FAA-RD-75-195

Project Report
ATC-58

Airport Survey for MLS Multipath Issues

D.A. Shnidman

15 December 1975

Lincoln Laboratory
MASSACHUSETTS INSTITUTE OF TECHNOLOGY
LEXINGTON, MASSACHUSETTS

Prepared for the Federal Aviation Administration,
Washington, D.C. 20591.

This document is available to the public through
the National Technical Information Service,
Springfield, VA 22161

This document is disseminated under the sponsorship of the Department of Transportation in the interest of information exchange. The United States Government assumes no liability for its contents or use thereof.

Technical Report Documentation Page

1. Report No. FAA-RD-75-195	2. Government Accession No.	3. Recipient's Catalog No.
4. Title and Subtitle Airport Survey for MLS Multipath Issues		5. Report Date 15 December 1975
		6. Performing Organization Code
7. Author(s) D. A. Shnidman		8. Performing Organization Report No. ATC-58
9. Performing Organization Name and Address Massachusetts Institute of Technology Lincoln Laboratory P. O. Box 73 Lexington, MA 02173		10. Work Unit No. (TRAIS) DOT-FA74WAI-461
		11. Contract or Grant No. DOT-FA74WAI-461
12. Sponsoring Agency Name and Address Department of Transportation Federal Aviation Administration Systems Research and Development Service Washington, DC 20591		13. Type of Report and Period Covered Project Report
		14. Sponsoring Agency Code

15. Supplementary Notes

The work reported in this document was performed at Lincoln Laboratory, a center for research operated by Massachusetts Institute of Technology under Air Force Contract F19628-76-C-0002.

16. Abstract

Eight major U.S. civilian airports were visited and data on the surface material of all sizable buildings visible from the runways were obtained. This information is catalogued herein. It is only with the aid of such information that we can address issues such as the likelihood of a system performance changes due to polarization, pattern control and coverage control.

A total of 93 buildings and 123 surfaces are included and the breakdown between the various surfaces is as follows:

74 surfaces were corrugated
17 surfaces were cinder block
16 surfaces were brick
9 surfaces were concrete
5 surfaces were smooth metal.

Of the 74 corrugated surfaces 18 were of the "flat" variety, 34 were one of five sub-categories and the remaining 22 needed 15 sub-categories for classification.

17. Key Words Microwave Landing Systems multipath building survey airports corrugation	18. Distribution Statement Document is available to the public through the National Technical Information Service, Springfield, Virginia 22151.

19. Security Classif. (of this report) Unclassified	20. Security Classif. (of this page) Unclassified	21. No. of Pages	

Form DOT F 1700.7 (8-72) Reproduction of completed page authorized

TABLE OF CONTENTS

1. Introduction

Brewster's law determines the reflection coefficient of a dielectric surface in terms of the polarization of the impinging electromagnetic wave.[1] In a similar manner, a corrugated surface will cause different levels of reflection for different polarizations.[2,3,4,5] Although these results are reasonably well known, it is difficult to quantify from them the impact of polarization on MLS system performance. This is due to the fact that small differences in multipath levels do not necessarily result in measurable differences in MLS system performance and one must have knowledge of the airport building surface materials in order to be able to specify, for each, the dependence of multipath levels on polarization. In order to obtain any insight into the problem, it is important to have some knowledge as to the distribution of types of reflecting surfaces at airports. This information can be utilized, in addition to the polarization issue, in considering topics, such as pattern control and coverage control, which are dependent on building multipath levels. In the spring of 1975 a representative of the FAA* surveyed eight large US airports to obtain data on the types and frequency of construction materials found on the surfaces of buildings visible from airport runways. As will be seen from the data, the number of different surfaces needed to characterize a majority of the buildings is not unwieldy. Most surfaces could be placed in one of the following categories: brick, concrete, cinder block, smooth metal, and five types of corrugations.

The eight airports in the survey were: John F. Kennedy (JFK) in New York, Philadelphia (PHL), O'Hare (ORD) in Chicago, Los Angeles (LAX), San Francisco (SFO), Miami (MIA), Tulsa (TUL), and Minneapolis/St. Paul (MSP). A summary of the data is presented in the next section and the detailed information given Lincoln Laboratory presented in Appendix A.

---

*Albert Stein

AIR FORCE (1) FEBRUARY 18, 1976--500

2. Summary of Survey Data

All sizable buildings, visible from runway surfaces (not just those oriented for the generation of MLS multipath), were included in the survey for a total of 93 buildings. Some buildings have more than one surface material of interest so that 123 surfaces (excluding glass, fiberglass, and parts of the building near the ground) were noted and recorded. The break-up of the buildings as to airport and the surfaces are categorized as in Table 1.

Table 1

Surfaces Categorized for Each Airport

Airport	Buildings	Surfaces	Corru-gated	Cinder Block	Brick	Concrete	Smooth Metal
JFK	19	28	13	3	7	1	4
PHL	12	17	11	3	2	1	
ORD	14	19	14	1	4		
LAX	11	15	9	1		4	1
SFO	4	4	3		1		
MIA	17	20	10	6	1	3	
TUL	10	12	9	2	1	1	
MSP	6	8	5	1		1	1
Totals	93	123	74	17	16	11	6

Glass (unless bronzed) and fiberglass were considered as transparent. The 74 corrugations were broken down and classified further. We defined seven different types of parameterized corrugations: sinusoidal, trapezoidal, rectangular, sine-flat, trap-flat, rect-flat, and trap-rect. The first three categories are obvious. The next three are typified by a large flat region and are expected to have reflection properties more in line with a flat surface than a corrugated one. The final category consists of trapezoidal corrugated surfaces which are nearly rectangular. Figure 1 depicts each category and defines the parameters for each.

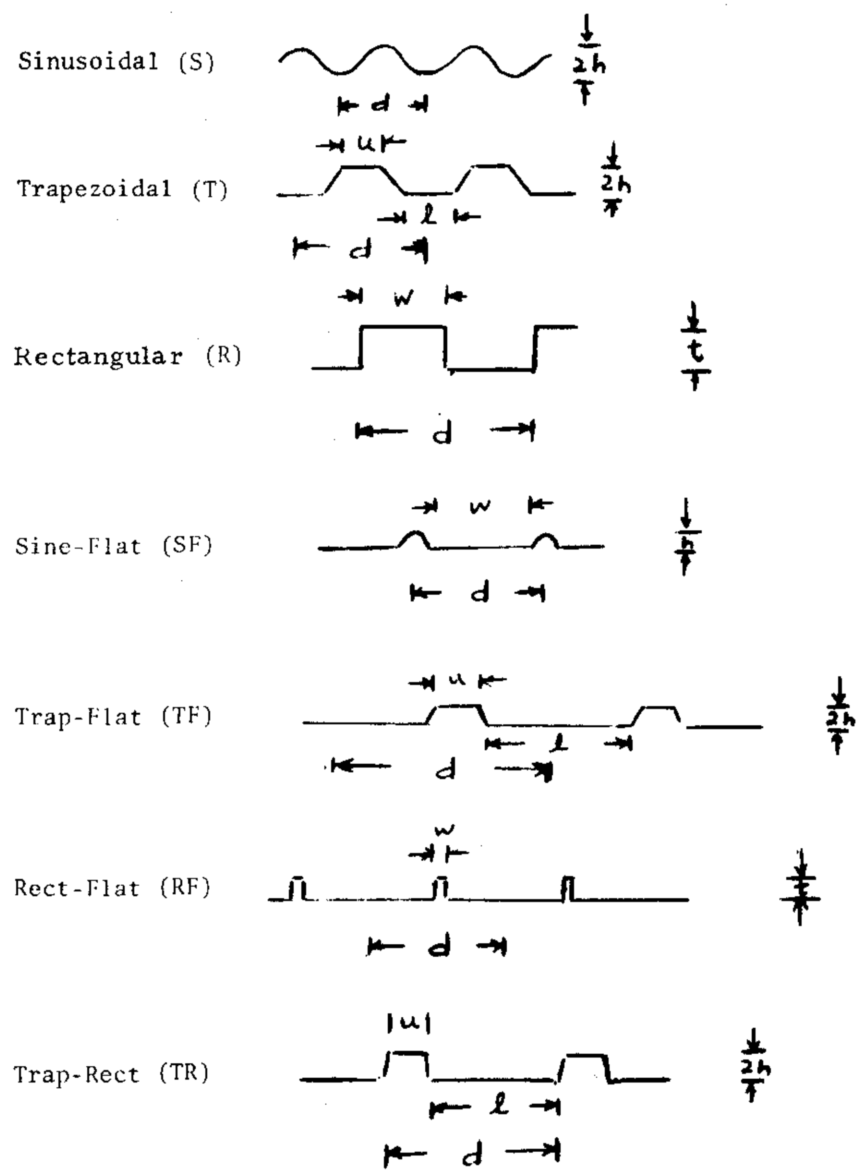

Fig. 1. Categories of corrugations.

Table 2 specifies the parameter values for each subcategory. There were six sets of parameters for the sinusoidal category. The trapezoidal category had six entries in which T1, T2, T3 and T6 are undistorted trapezoids. Trapezoids T4 and T5 have additional bumps and are depicted in Fig. 2. The rectangles have 3 subcategories of which the third has additional bumps and notches and is depicted in Fig. 3. The single sine-flat corrugation has a period d = 6.0" and is depicted in Fig. 4. Trap-flat TF1, TF3, TF5, and TF6 are undistorted trapezoids while TF2, TF4, and TF7 have extra bumps and are depicted in Fig. 5. The single rect-flat, having a period of 6 inches, is shown in Fig. 6. The final category of trap-flat has 5 subdivisions of which 3 are undistorted trapezoids. The remaining are shown in Fig. 7.

Table 3 specifies the number and location of each category. The detailed information together with airport maps are given in Appendix A.

Table 2

Parameter Values for Each Sub-category

S1	d = 2.75"			h = 0.25"
S2	d = 3.0"			h = 0.375"
S3	d = 5.5"			h = 0.75"
S4	d = 6.0"			h = 0.875"
S5	d = 4.5"			h = 0.5625"
S6	d = 4.0"			h = 0.375"
T1	d = 8.0"	u = 2.0"	ℓ = 2.0"	h = 0.75"
T2	d = 5.5"	u = 1.0"	ℓ = 1.0"	h = 0.75"
T3	d = 5.0"	u = 4.0"	ℓ = 1.5"	h = 0.625"
T4	d = 12.0"	u = 4.0"	ℓ = 2.0"	h = 1.75"
T5	d = 12.0"	u = 2.0"	ℓ = ?	h = 1.75"
T6	d = 6.0"	u = 2.0"	ℓ = 2.5"	h = 0.625"
R1	d = 6.0"	w = 4.0"	t = 1.5"	
R2	d = 12.0"	w = 6.0"	t = 1.125"	
R3	d = 12.0"	w = 6.0"	t = 1.4375"	
TF1	d = 12.0"	u = 1.0"	ℓ = 10.0"	h = 0.5"
TF2	d = 12.0"	u = 1.375"	ℓ = 9.0"	h = 0.75"
TF3	d = 16.0"	u = 10.25"	ℓ = 4.25"	h = 0.75"
TF4	d = 12.0"	u = 1.0"	ℓ = 8.0"	h = ?
TF5	d = 7.0"	u = 5.0"	ℓ = 1.0"	h = 0.5"
TF6	d = 12.0"	u = 7.75"	ℓ = 1.5"	h = 0.75"
TF7	d = 12.0"	u = 1.0"	ℓ = 9.25"	h = 0.5"
TR1	d = 12.0"	u = 6.0"	ℓ = 4.0"	h = 0.75"
TR2	d = 4.0"	u = 2.0"	ℓ = 1.5"	h = 0.5"
TR3	d = 7.0"	u = 4.0"	ℓ = 1.5"	h = 0.75"
TR4	d = 8.0"	u = 1.5"	ℓ = 5.5"	h = 0.5"
TR5	d = 12.0"	u = 5.5"	ℓ = 3.5"	h = 0.75"

ATC-58 (2)

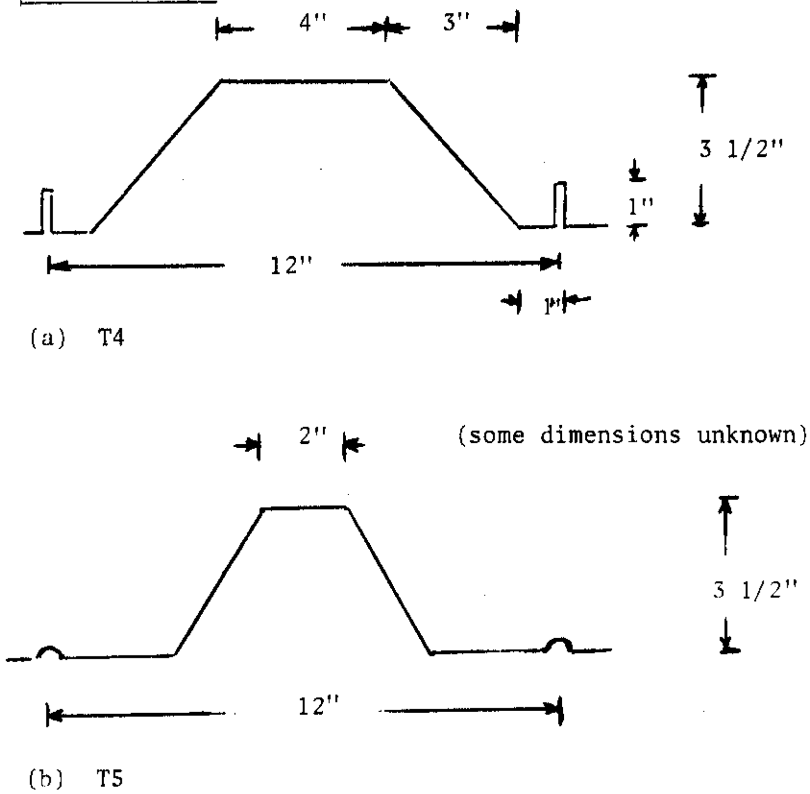

Fig. 2. T4 and T5 corrugation details.

ATC-58 (3)

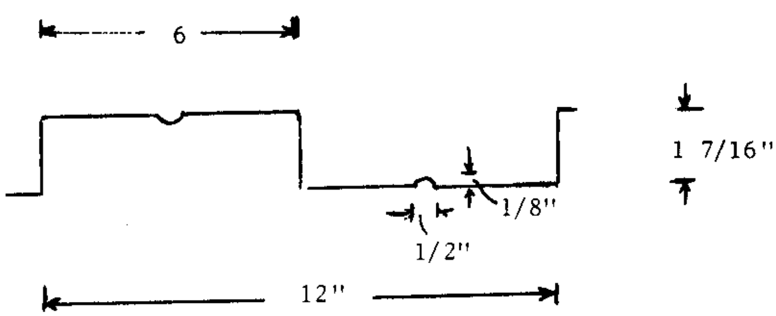

Fig. 3. R3 corrugation detail.

ATC-58 (4)

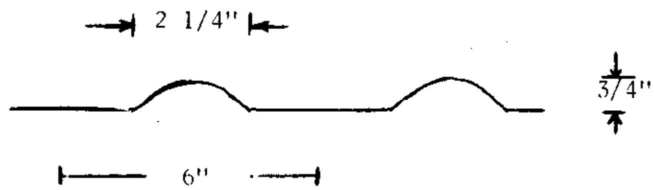

Fig. 4. SF1 corrugation detail.

ATC-58 (5a,b,c)

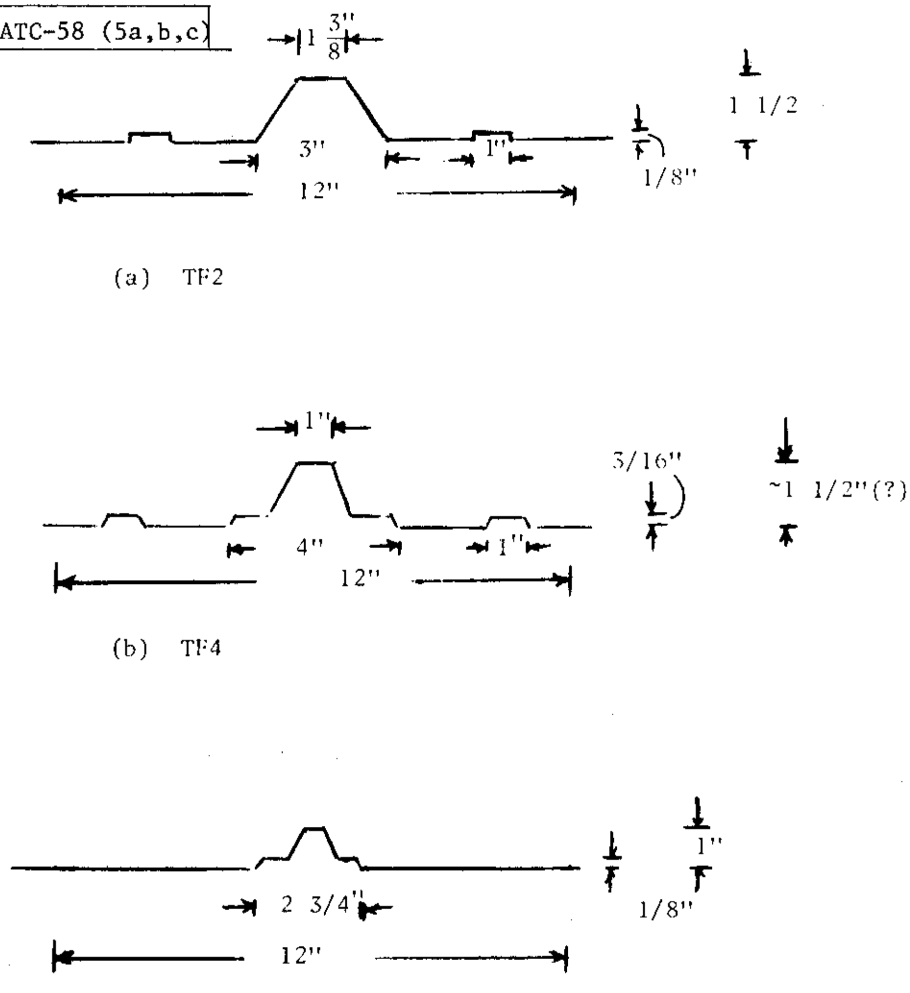

Fig. 5. TF2, TF4 and TF7 corrugation detail.

ATC-58 (6)

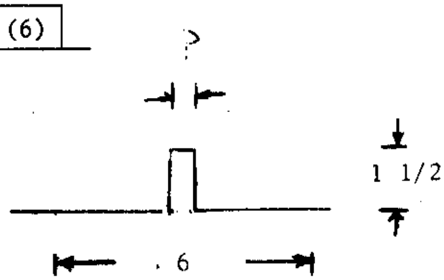

Fig. 6. RF1 corrugation detail.

ATC-58 (7a,b)

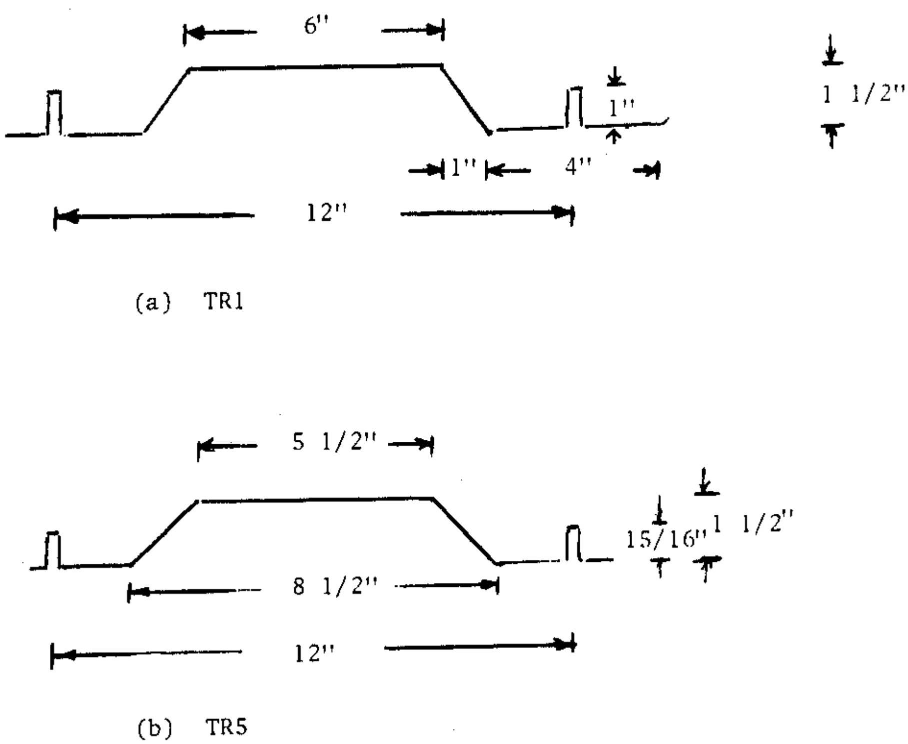

Fig. 7. TR1 and TR5 corrugation detail.

Table 3

Number and Locations of Each Sub-Category

Category	Number	Location
S1	9	LAX(3), SFO(2), MSP(2), TUL(2)
S2	4	JFK(3), MIA (1)
S3	3	JFK(3)
S4	1	JFK(1)
S5	1	MIA(1)
S6	1	ORD(1)
T1	10	JFK(1), LAX(2), SFO(1), MSP(1), MIA(3) ORD(2)
T2	5	MSP(2), MIA(1), ORD(2)
T3	2	LAX(2)
T4	1	JFK(1)
T5	1	JFK(1)
T6	1	ORD(1)
R1	6	PHL(1), LAX(2), TUL(2), ORD(1)
R2	2	PHL(1), ORD(1)
R3	1	PHL(1)
SF1	3	MIA(3)
TFL	1	PHL(1)
TF2	5	PHL(3), ORD(2)
TF3	3	PHL(3)
TF4	2	TUL(1), MIA(1)
TF5	1	TUL(1)
TF6	1	TUL(1)
TF7	1	ORD(1)
RF1	1	JFK(1)
TR1	2	JFK(1), PHL(1)
TR2	1	JFK(1)
TR3	3	TUL(2), ORD(1)
TR4	1	ORD(1)
TR5	1	ORD(1)

3. *Summary of Conclusions*

(a) Of the 93 buildings surveyed 71%(67) had at least one corrugated surface.

(b) Of the 123 surfaces 60%(74) were corrugated, 14%(17) were cinder block, 13%(16) were brick, 9%(11) were concrete, and 5%(6) were smooth metal.

(c) 24%(18) of the corrugated surfaces were of the "flat" variety which are expected to have reflection properties similar to flat surfaces.

(d) Of the 56 remaining corrugated surfaces 61%(34) are one of the five dominant types T1, T2, S1, S2, and R1.

(e) It required 15 subcategories of corrugation to cover the remaining 22 surfaces. In addition only R2 (one at PHL and one at ORD), TR1 (one at JFK and one at PHL), and TR3 (two at TUL and one at ORD) appear at more than a single airport.

(f) Estimates of the squares of peak reflection coefficients, assuming perfect conductivity properties, for S1, S2, and R1, have been determined by J. Mink of ECOM and are presented in Appendix B. They indicate that the possibility of significantly different levels of reflections for different polarizations exists.

(g) An experimental program in order to characterize the prevalent surfaces should be undertaken and include a determination of the conductivity of commonly used nonmetalic materials such as galbestos and bronzed glass.

Appendix A

DETAILED SURVEY DATA

The detailed survey data and comments are reproduced here to the same degree of completeness as was received by Lincoln Laboratory. They were redone solely to improve on the legability and reproducibility of the figures. Airport maps are also included to help locate the buildings described. The airports are presented alphabetically according to airport codes.

Airport	Pages	Date Visited
JFK	12-21	29 April 1975
LAX	22-32	6 June 1975
MIA	33-41	2 June 1975
MSP	42-46	3 June 1975
ORD	47-54	2 June 1975
PHL	55-60	20 March 1975
SFO	61-64	5 June 1975
TUL	65-70	4 June 1975

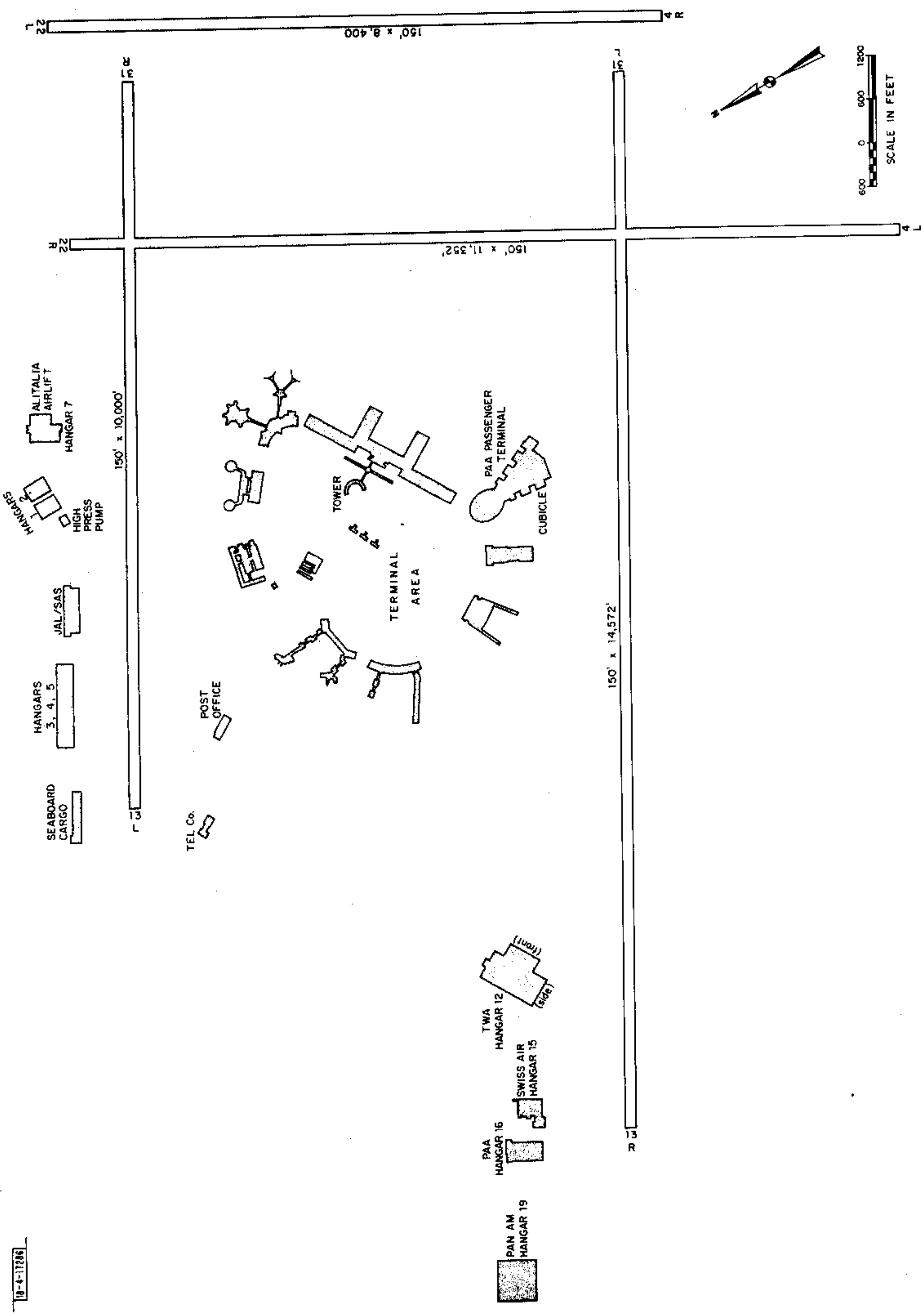

Fig. A1. John F. Kennedy International Airport (JFK).

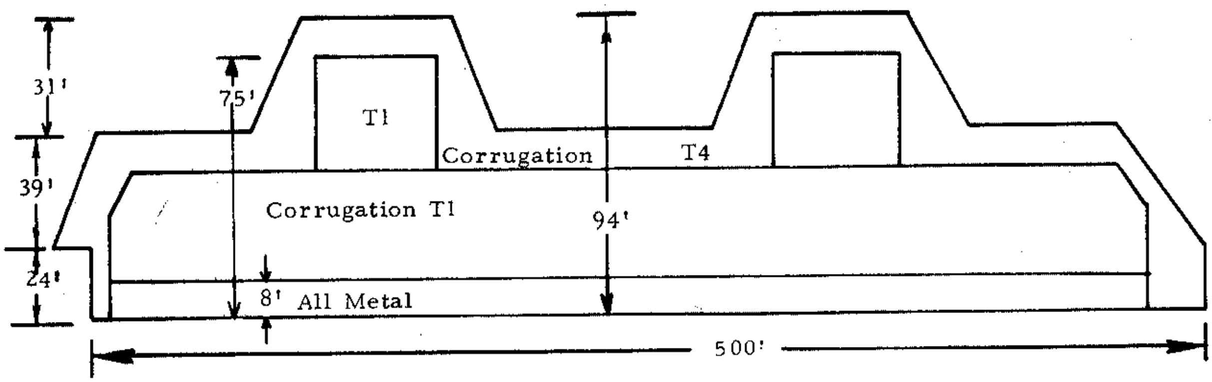

(a) PAA Hangar 19 (Front)

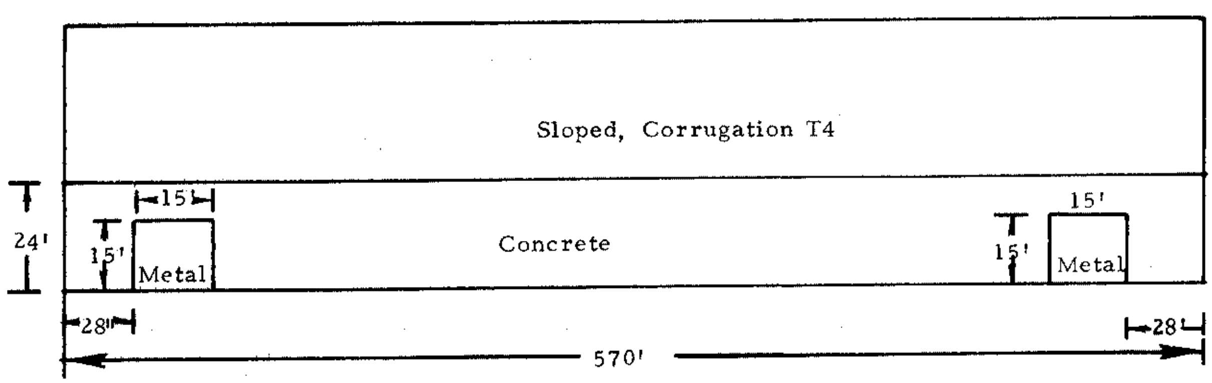

(b) PAA Hangar 19 (Side)

Fig. A2. JFK, PAA hangar 19.

ATC-58 (A3)

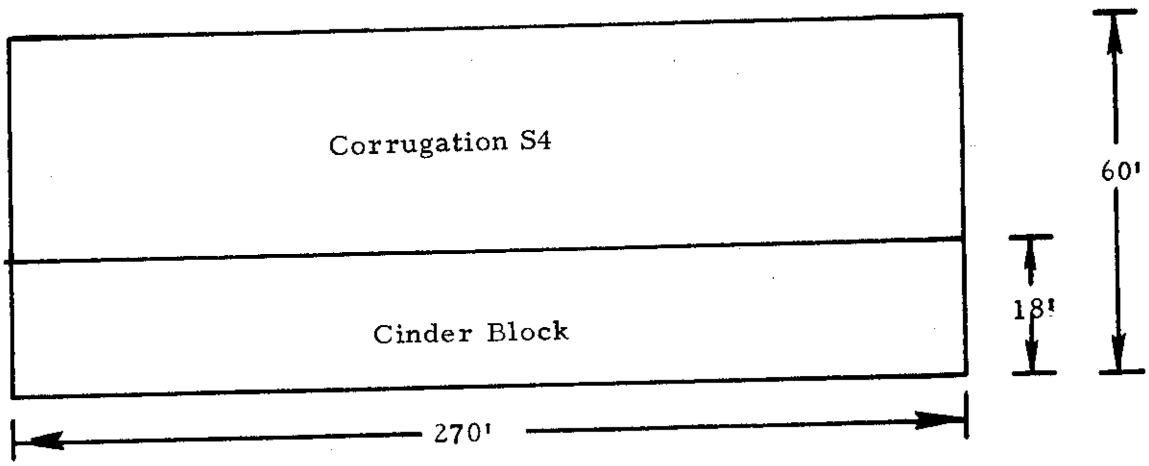

Fig. A3. JFK, PAA hangar 16.

ATC-58 (A4)

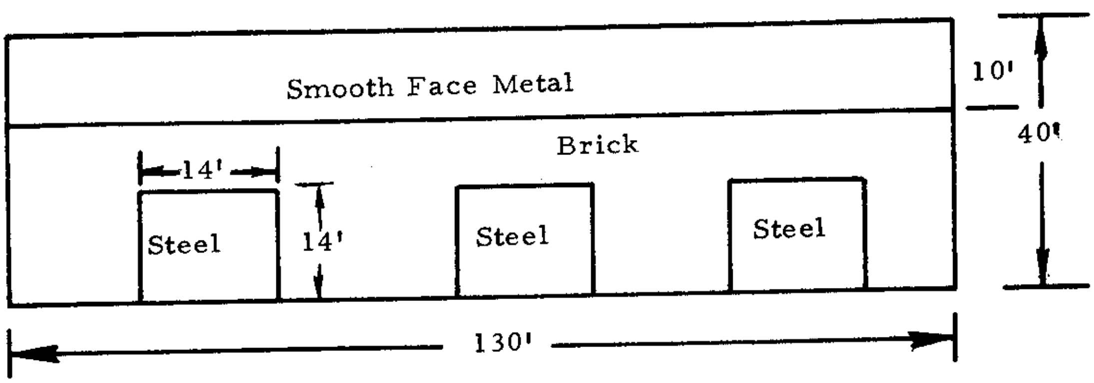

Fig. A4. JFK, Swiss Air hangar 15.

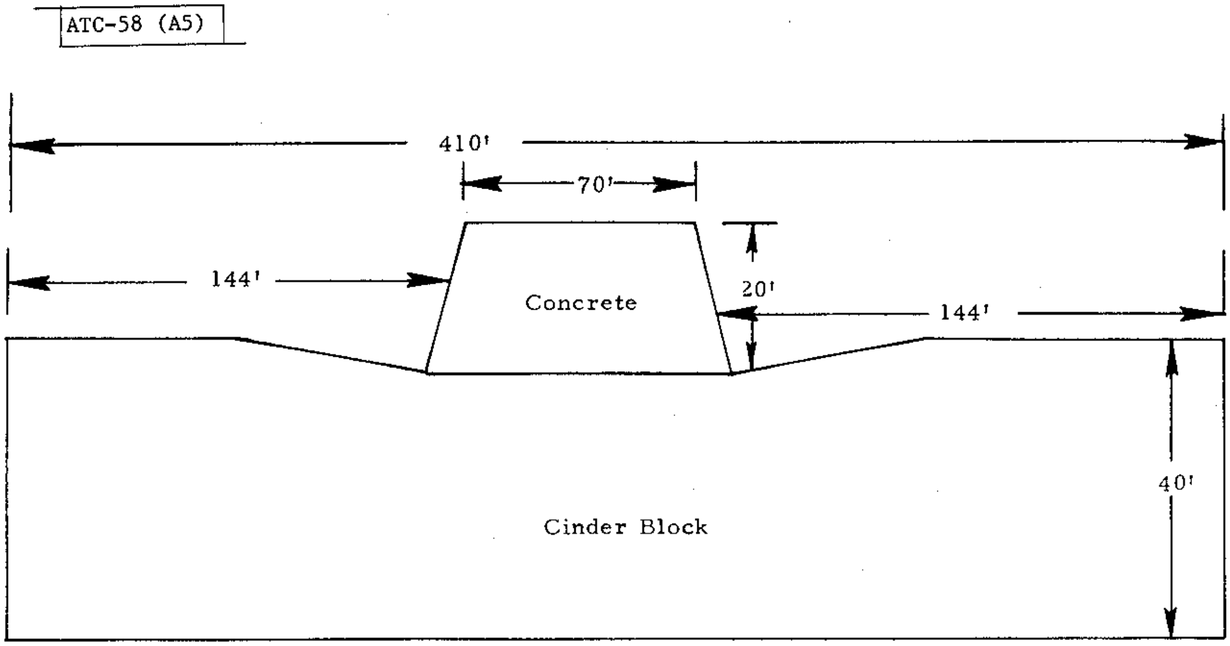

Fig. A5. JFK, TWA hangar 12 (side).

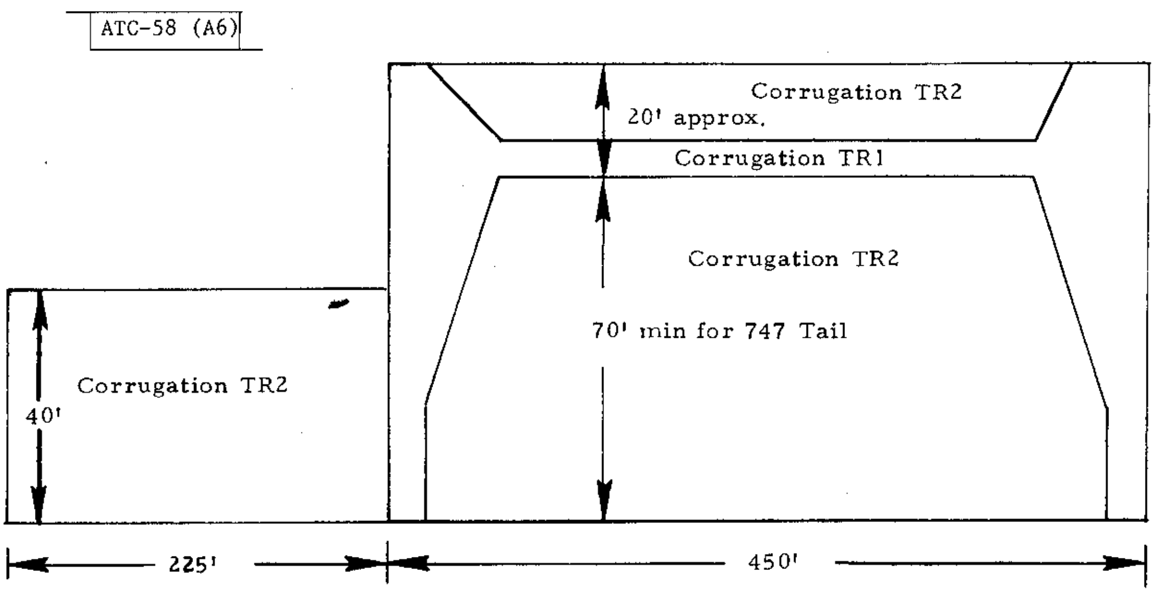

Fig. A6. JFK, TWA hangar 12 (front).

ATC-58 (A7)

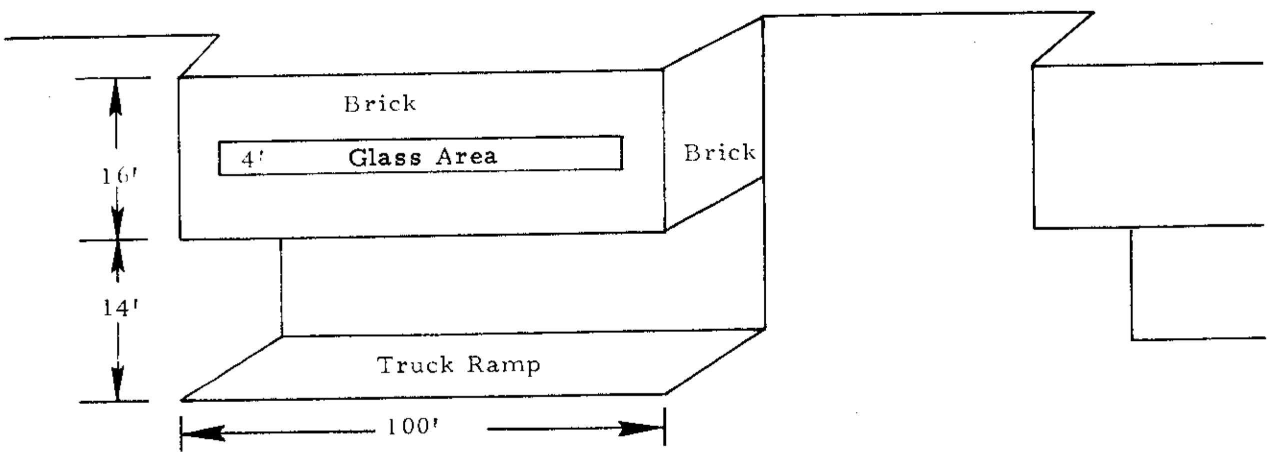

Fig. A7. JFK, Pan Am passenger terminal.

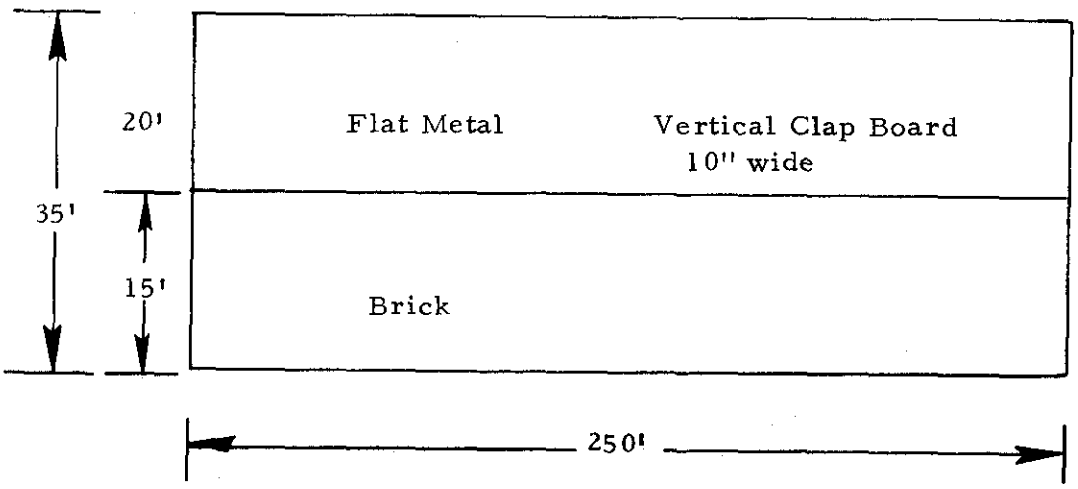

Fig. A8. JFK, Telephone Company building.

ATC-58 (A9)

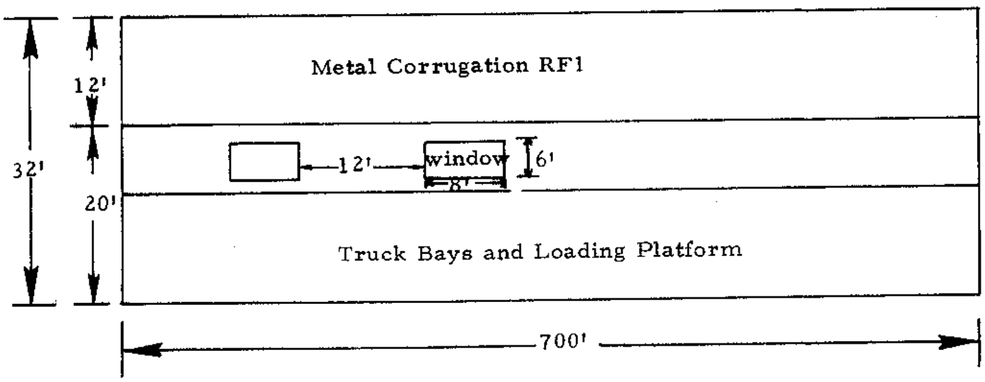

Fig. A9. JFK, Sea Board building.

ATC-58 (A10)

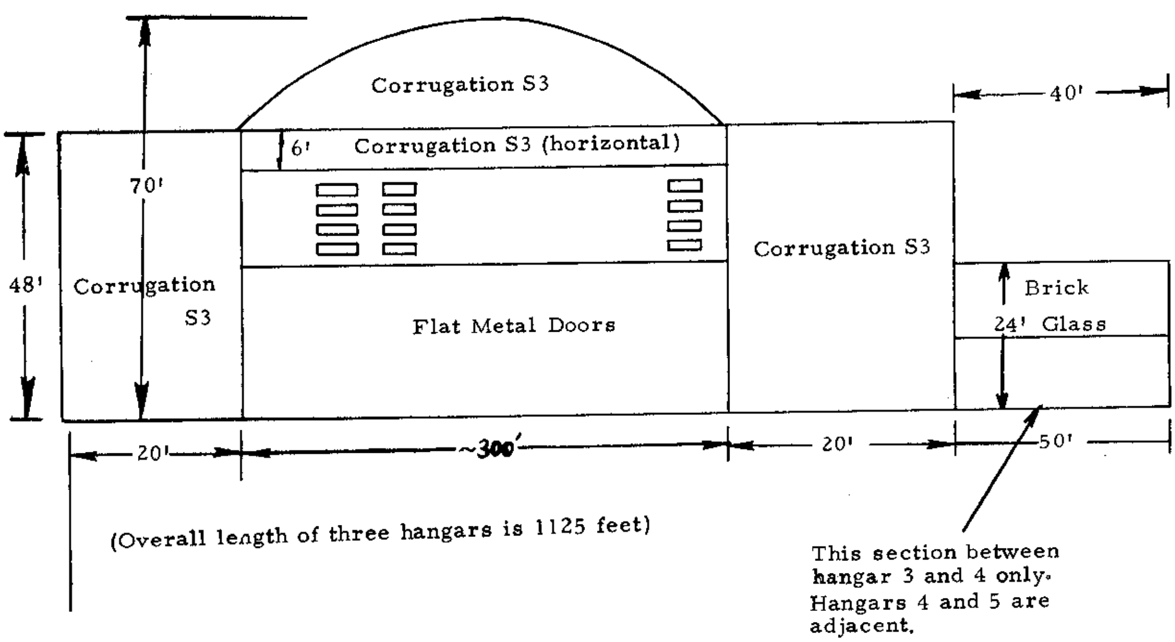

Fig. A10. JFK, hangars 3, 4, 5.

ATC-58 (A11)

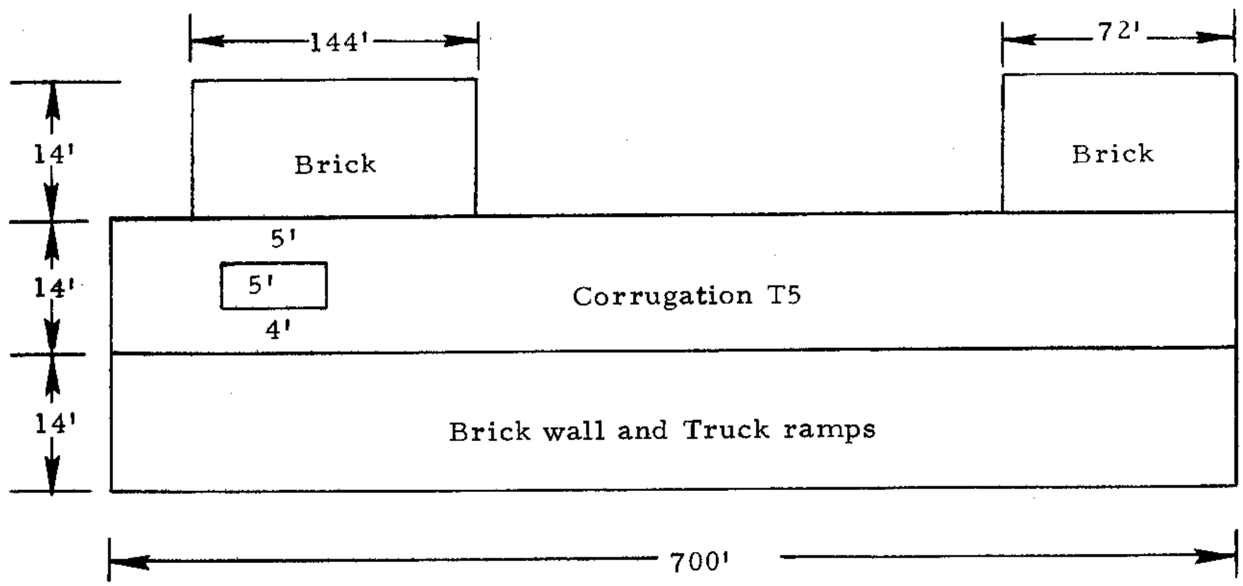

Fig. A11. JFK, JAL/SAS building.

ATC-58 (A12)

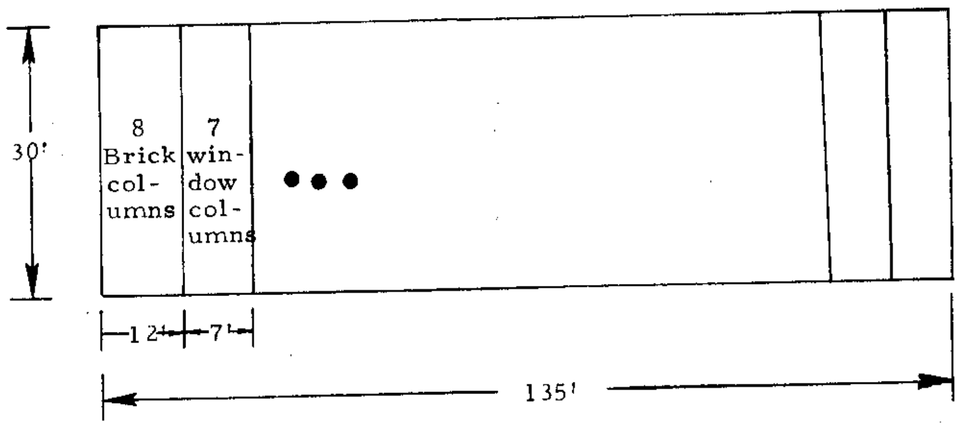

Fig. A12. JFK, High Pressure Pump Station.

ATC-58 (A13)

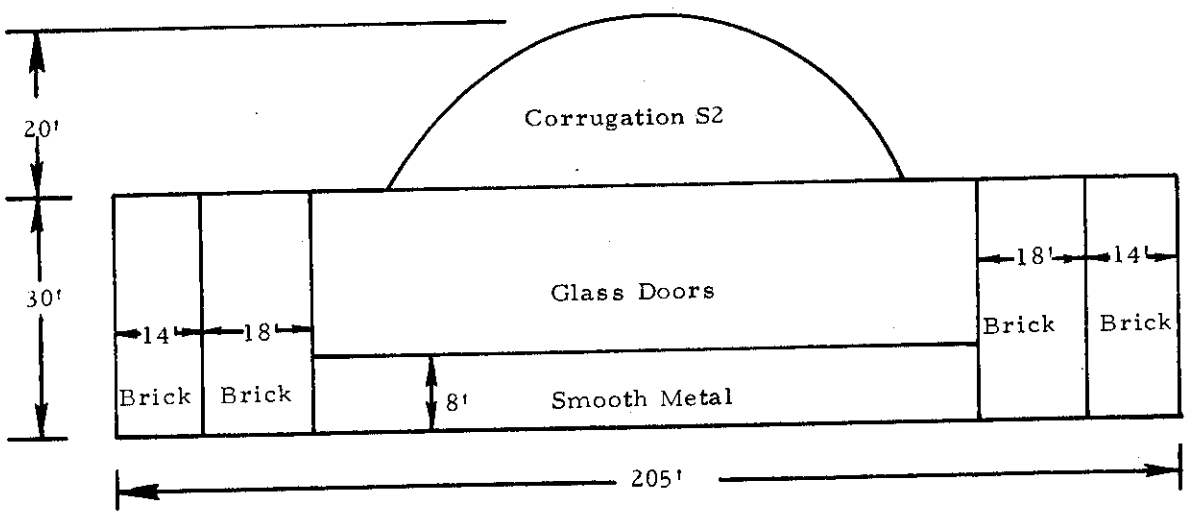

Fig. A13. JFK, hangars 1 and 2 (identical).

ATC-58 (A14)

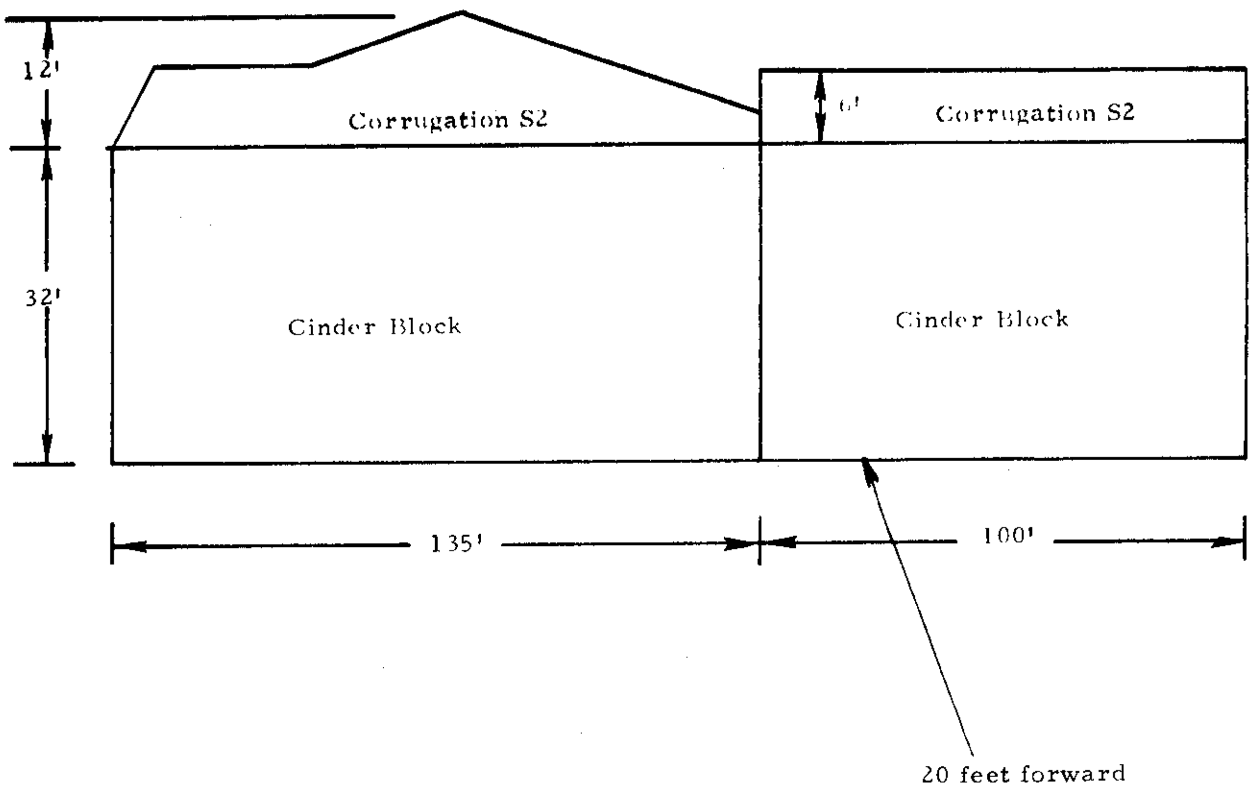

Fig. A14. JFK, hangar 7.

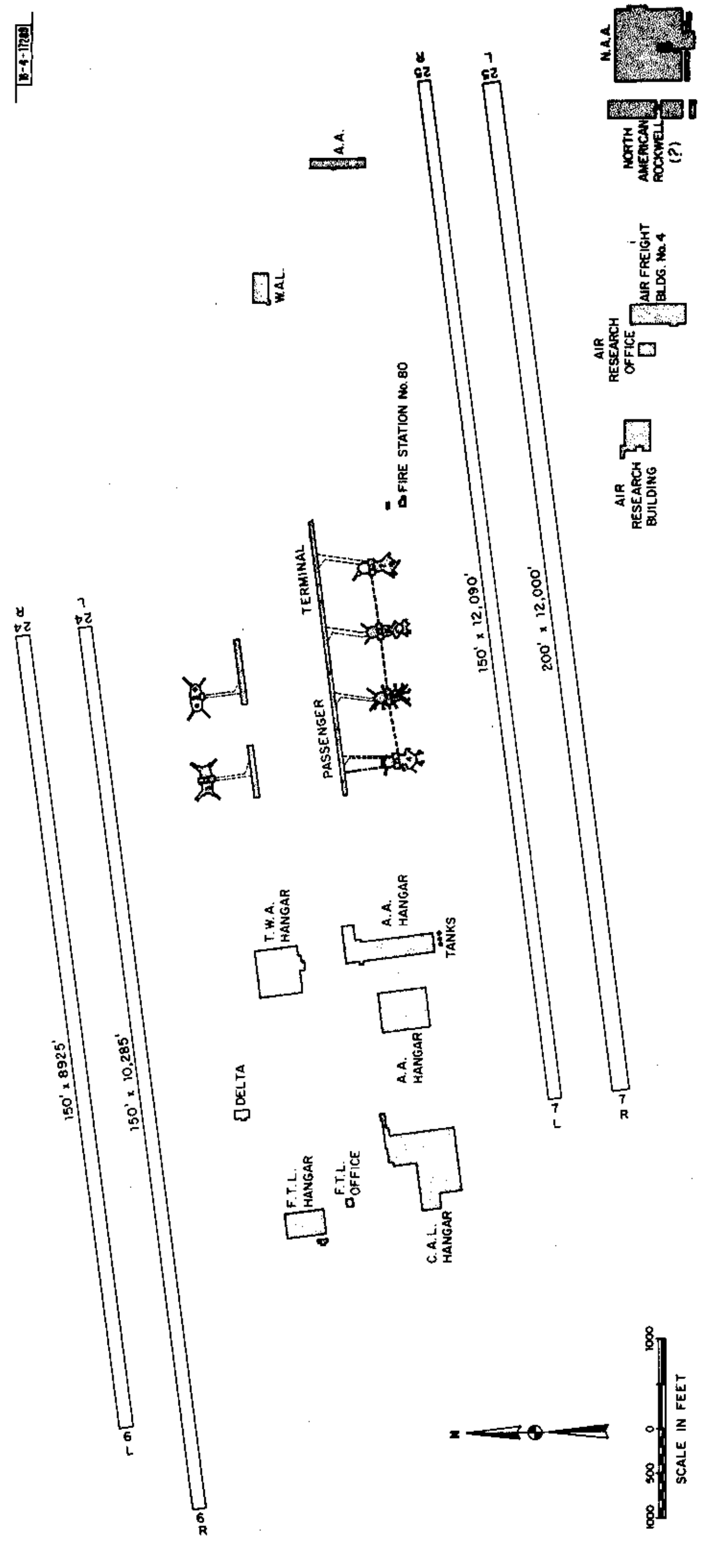

Fig. A15. Los Angeles International Airport (LAX).

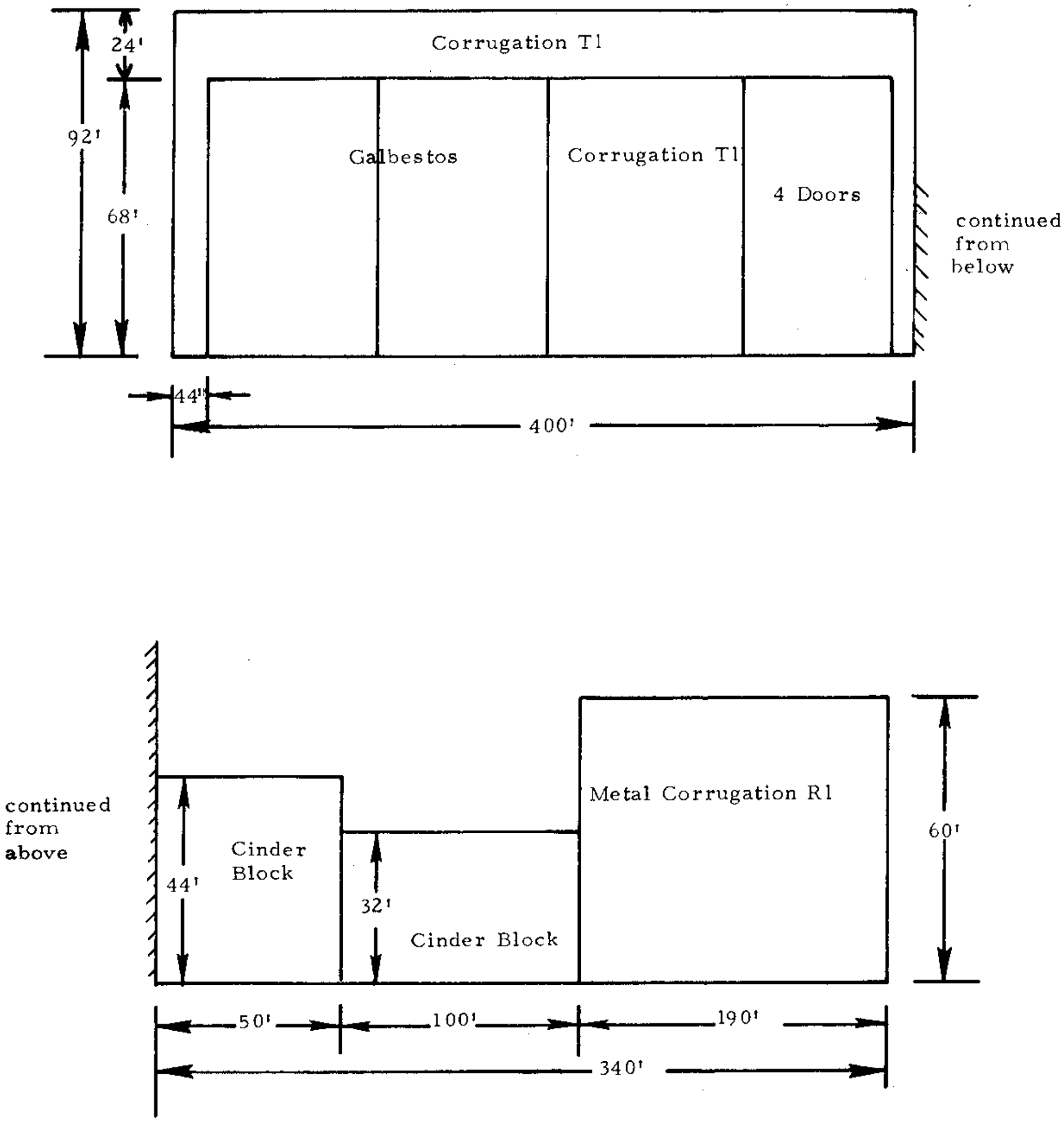

Fig. A16. LAX, Continental hangar.

ATC-58 (A17)

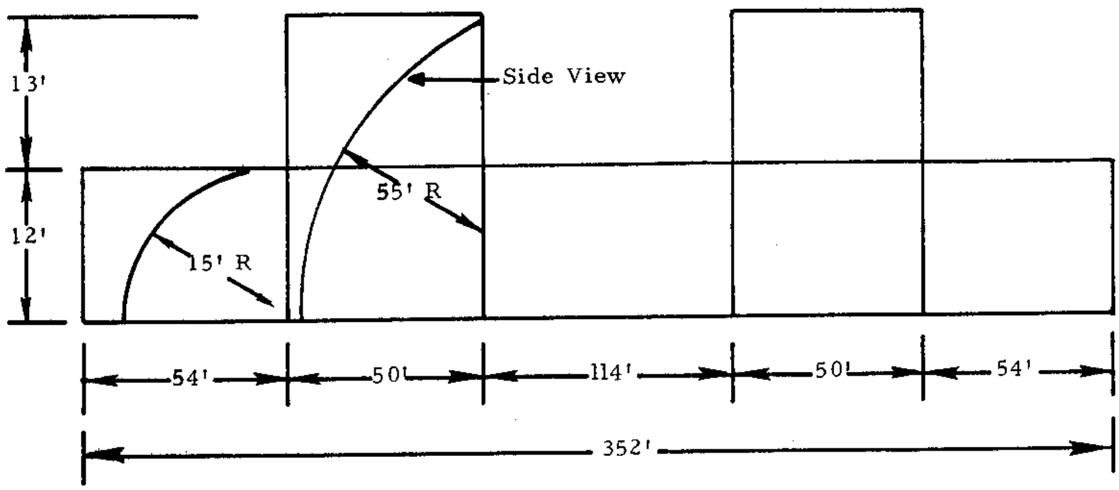

Fig. A17. LAX, blast fence.

ATC-58 (A18)

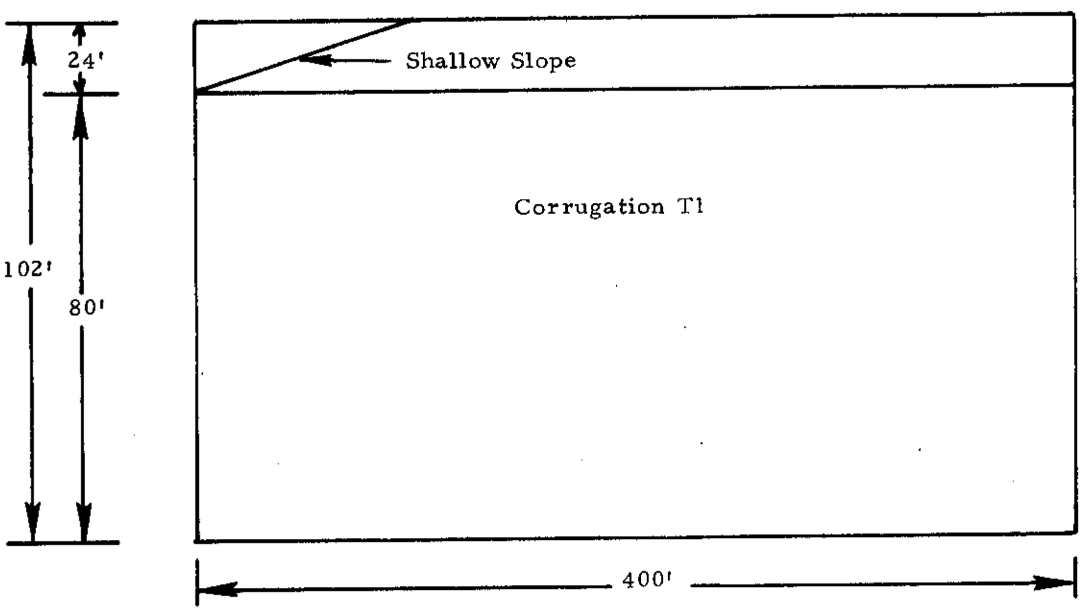

Fig. A18. LAX, American Airlines hangar.

ATC-58 (A19)

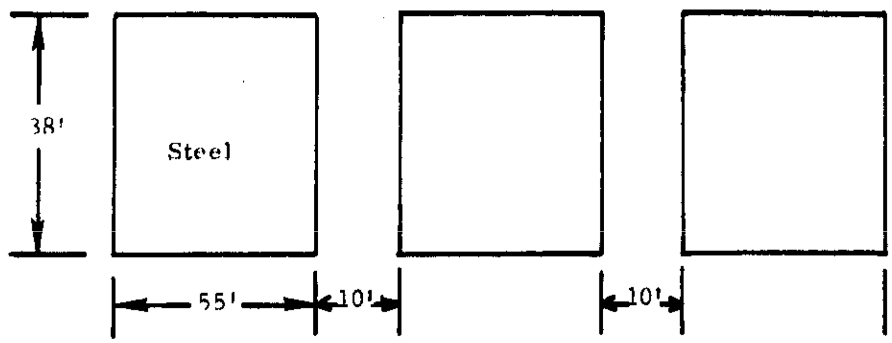

Fig. A19. LAX, tanks (same as San Francisco).

ATC-58 (A20)

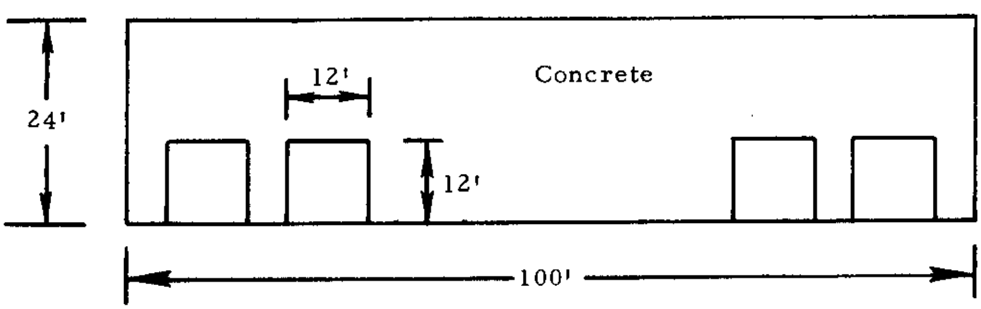

Fig. A20. AA Freight Building.

ATC-58 (A21)

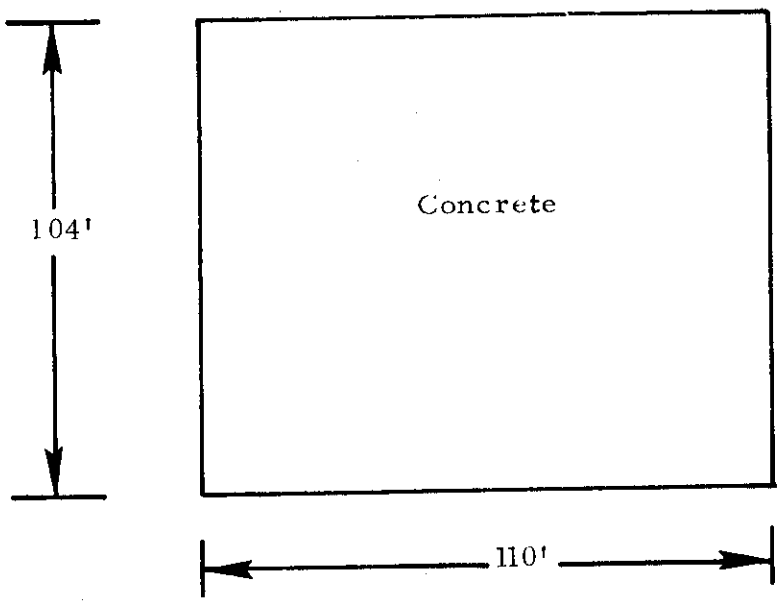

Fig. A21. LAX, Western Airline building.

ATC-58 (A22)

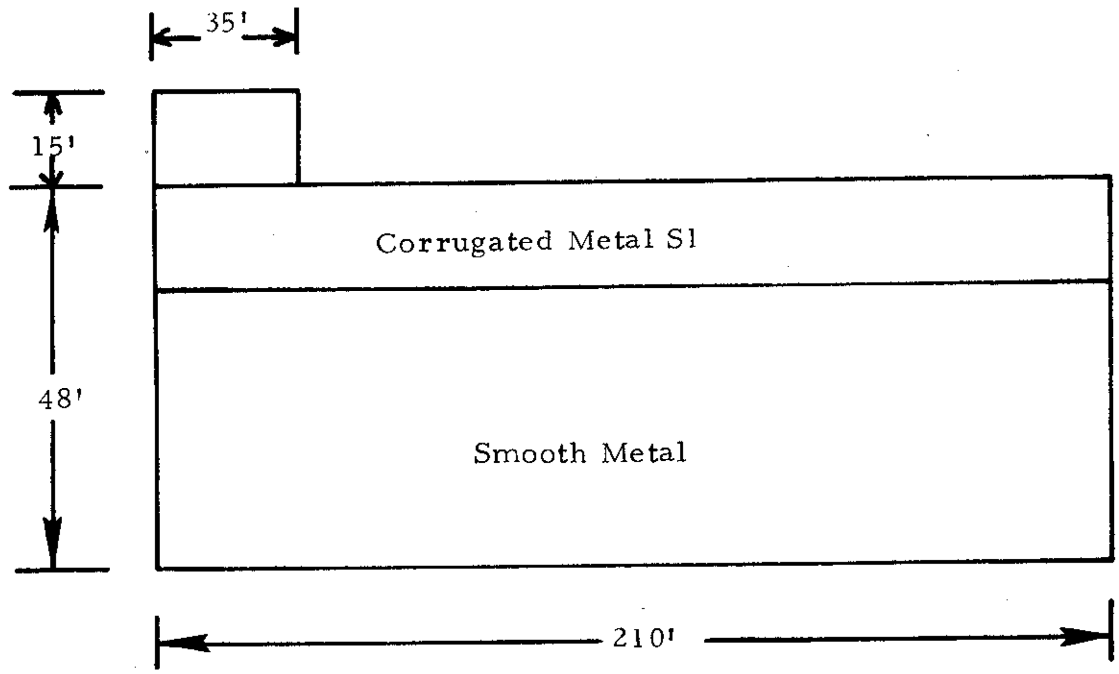

Note: Two N.A. Rockwell Office Buildings to the rear are all glass facing except that the upper 12' are concrete.

Fig. A22. LAX, North American Rockwell.

ATC-58 (A23)

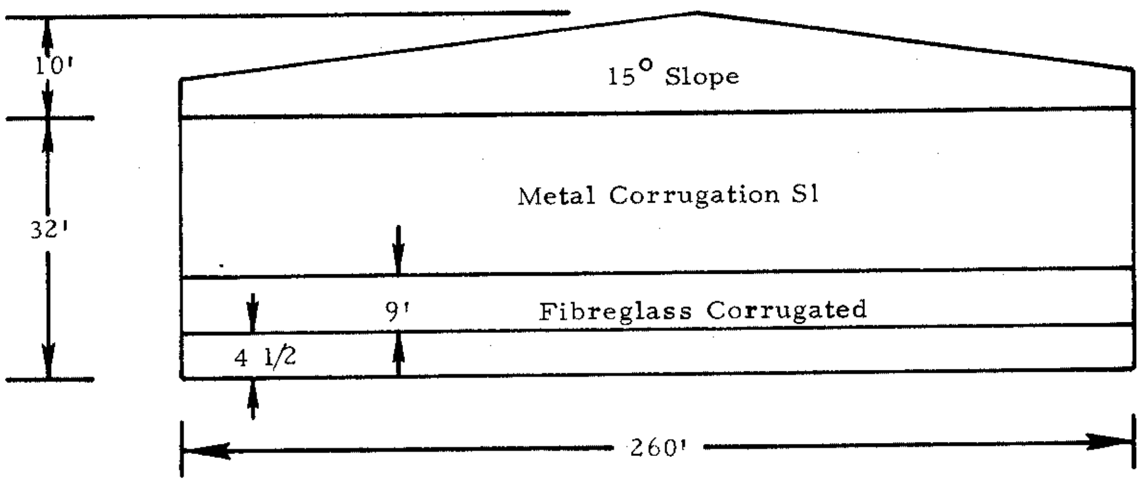

Fig. A23. LAX, Air Research building.

ATC-58 (A24)

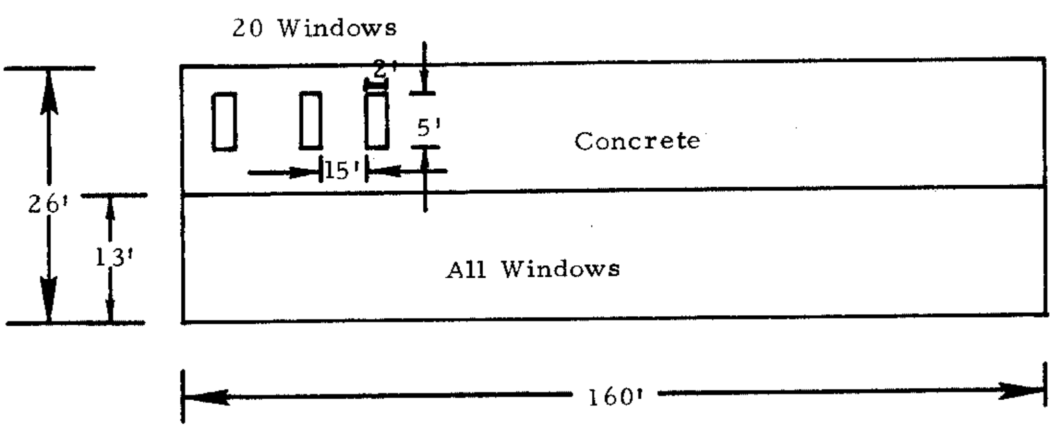

Fig. A24. LAX, Air Research Office.

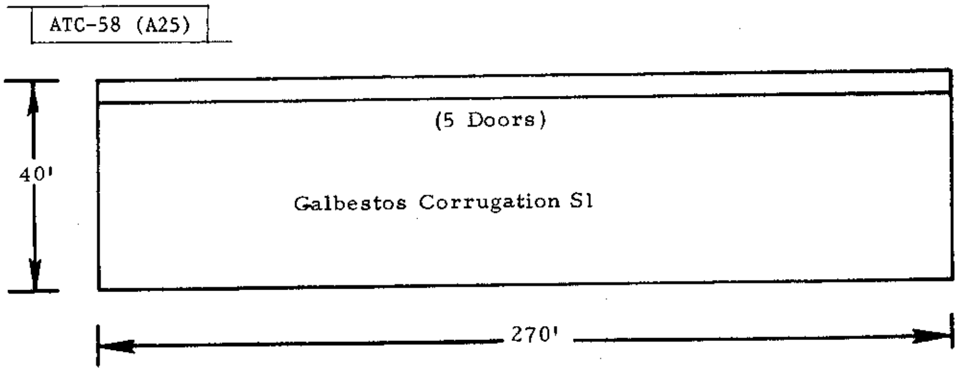

Fig. A25. LAX, building B-4 (hangar).

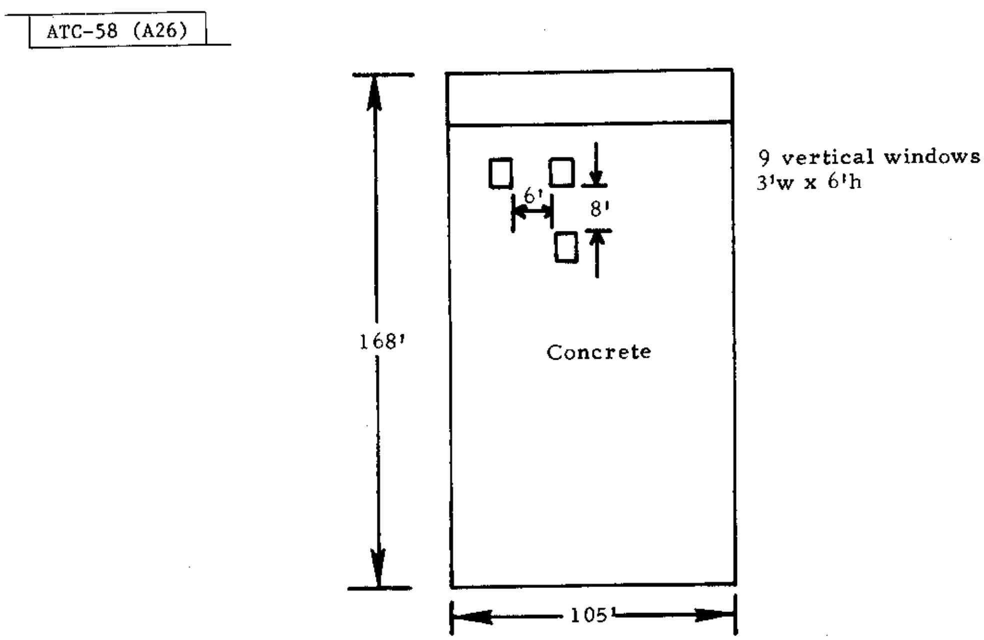

Fig. A26. LAX, Flying Tiger Office building.

ATC-58 (A27)

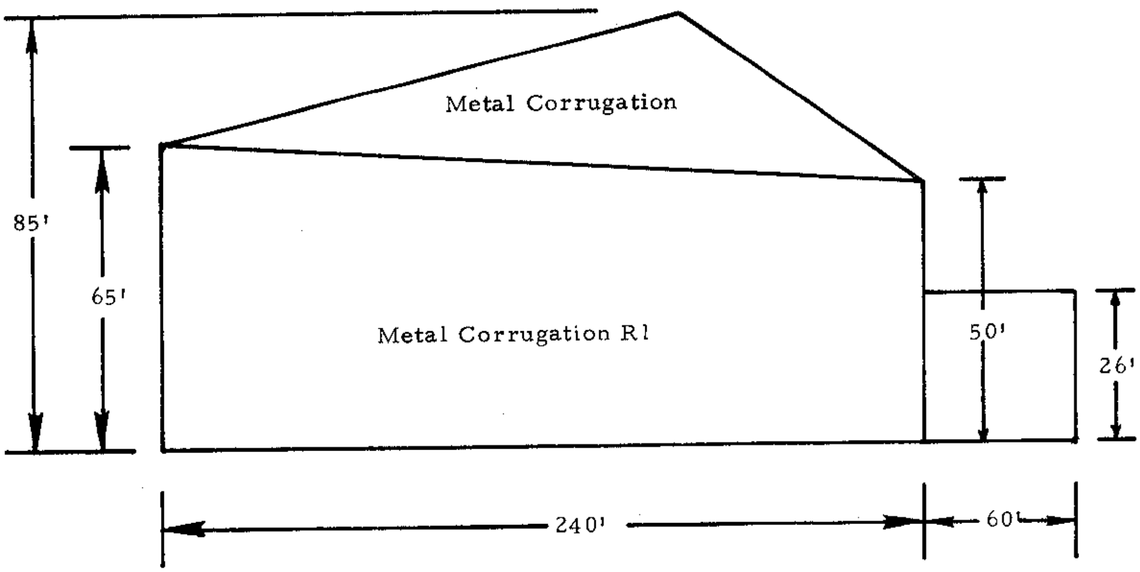

Fig. A27. LAX Flying Tiger hangar.

ATC-58 (A28)

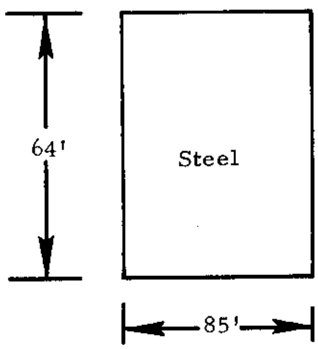

Fig. A28. LAX, tanks.

ATC-58 (A29)

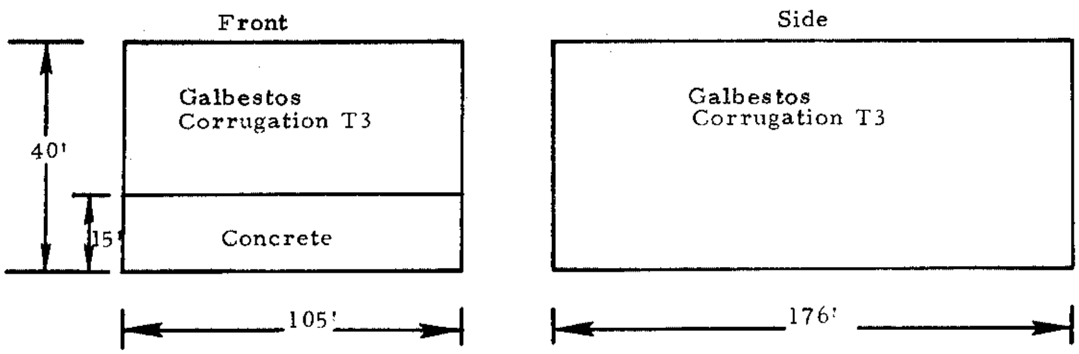

Fig. A29. LAX, Delta hangar.

ATC-58 (A30)

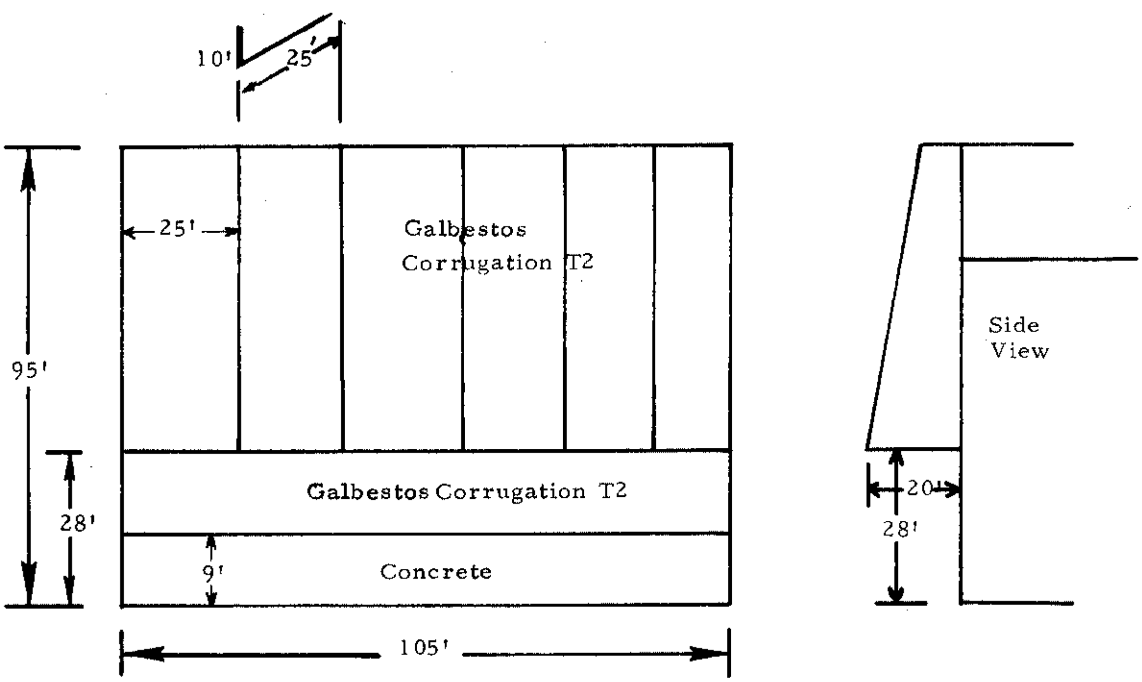

Fig. A30, LAX, TWA hangar building.

ATC-58 (A31)

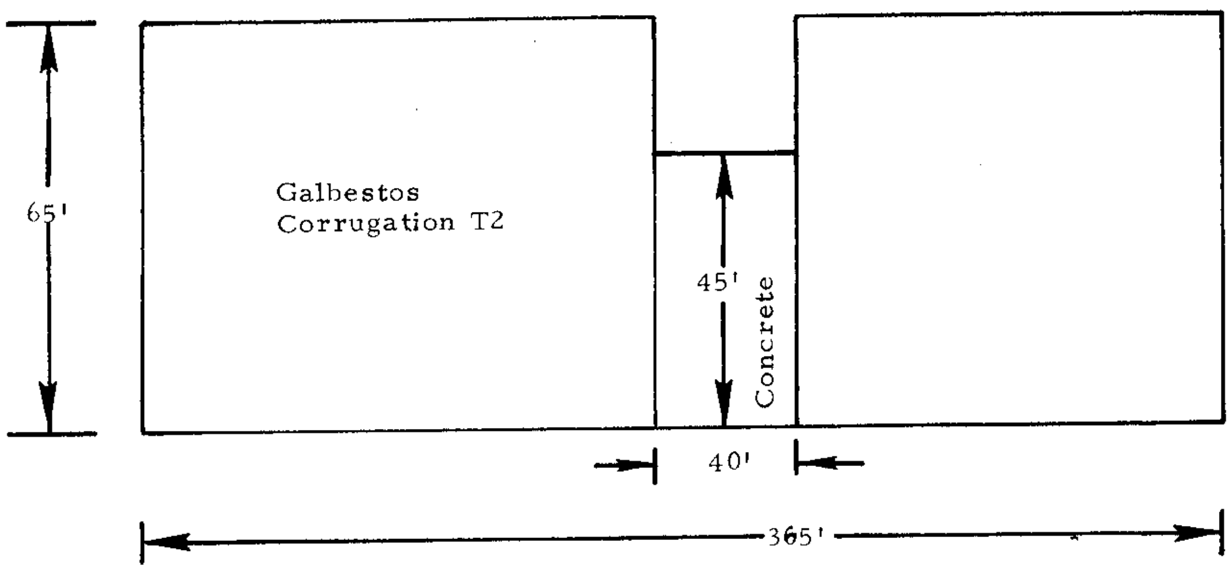

Fig. A31. LAX, TWA hangar.

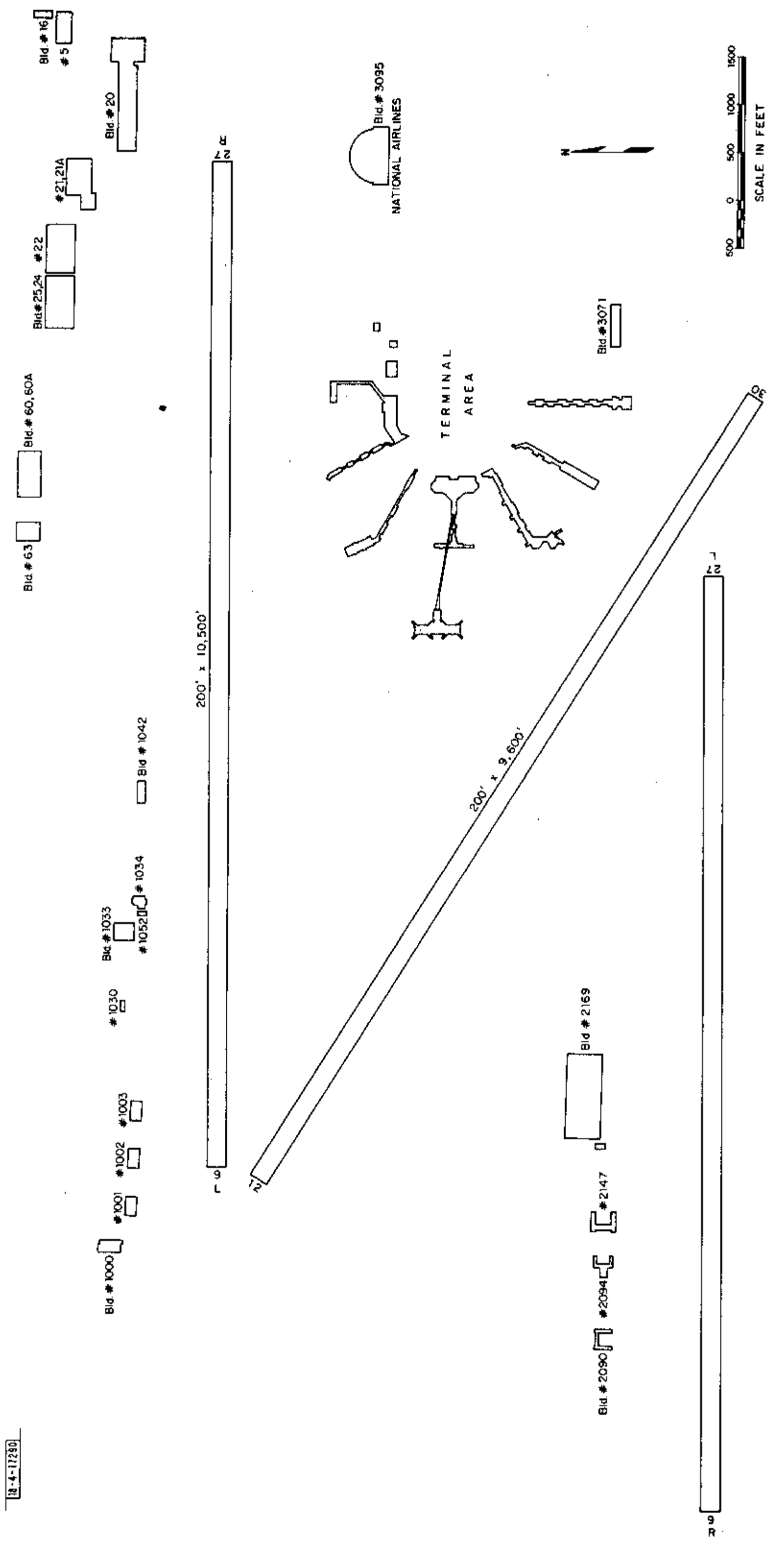

Fig. A32. Miami International Airport.

ATC-58 (A33)

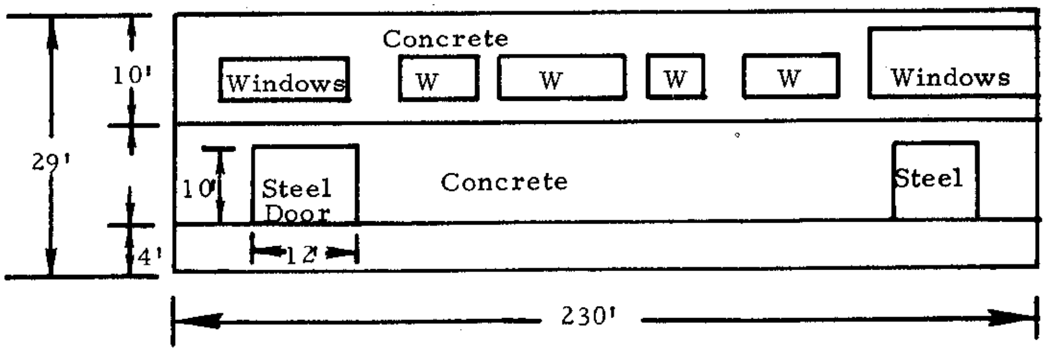

Fig. A33. MIA, building 1000.

Buildings 1001, 1002, 1003 same as Building 1000 for style and length

3- 12'w x 10' h Metal Doors   Buildings are 29' high

ATC-58 (A34)

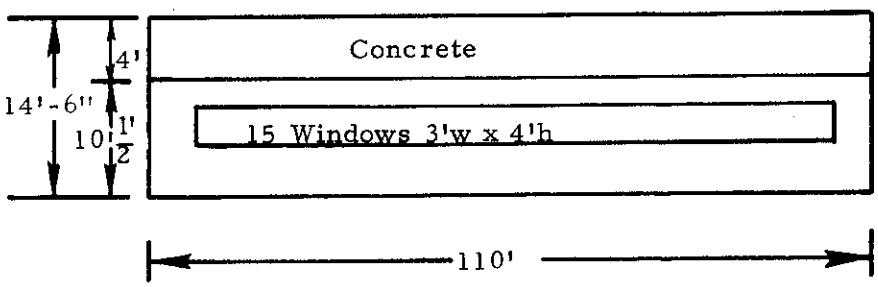

Fig. A34. MIA, building 1030.

ATC-58 (A35)

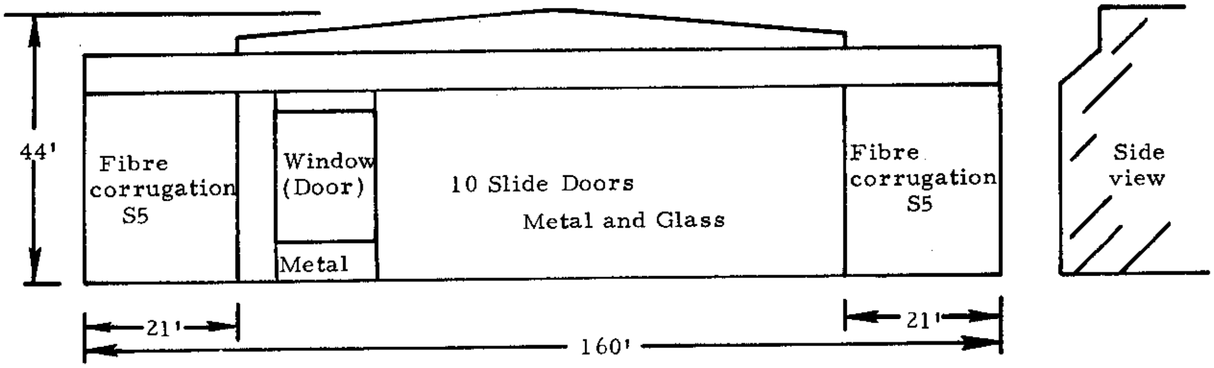

Fig. A35. MIA, building 1033 (hangar).

ATC-58 (A36)

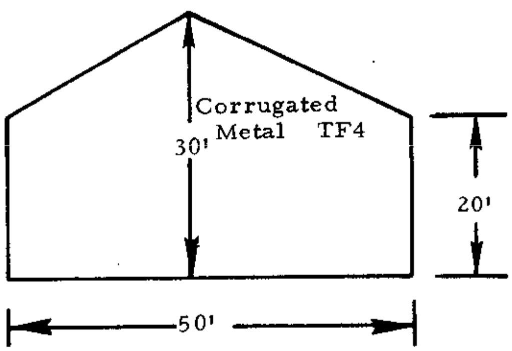

Fig. A36. MIA, building 1052.

ATC-58 (A37)

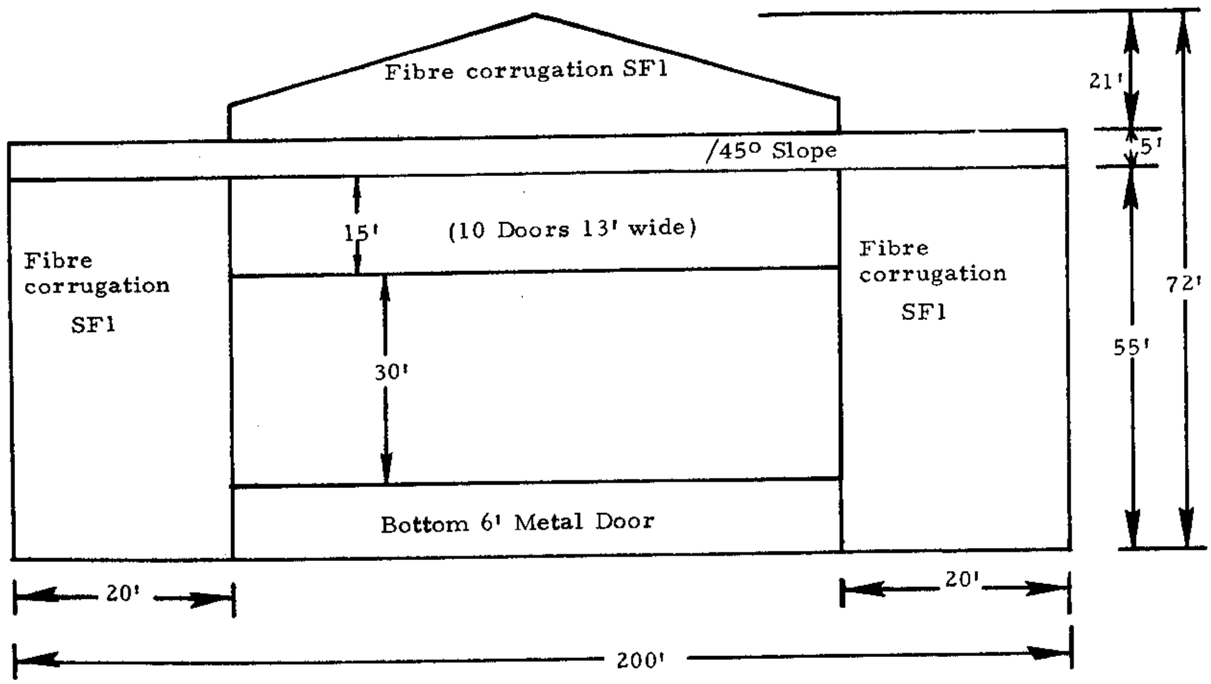

Note on Building 1042, 23' tall - 230 feet long, concrete

Parked DC-6's are more obstruction to 9L than building.

Fig. A37. MIA, hangar building 63.

ATC-58 (A38)

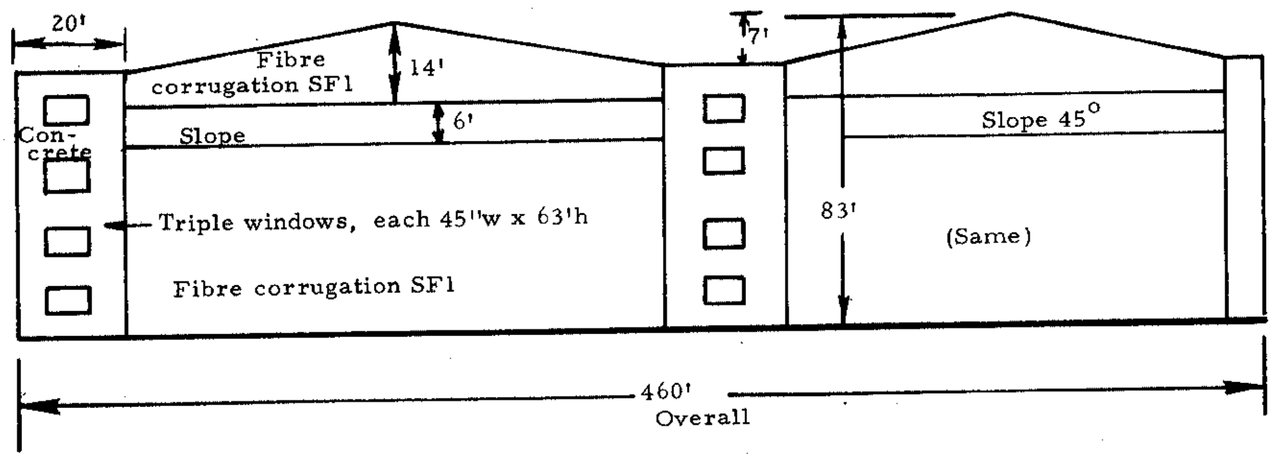

Fig. A38. MIA, hangar buildings 60-60A.

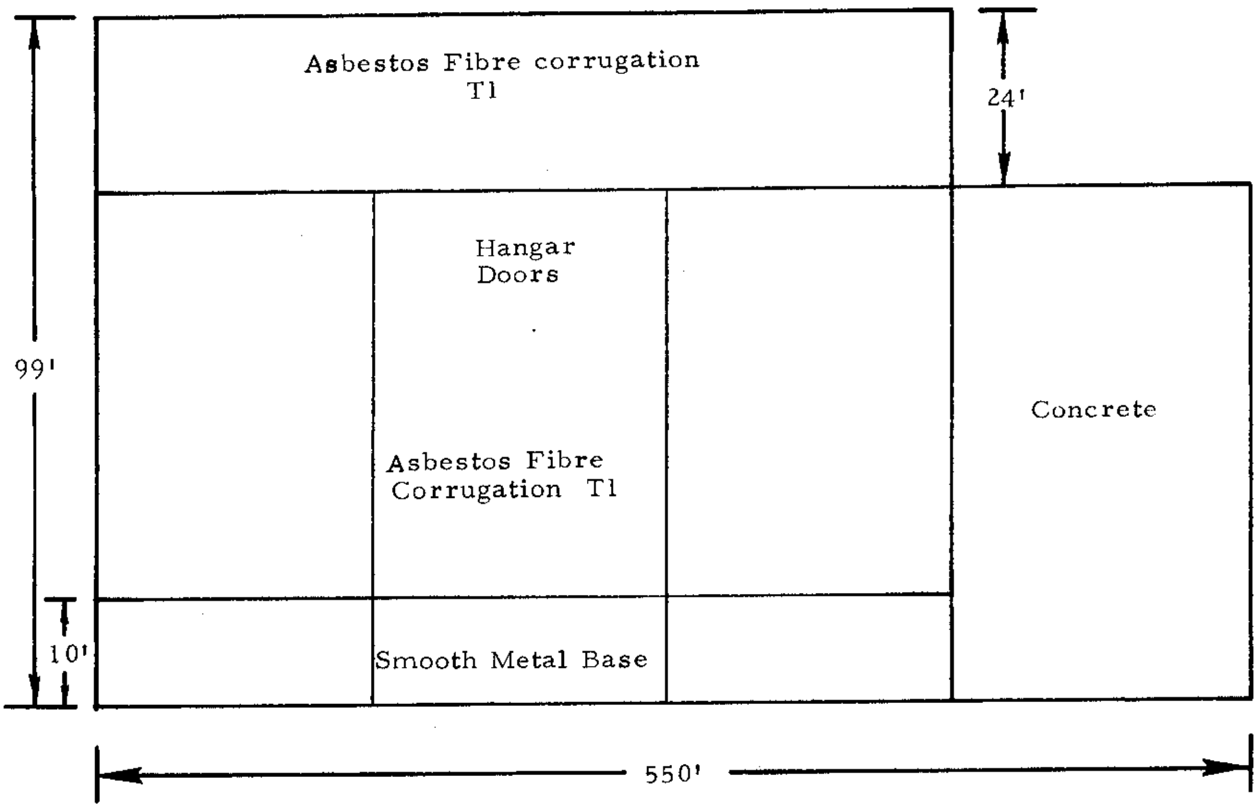

Fig. A39. MIA, building 25-24 (hangar).

ATC-58 (A40)

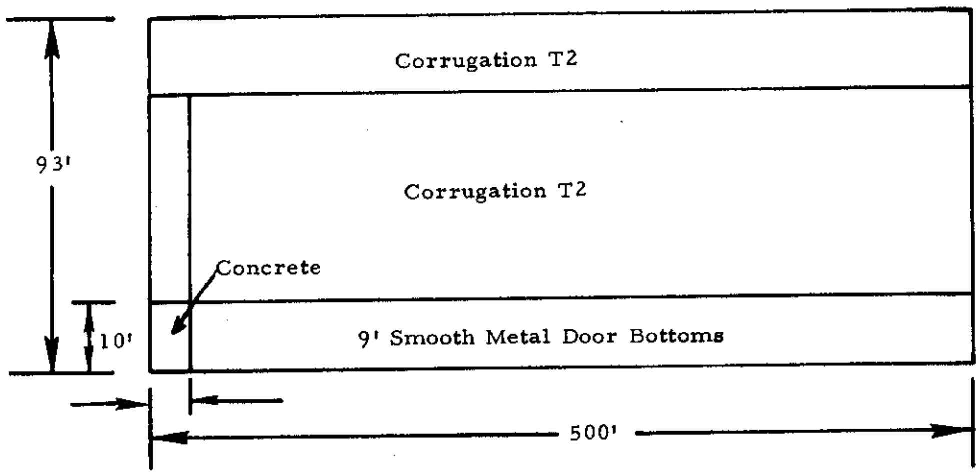

Fig. A40. MIA, building 22 (hangar).

ATC-58 (A41)

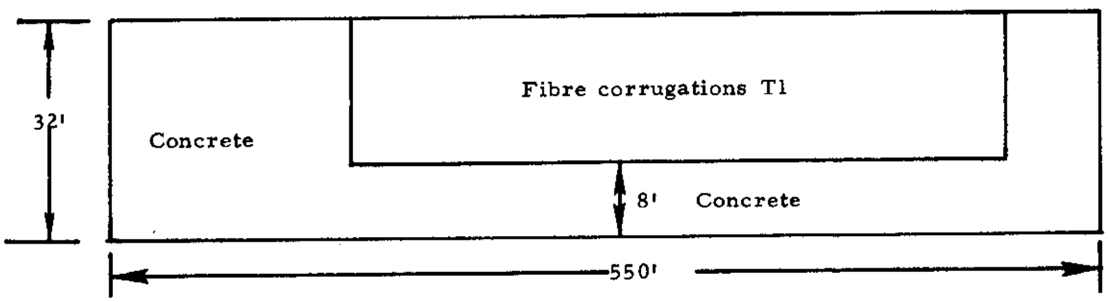

Note on Buildings 5 and 16

Building 5 is shadowed but Building 16 at 146' high may be a factor.

Building 16 width ≈ 60'

Fig. A41. MIA, building 21A.

ATC-58 (A42)

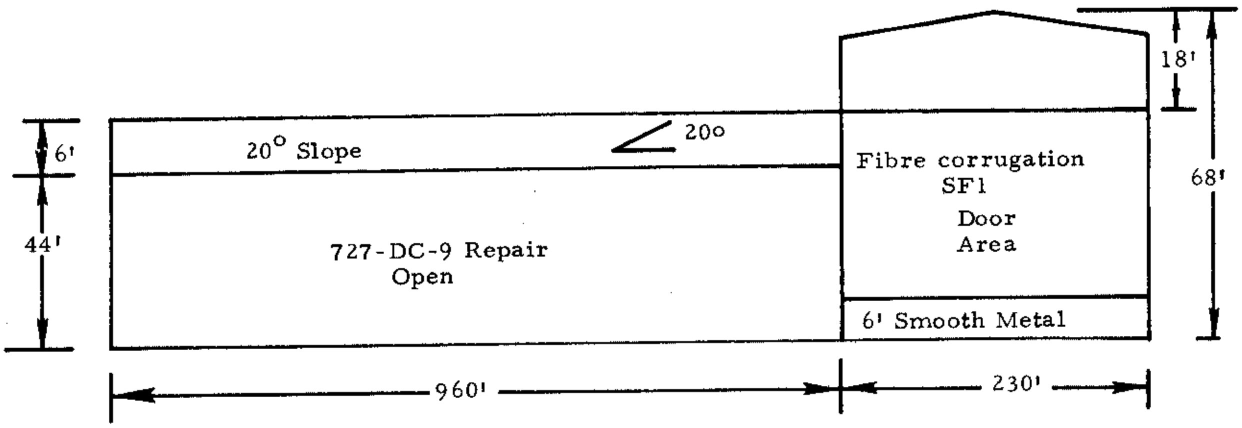

Note: Building 3035 - No problem

Building 3095, 90' to roof DC-10 Hangar

Satellite Building (51' High) concrete facing

Fig. A42. MIA, building 20 (hangar).

ATC-58 (A43)

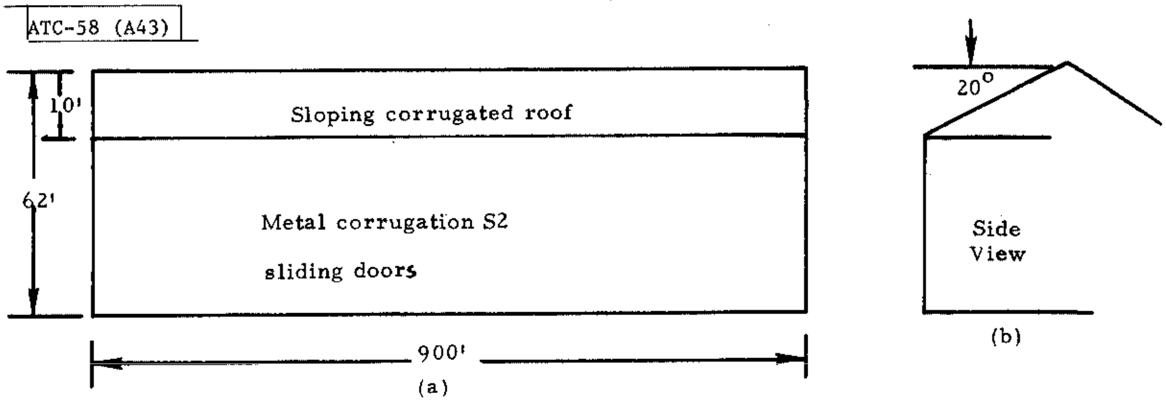

Fig. A43. MIA, building 2169 (hangar).

ATC-58 (A44)

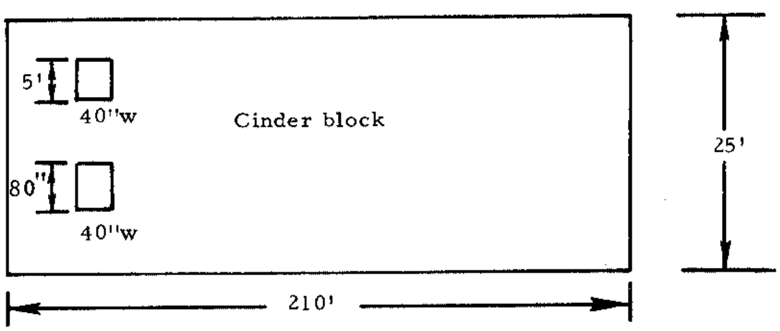

Fig. A44. MIA building 2147.

ATC-58 (A45)

Note: Building 2094 same as 2147 - Cinder block 20' high.

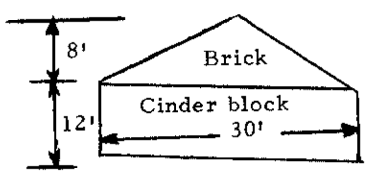

Fig. A45. MIA, building 2090, brick and cinder block.

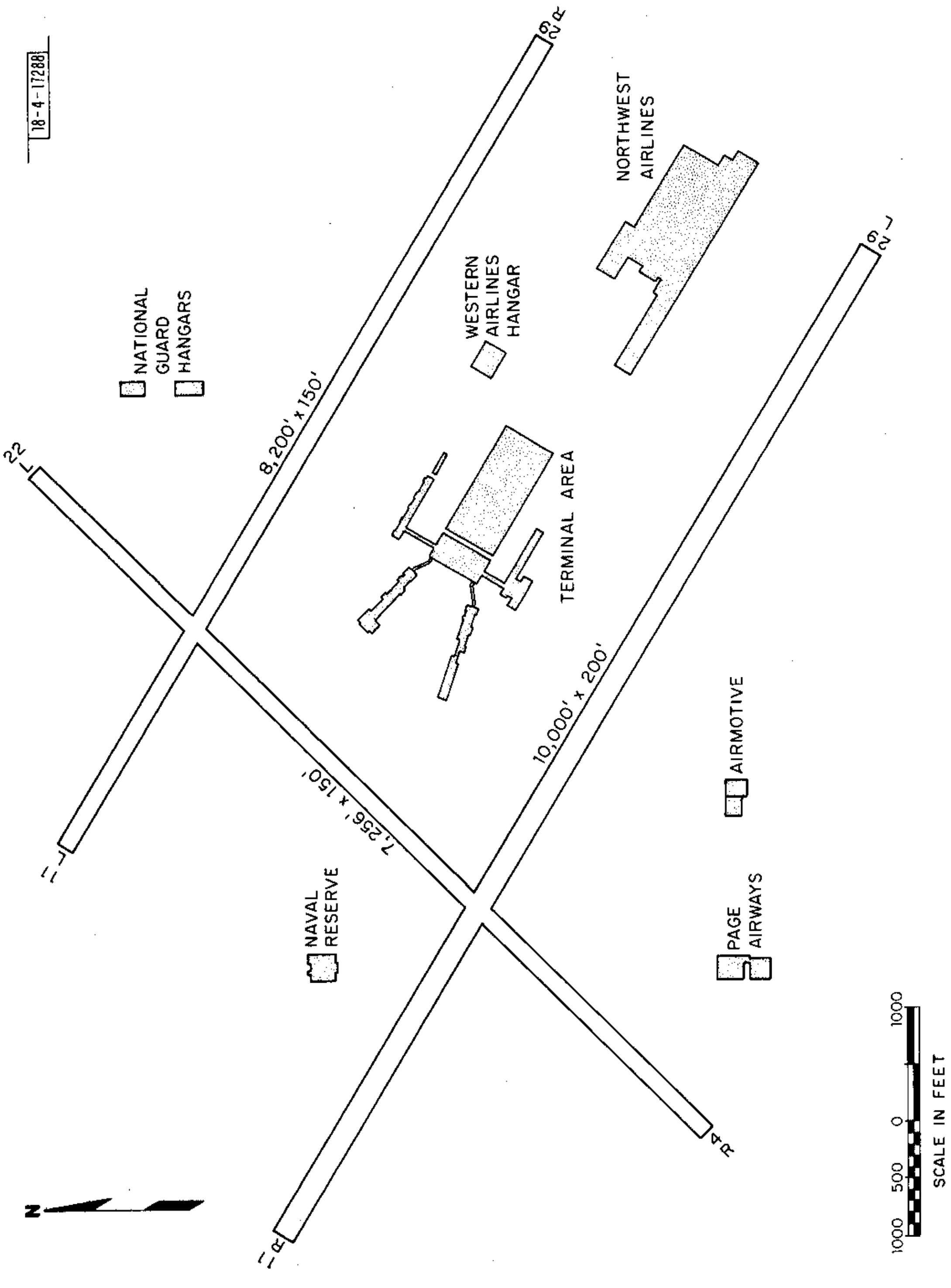

Fig. A46. Minneapolis-St. Paul (Wold-Chamberlain Field) (MSP).

ATC-58 (A47)

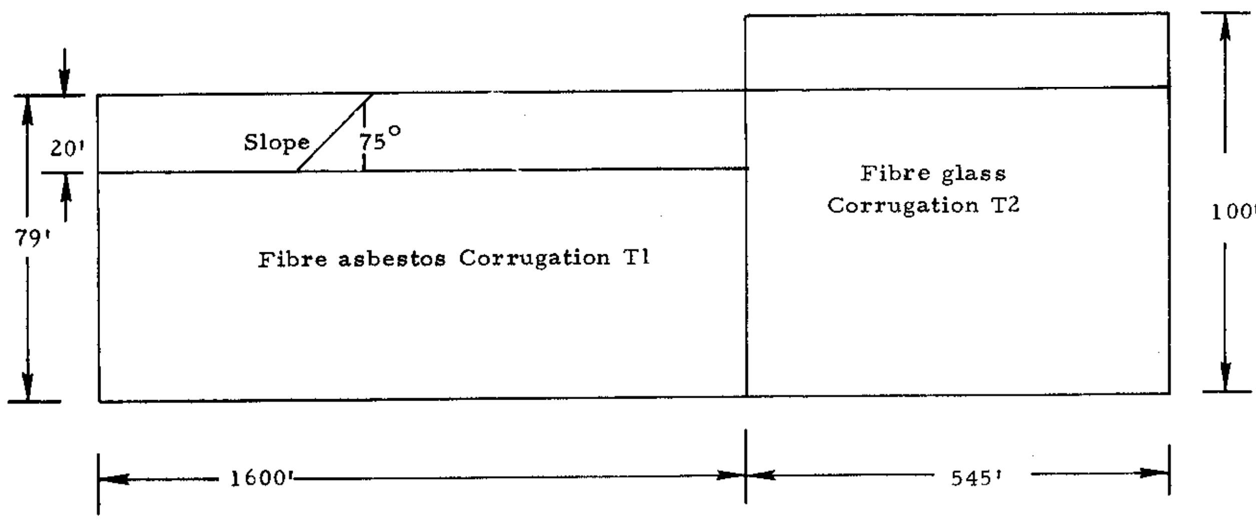

Fig. A47. MSP, Northwest Orient hangar.

ATC-58 (A48)

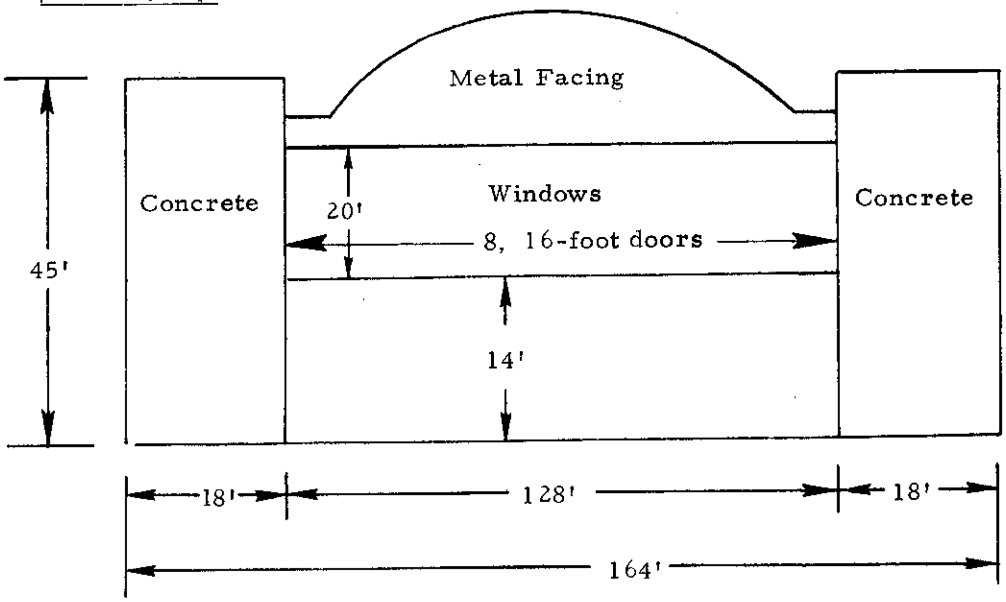

Fig. A48. MSP, Naval Reserve hangar.

ATC-58(A49)

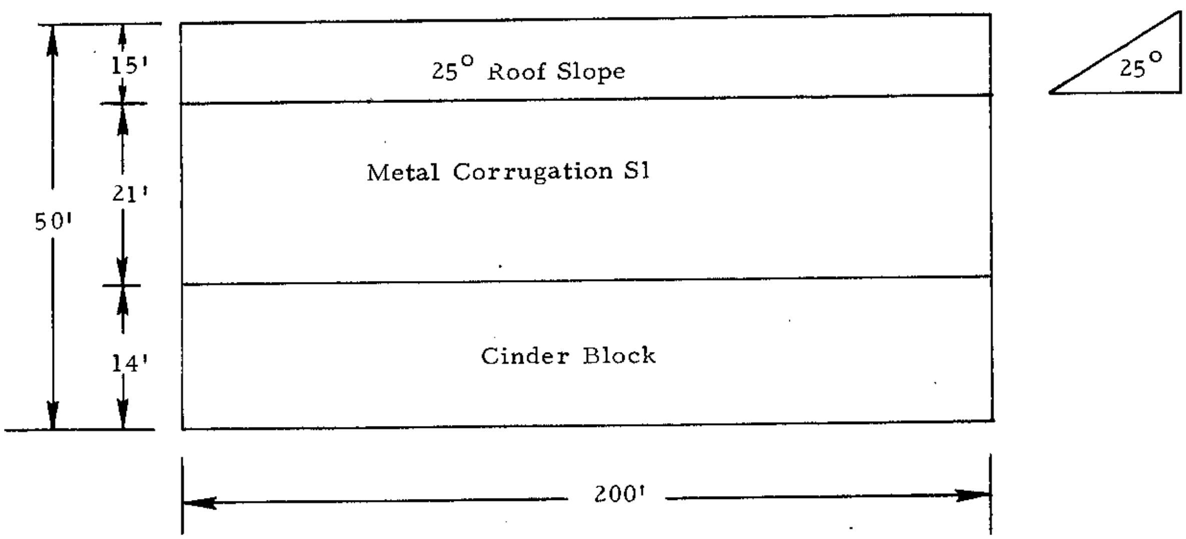

Fig. A49. MSP, Page Airways.

ATC-58(A50)

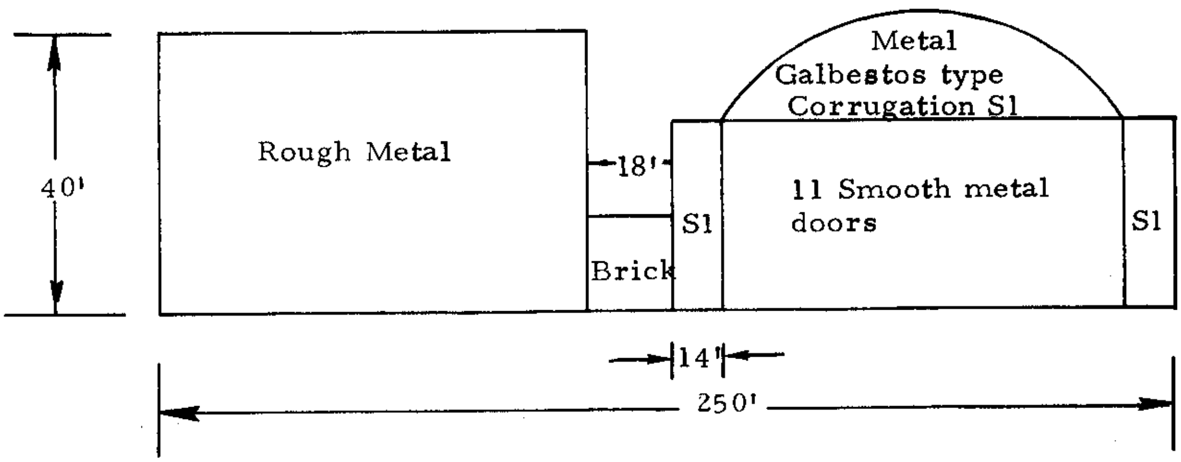

Fig. A50. MSP, Airmotive.

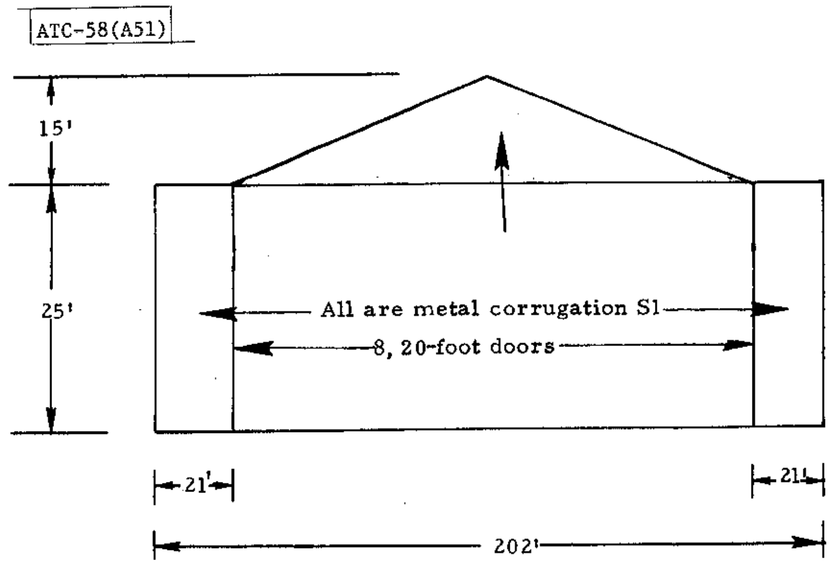

Fig. A51. MSP, 2 National Guard hangars.

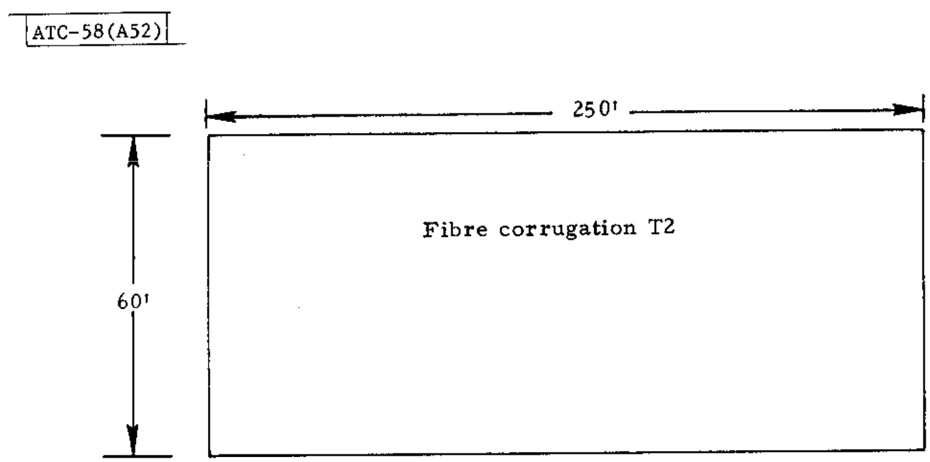

Fig. A52. MSP, Western Airways hangar.

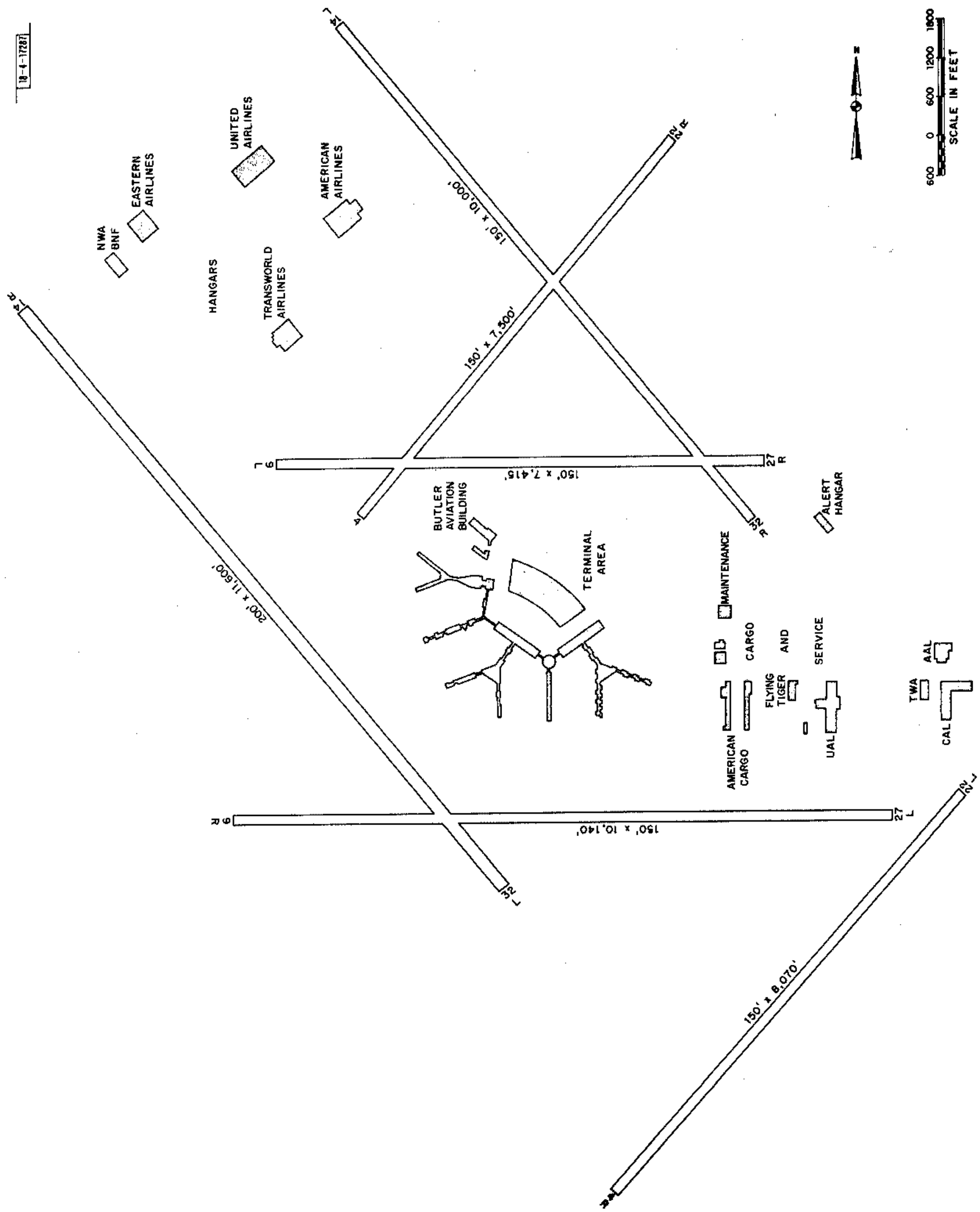

Fig. A53. O'Hare International Airport (ORD).

ATC-58(A54)

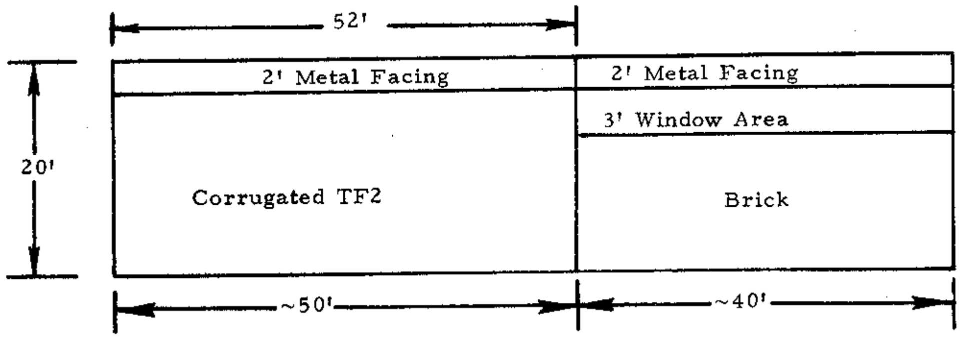

Fig. A54. ORD, American Cargo.

Note: Pan American Cargo building same as American but inverse left to right.

ATC-58(A55)

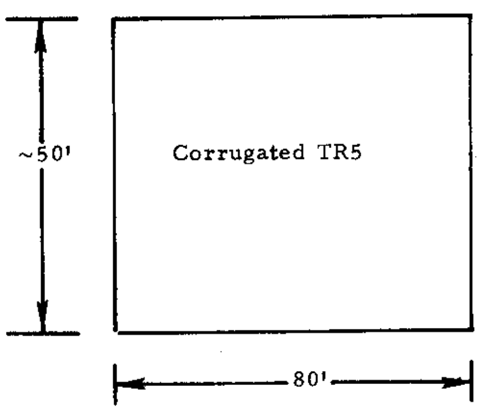

Fig. A55. ORD, Flying Tiger building.

ATC-58(A56)

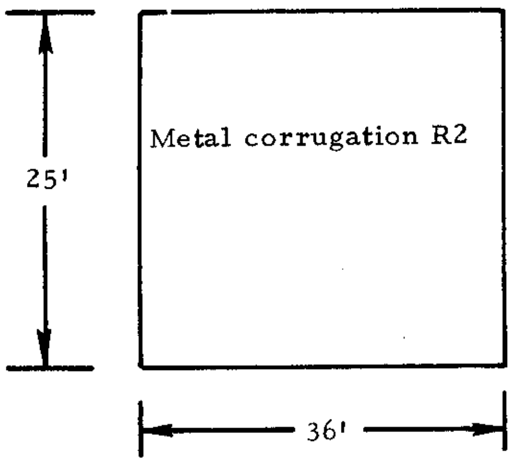

Fig. A56. ORD, Workshop.

ATC-58(A57)

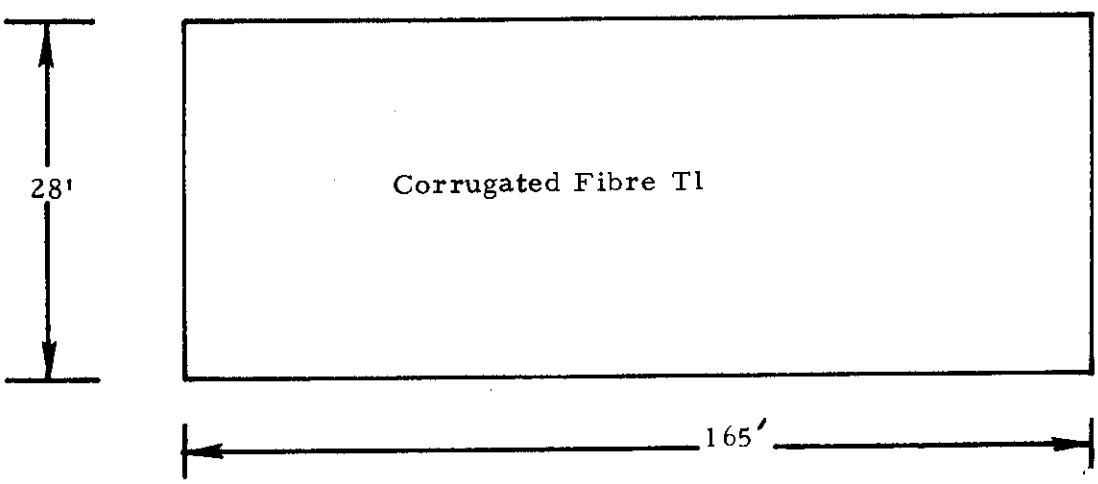

Fig. A57. ORD, United Airlines (cargo).

ATC-58(A58)

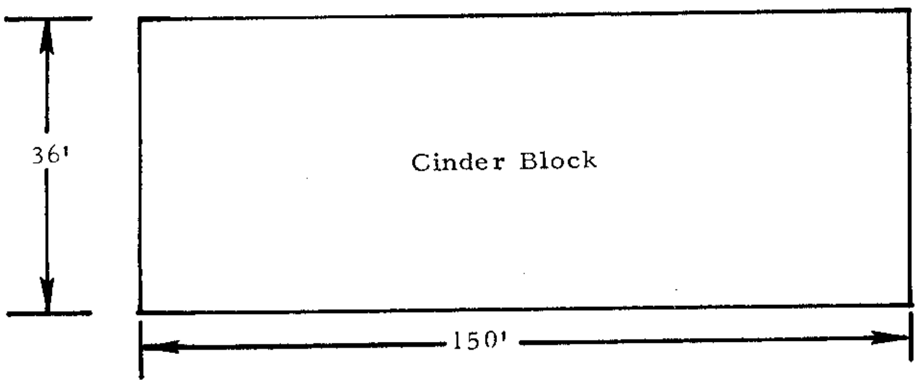

Fig. 58. ORD, Continental Cargo building.

ATC-58(A59)

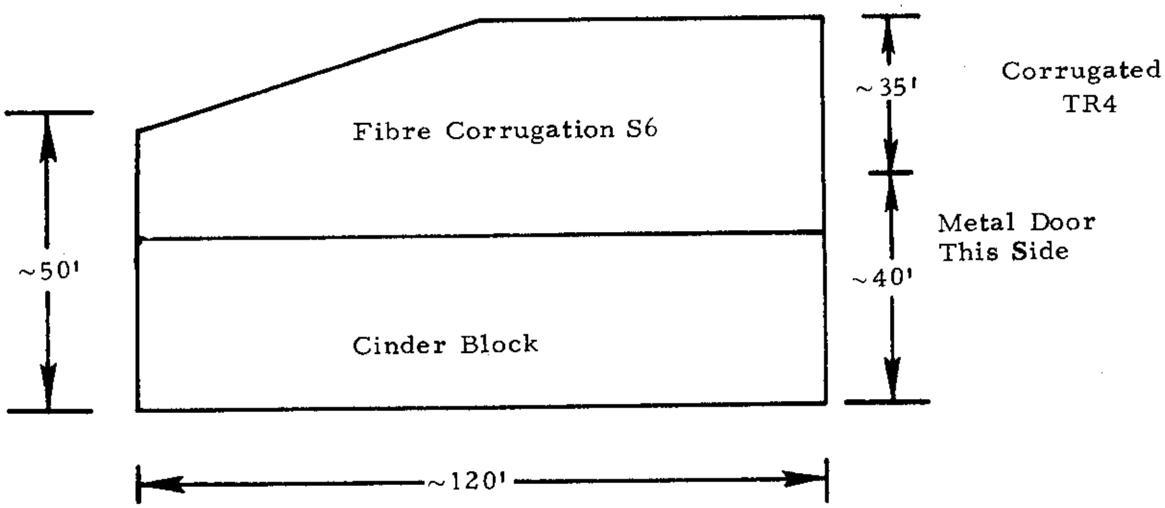

Fig. 59. ORD, Butler Aviation building.

ATC-58(A60)

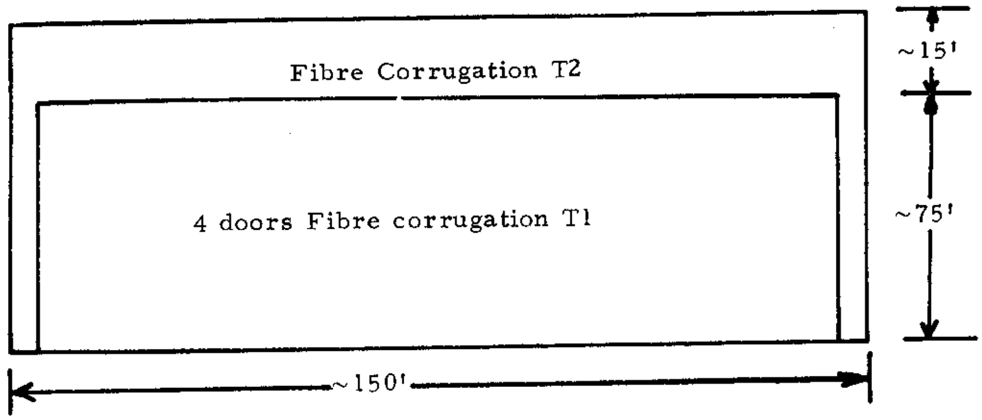

Fig. A60. ORD, Northwest hangar.

ATC-58(A61)

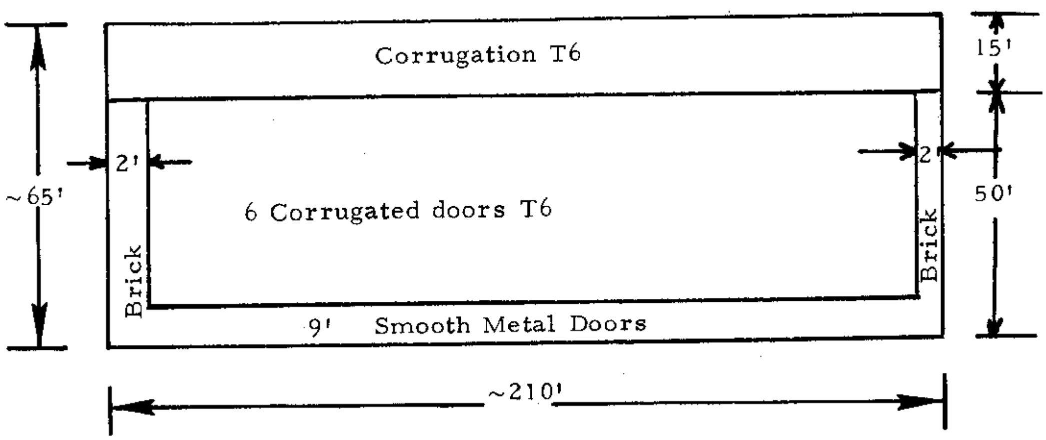

Fig. A61. ORD, Eastern hangar.

ATC-58(A62)

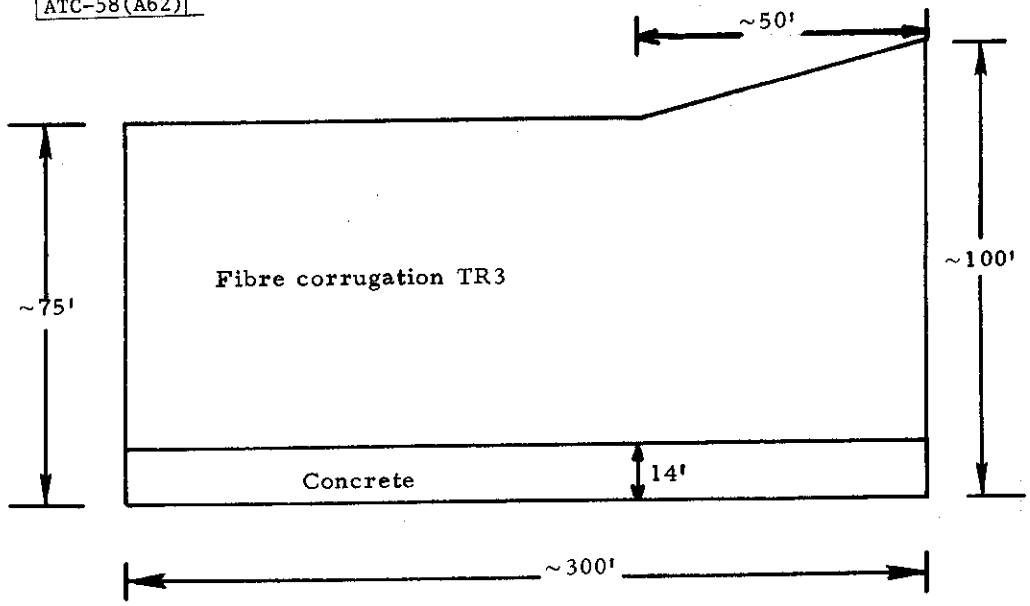

Fig. A62. ORD, United hangar.

ATC-58(A63)

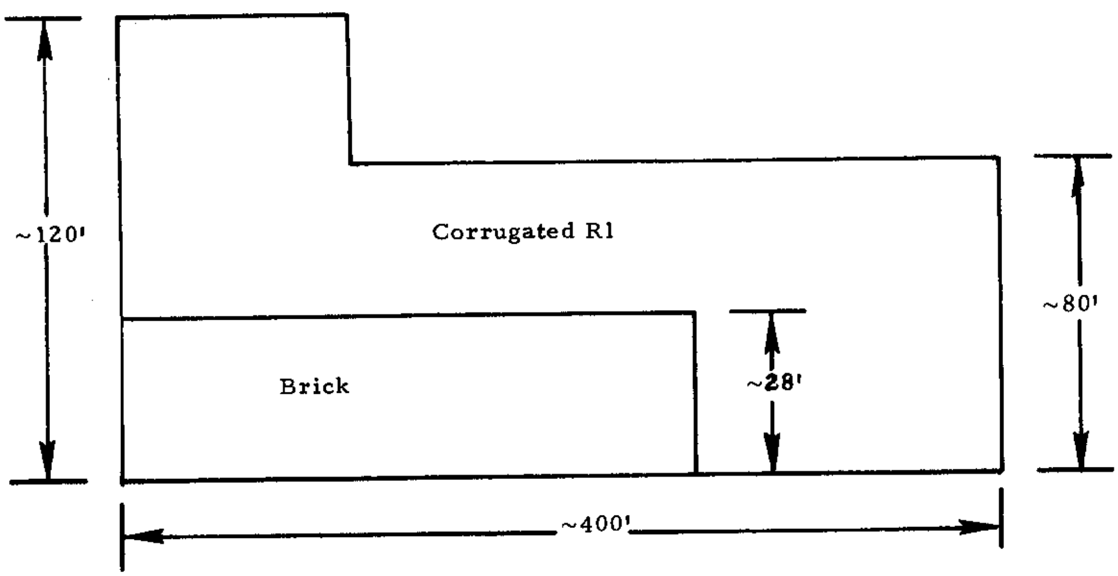

Fig. A63. ORD, American hangar.

ATC-58(A64)

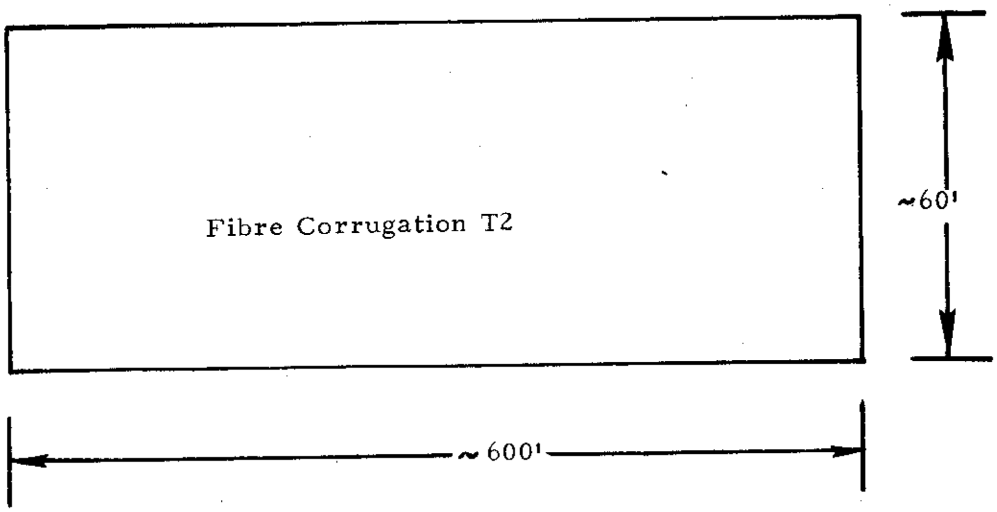

Fig. A64. ORD, TWA hangar.

ATC-58(A65)

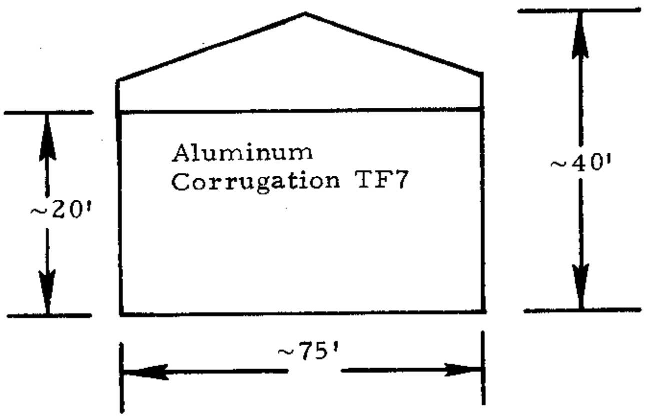

Fig. A65. ORD, Alert hangar (one of four).

ATC-58(A66)

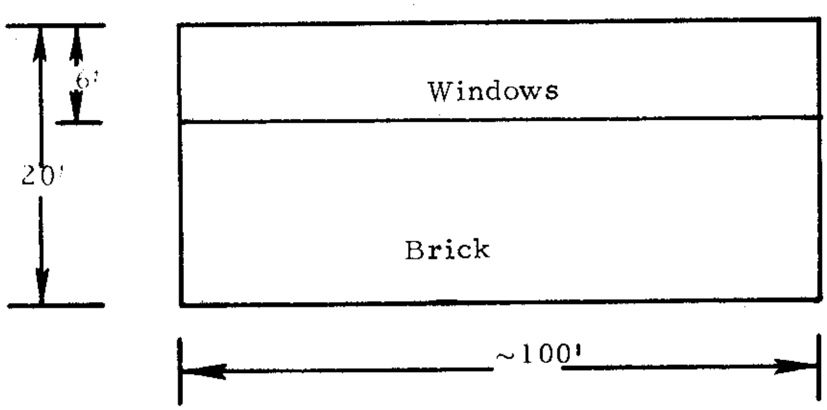

Fig. A66. ORD, Maintenance building.

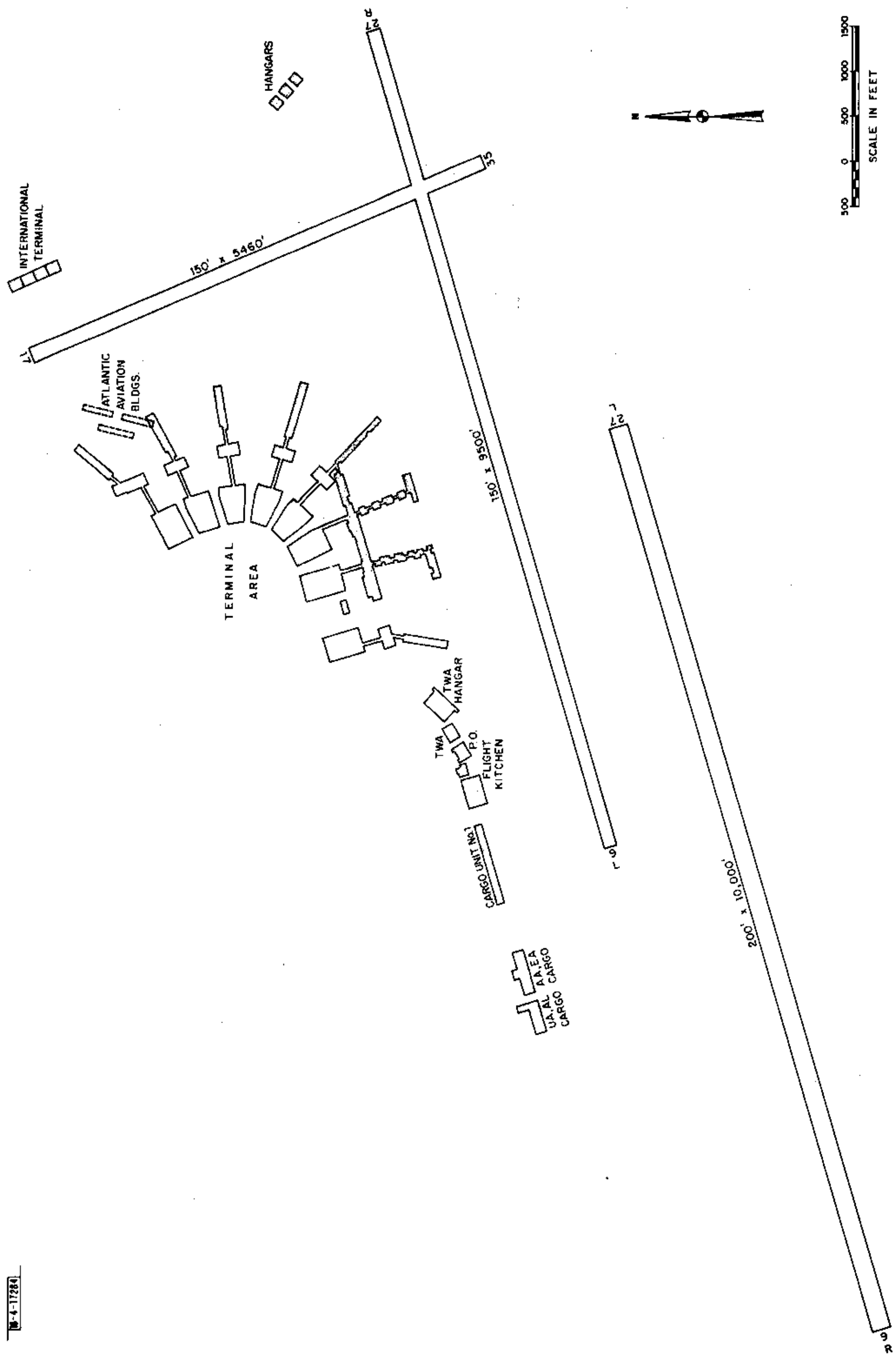

Fig. A67. Philadelphia International Airport (PHL).

ATC-58(A68)

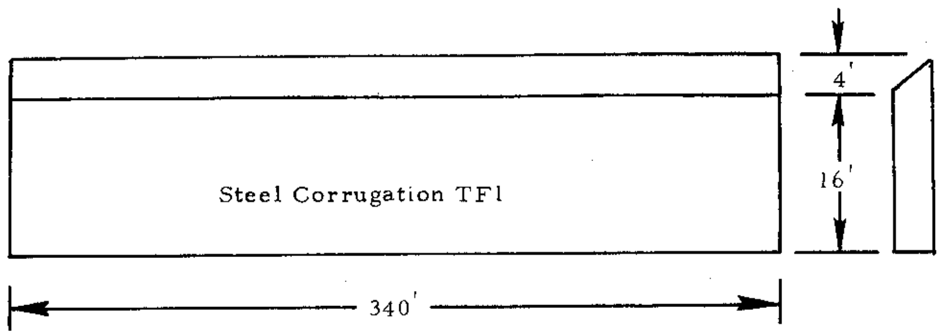

Fig. A68. PHL, Atlantic Aviation buildings - 2 required.

ATC-58(A69)

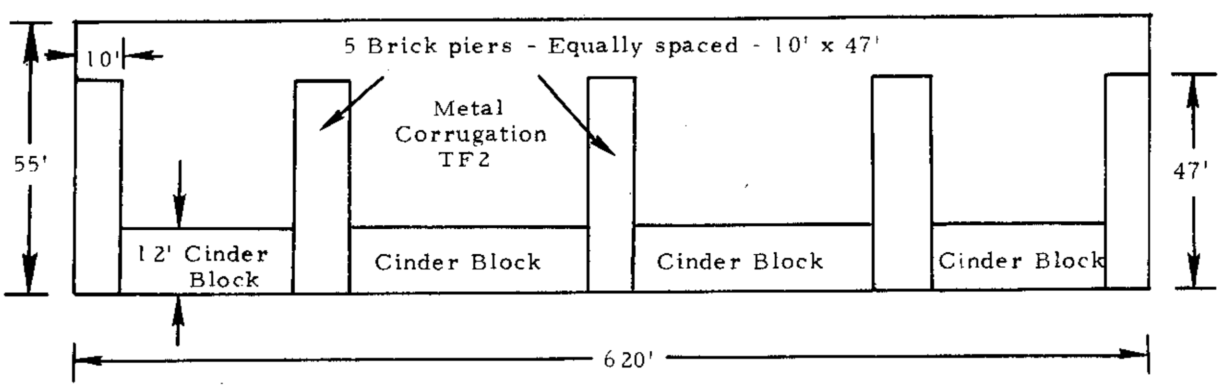

Fig. A69. PHL, International Terminal building.

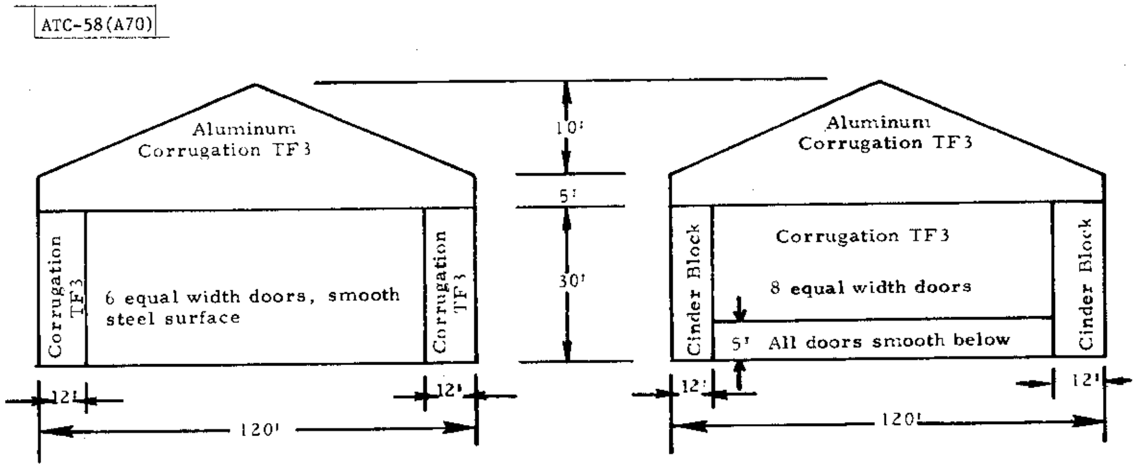

Fig. A70. PHL, 3 hangars; one as on left, two as in right.

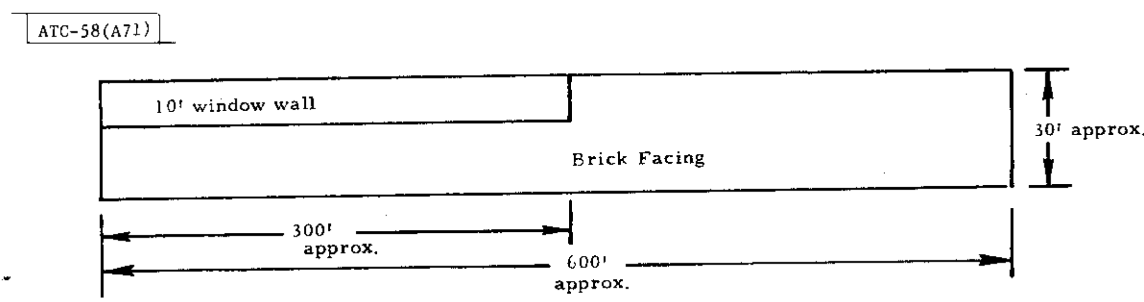

Fig. A71. PHL, warehouse building across highway-behind hangars.

ATC-58(A72)

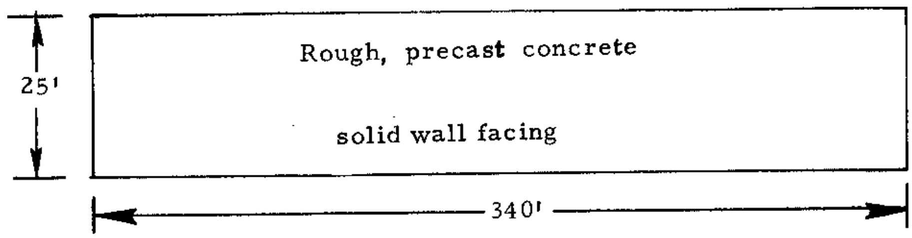

Fig. A72. PHL, United Fruit kitchen.

ATC-58(A73)

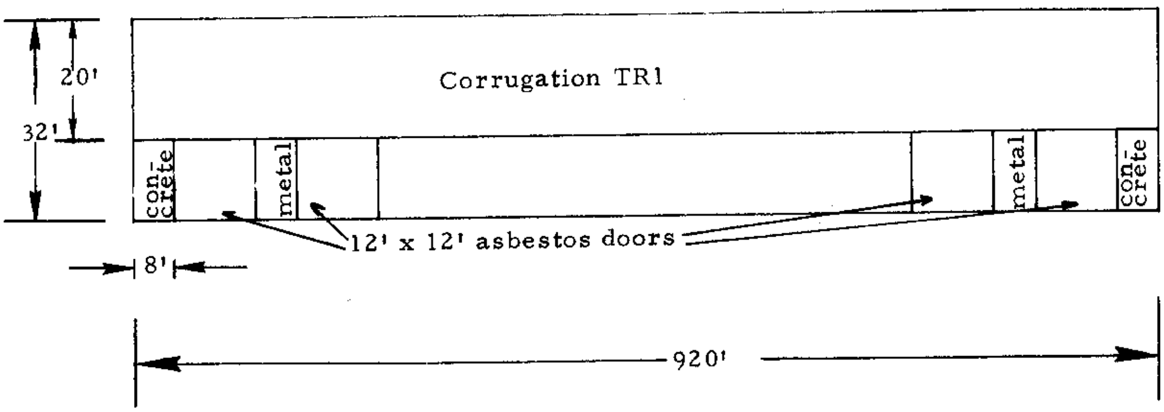

Fig. A73. PHL, cargo unit number 1.

ATC-58(A74)

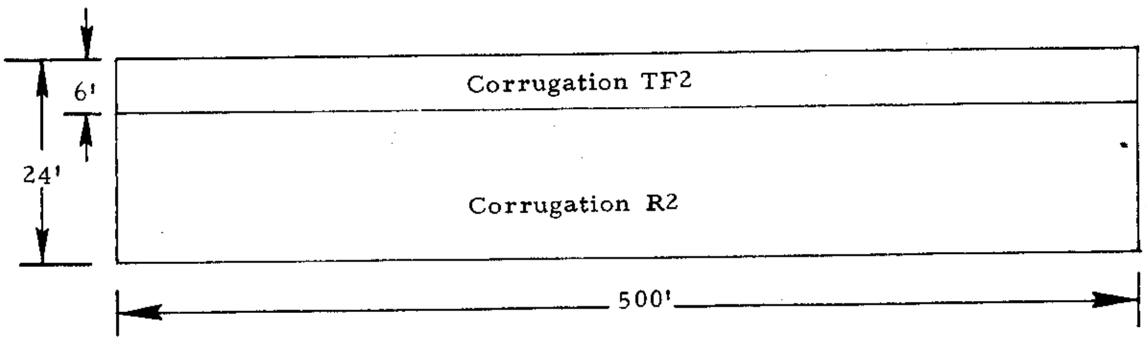

Fig. A74. PHL, American/Eastern freight building.

ATC-58(A75)

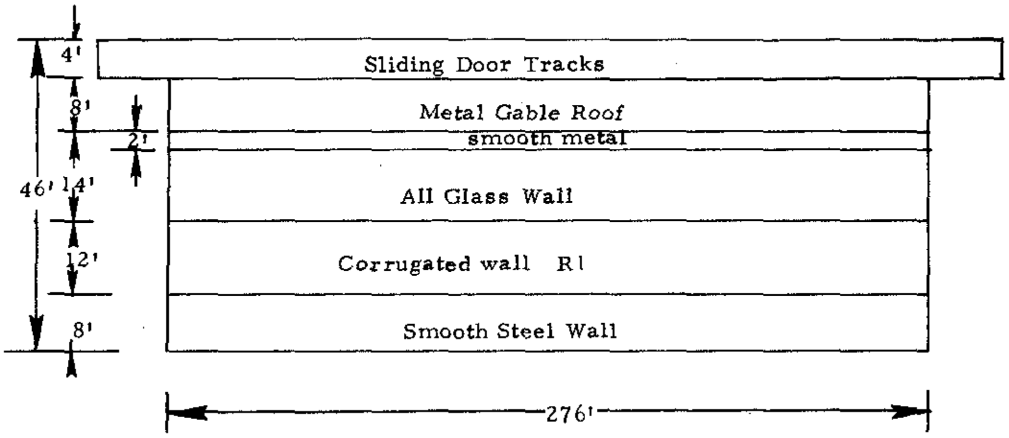

Fig. A75. PHL, TWA hangars.

ATC-58(A76)

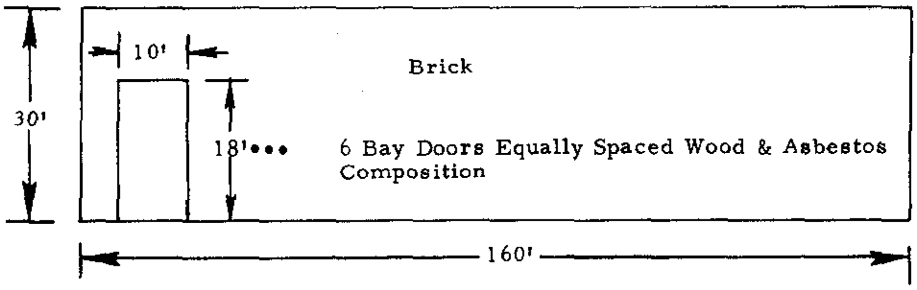

Fig. A76. PHL, TWA freight building.

ATC-58(A77)

Note: All kinds of vehicles & carts in front of P.O. building

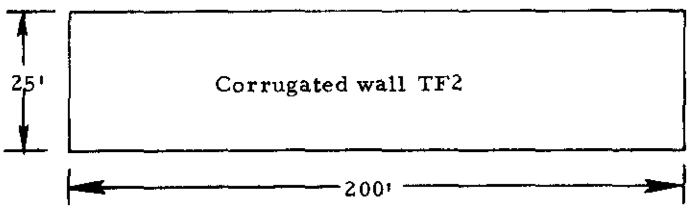

Fig. A77. PHL, Post Office.

ATC-58(A78)

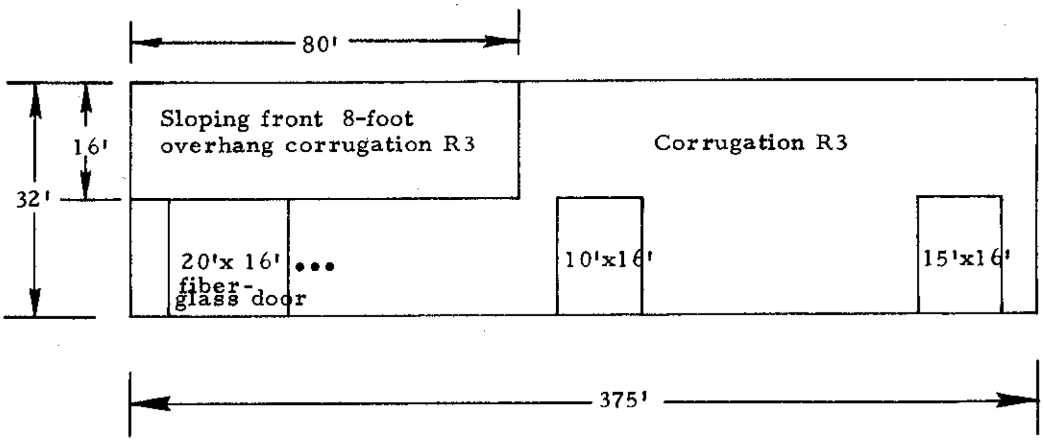

Fig. A78. PHL, United Air Freight building.

ATC-58(A79)

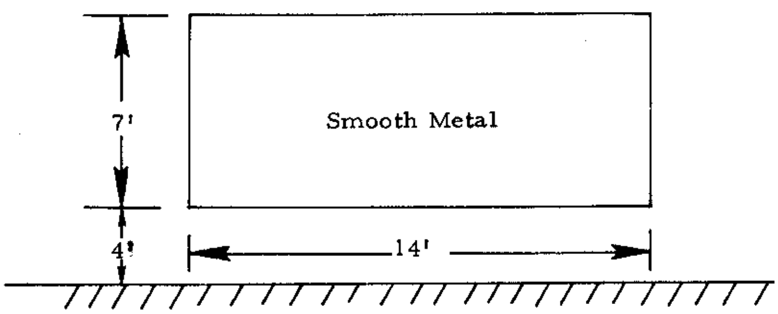

Fig. A79. PHL, Marriot Food Truck Side.

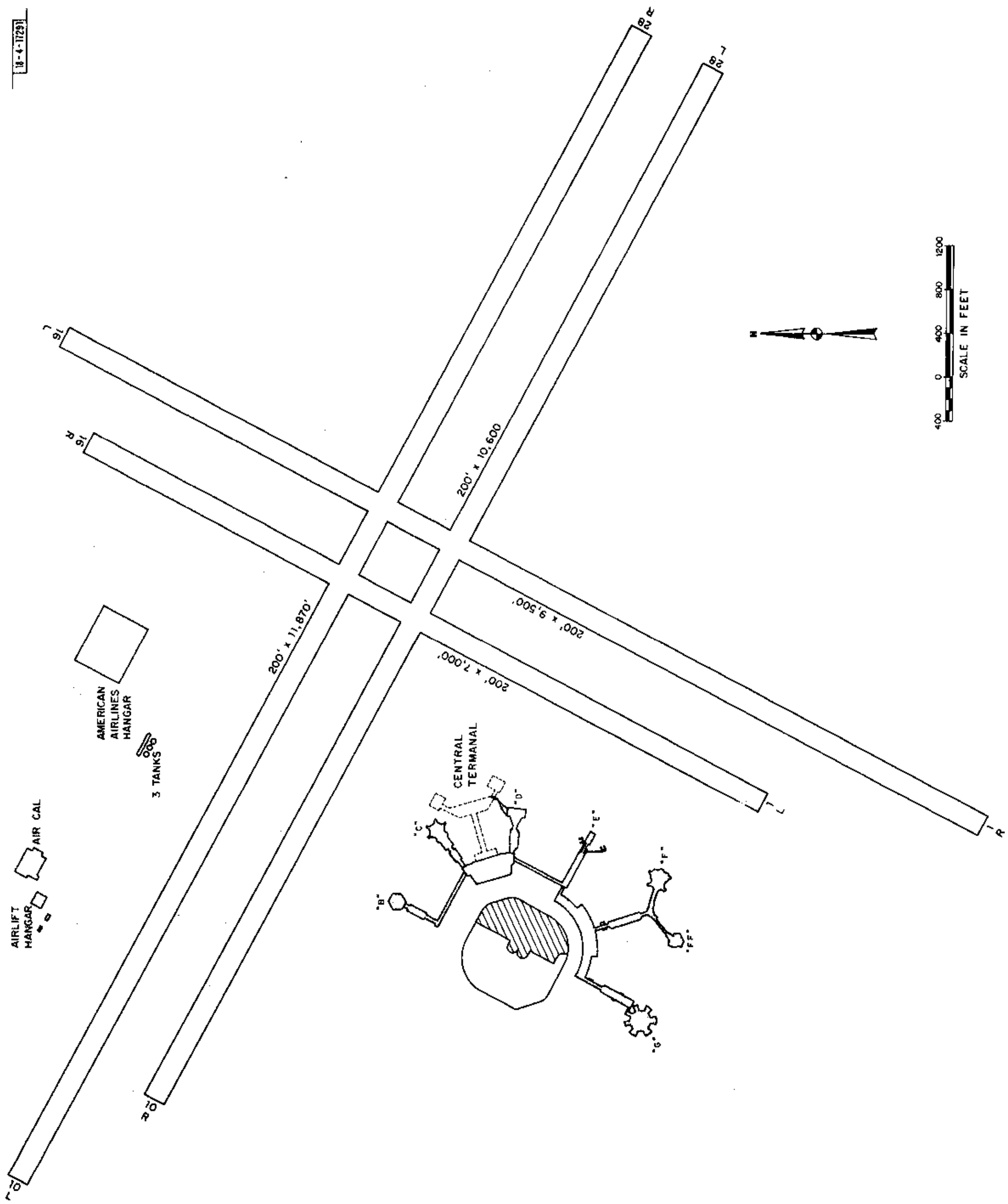

Fig. A80. San Francisco International Airport (SFO).

ATC-58(A81)

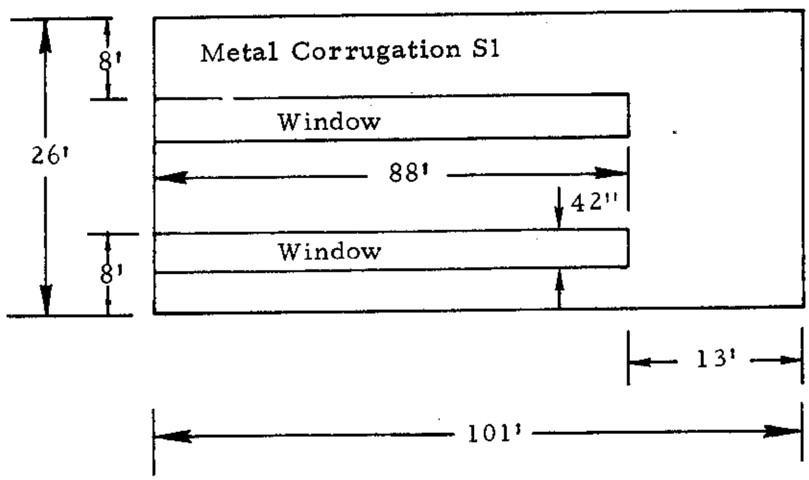

Fig. A81. SFO, Air Lift hangar.

ATC-58(A82)

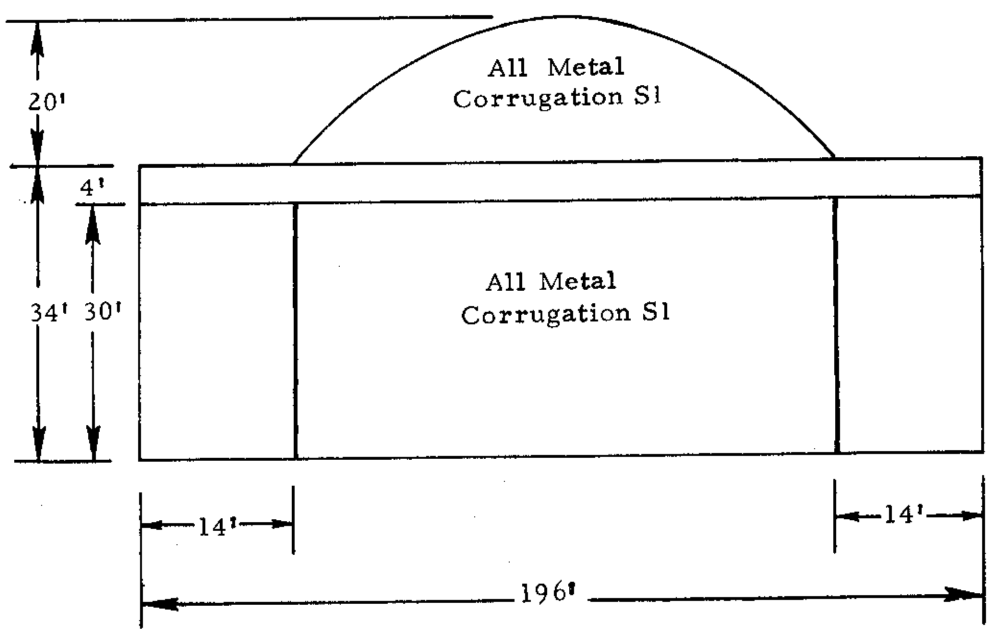

Fig. A82. SFO, Air Cal hangar.

ATC-58(A83)

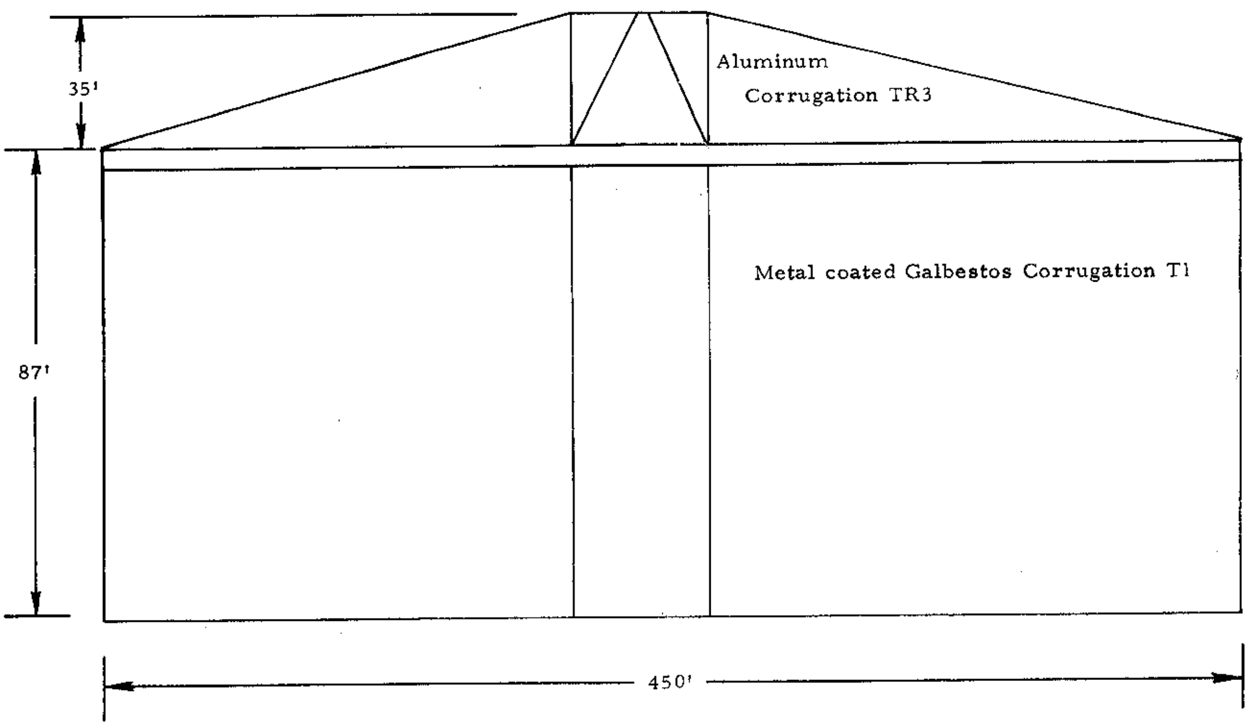

Fig. A83. SFO, American Airlines hangar.

ATC-58(A84)

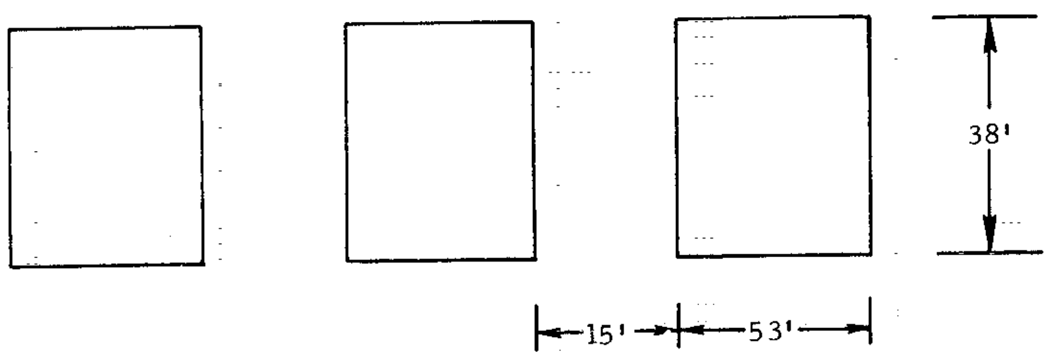

Fig. A84. SFO, 3 water tanks.

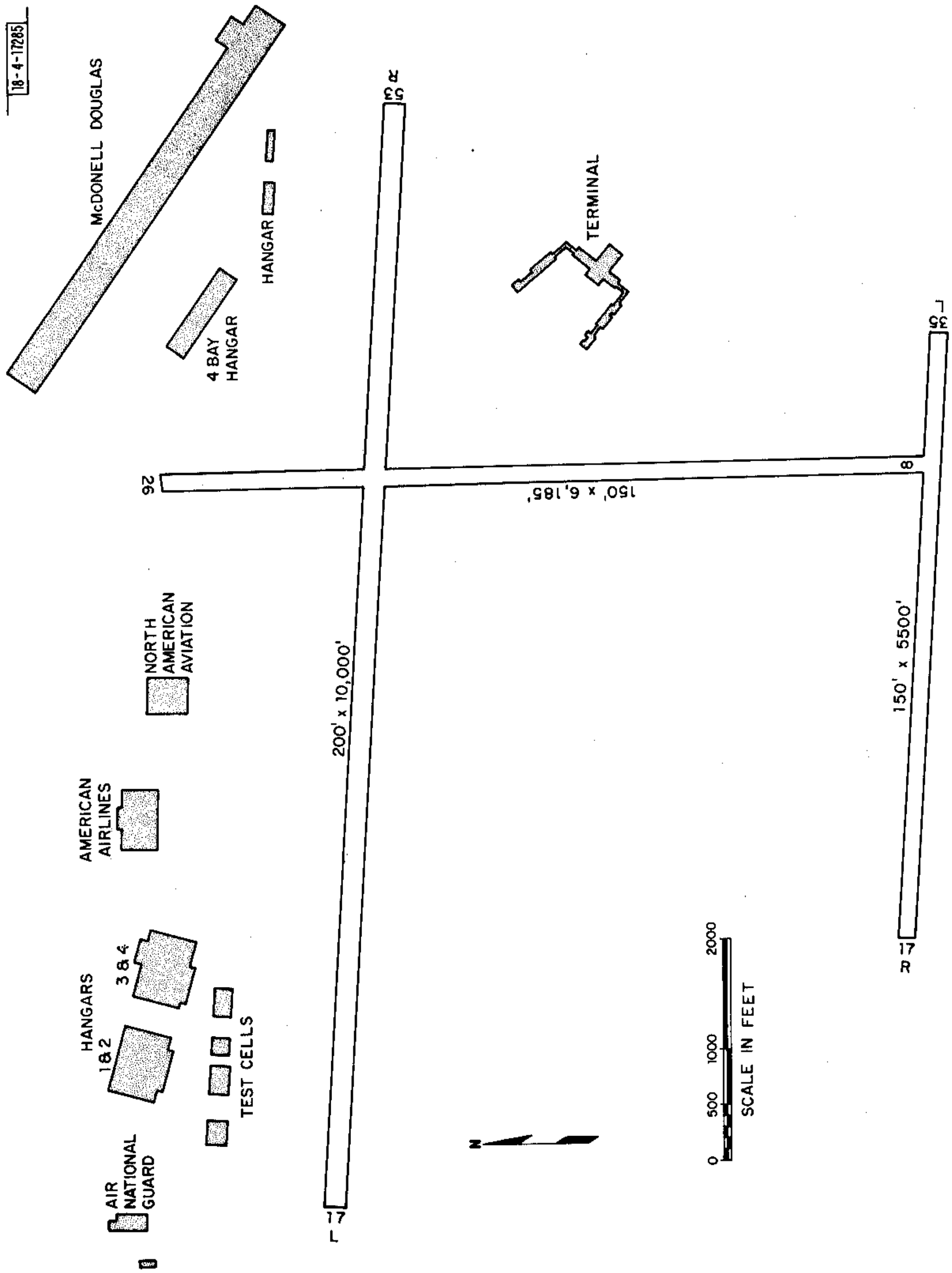

Fig. A85. Tulsa International Airport (TUL).

ATC-58(A86)

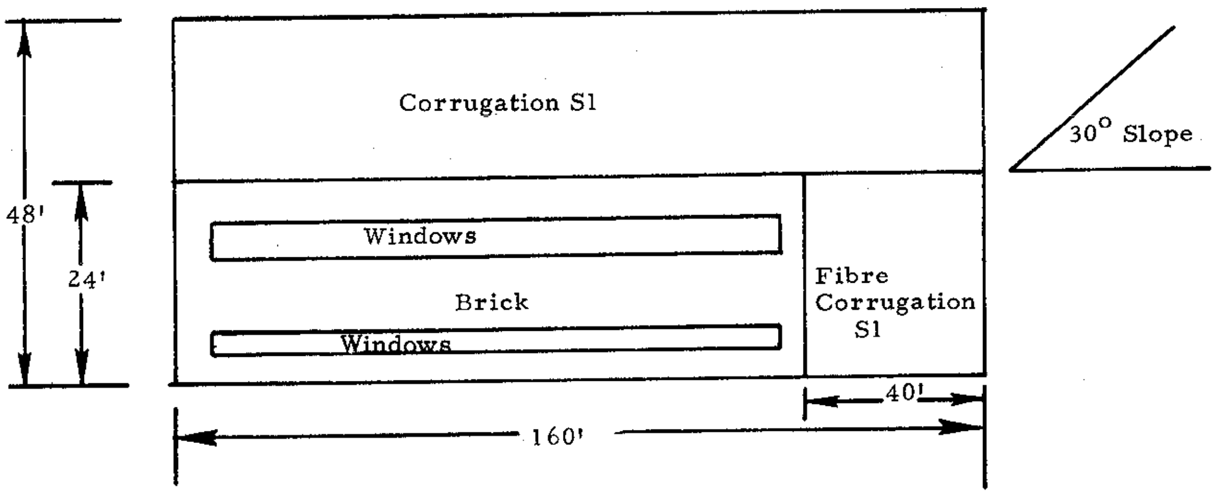

Fig. A86. TUL, National Guard building.

ATC-58(A87)

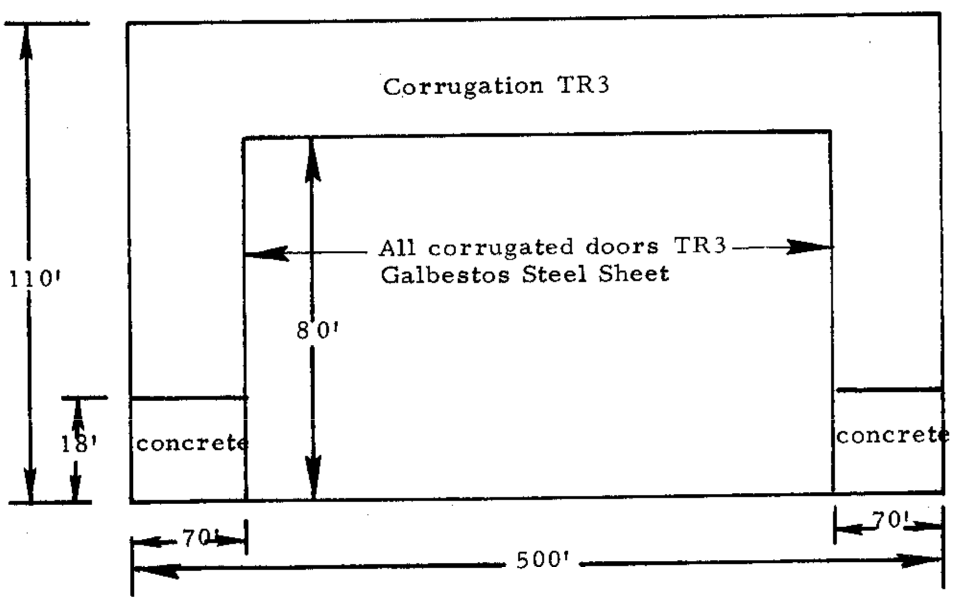

Fig. A87. TUL, American Airline hangar 5,

ATC-58(A88)

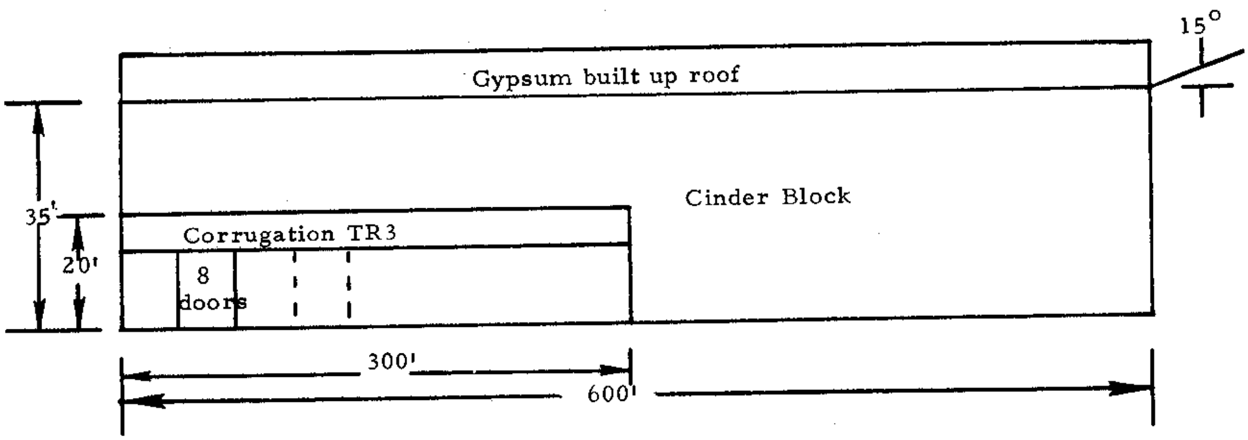

Fig. A88. TUL, American Airlines hangar 3 (west side).

ATC-58(A89)

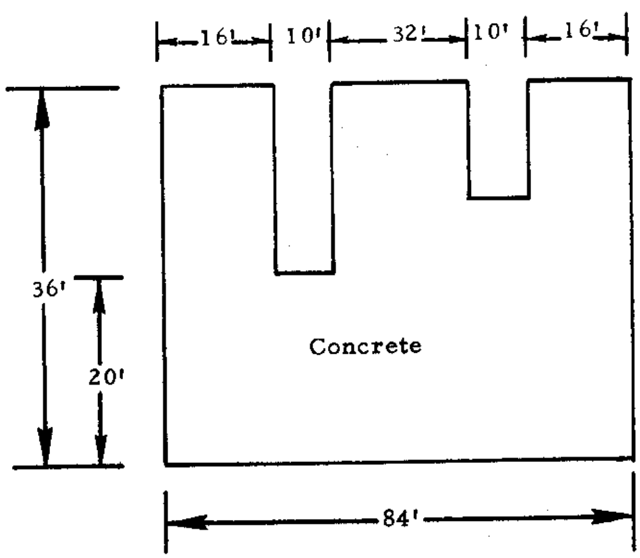

Fig. A89. TUL, concrete engine test cell 1, 2, 3.

ATC-58(A90)

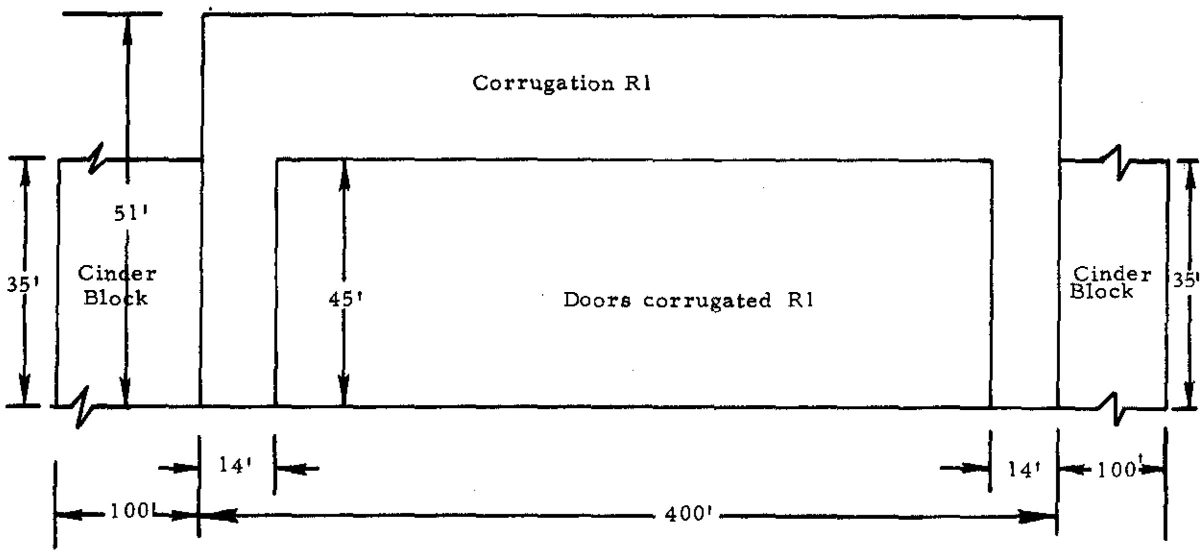

Fig. A90. TUL, American Airline hangars 1 and 2 west side.

ATC-58(A91)

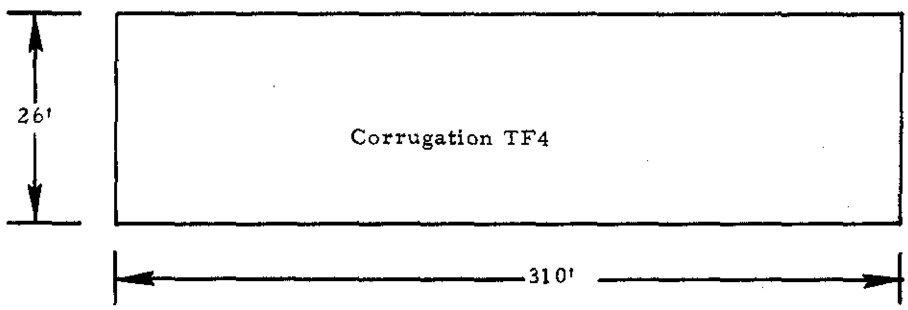

Fig. A91. TUL, North American Aviation.

ATC-58(A92)

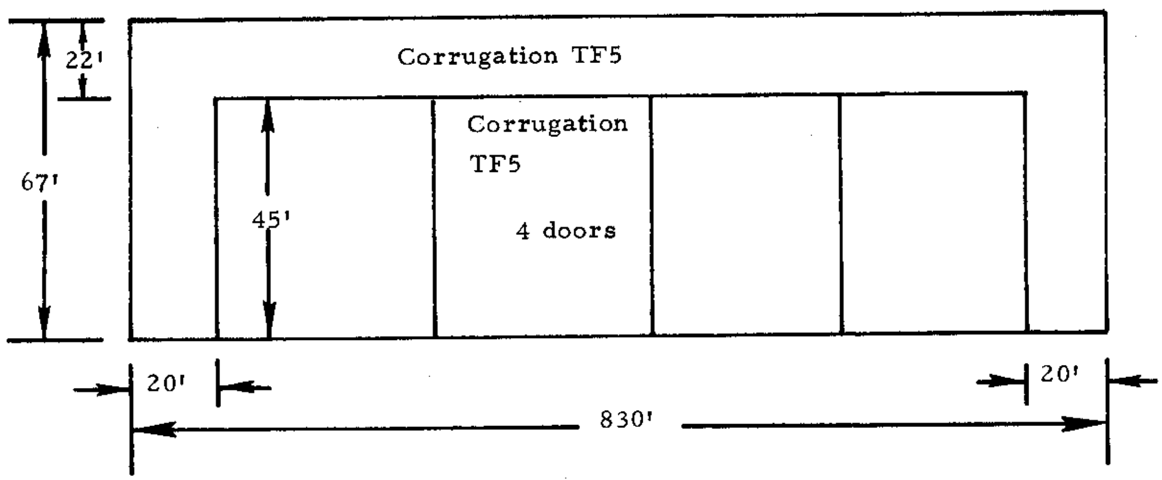

Fig. A92. TUL, 4-bay hangar.

ATC-58(A93)

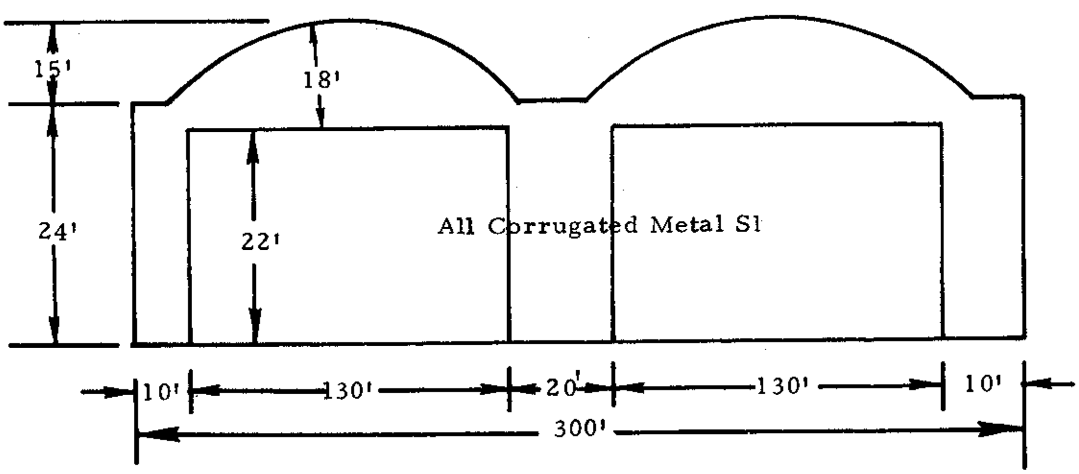

Fig. A93. TUL, Quonset roof hangar.

ATC-58(A94)

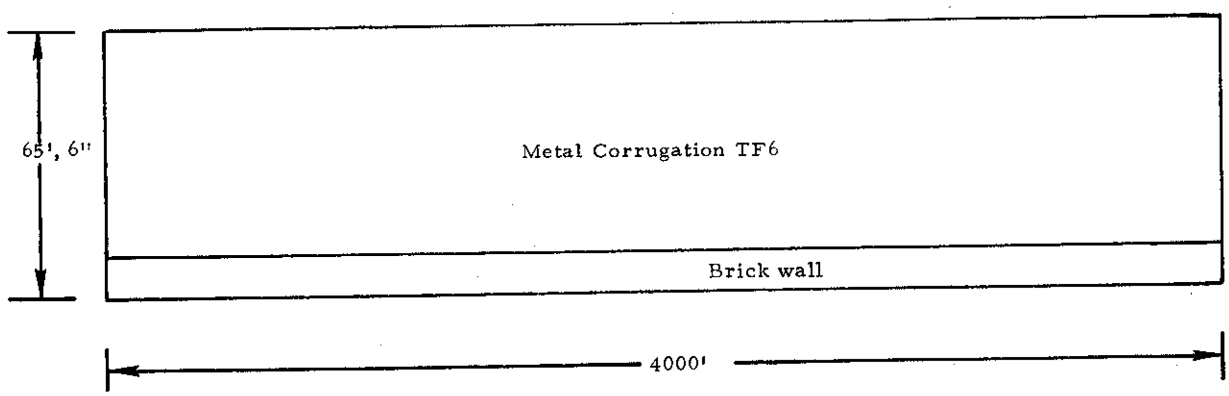

Fig. A94. TUL, large McDonnell Douglas building.

Appendix B

SQUARES OF PEAK REFLECTION COEFFICIENTS FOR SELECTED CORRUGATED SURFACES

A periodically regular surface, such as a vertical corrugation, produces a multimodal reflection which is dependent on the incident angle θ_1. In Fig. 1, the multimodal reflections are denoted by an index k and the reflection angle denoted by $\theta_{2,k}$ where

$$\theta_{2,0} = \theta_1$$

The equation specifying the angles $\theta_{2,k}$ is

$$\sin \theta_{2,k} = \sin \theta_1 + k \frac{\lambda}{d} , \quad \text{for } k = 0, \ \pm 1, \pm 2, \ldots \tag{B1}$$

where d is the period and λ the wavelength of the incident wave, provided that the right hand side of (B1) has magnitude less than or equal to one. This requirement limits the acceptable range on values of k. Let us define $\rho(\theta_1, \theta_2)$ as the reflection coefficient at reflection angle θ_2 when the angle of incidence is θ_1. An example of $|\rho(\theta_1, \theta_2)|$ for $\theta_1 = 45°$ is shown in Fig. 2. We define $P_k(\theta_1)$ as

$$P_k(\theta_1) = |\rho(\theta_1, \theta_{2,k})|^2 \tag{B2}$$

The values of $P_k(\theta_1)$ vs θ_1 are presented here for the subcategories S1, S2, and R1 for the case in which the corrugated surfaces are perfectly conducted. Analytically determined, they were calculated by J. Mink of ECOM. They are plotted as a function of incidence angle for each mode over the range for which the mode exists. They are presented for a carrier at 5 GHz (λ = 2.362") for vertical and horizontal polarization.

Corrugation	Pages
S1	73-75
S2	76-78
R1	79-81

ATC-58(B1)

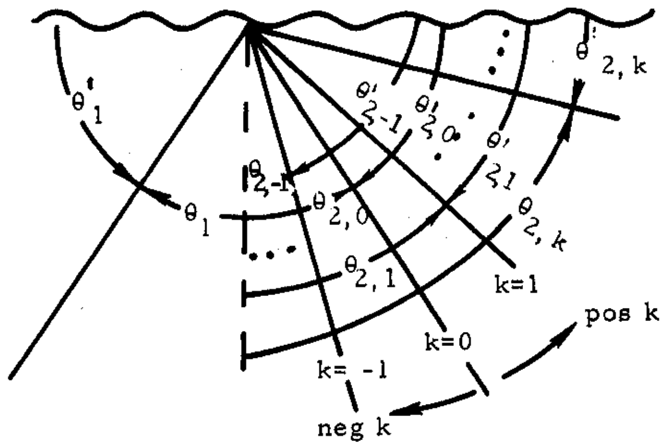

Fig. B1. Multimoded reflections for periodic surface.

ATC-58(B2)

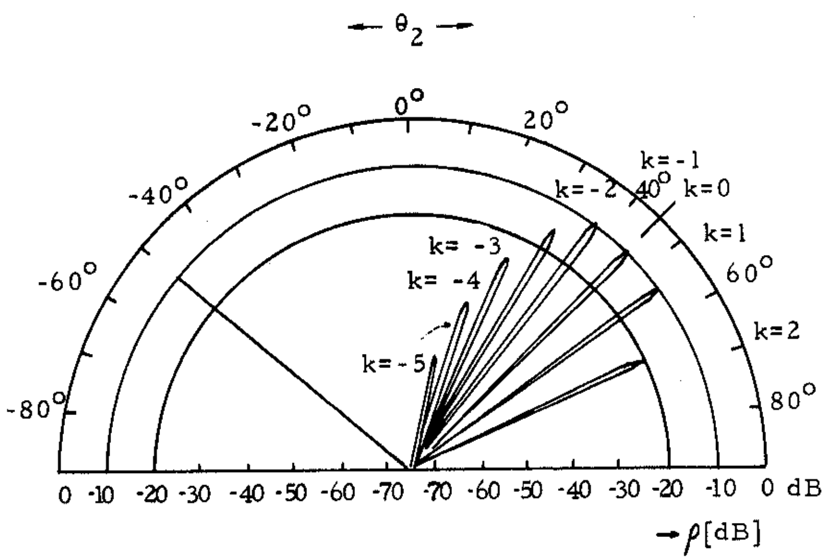

Fig. B2. Scattering by a sinusoidal surface. $d = 10\lambda$, $\theta_1 = 45°$.

ATC-58(B3)

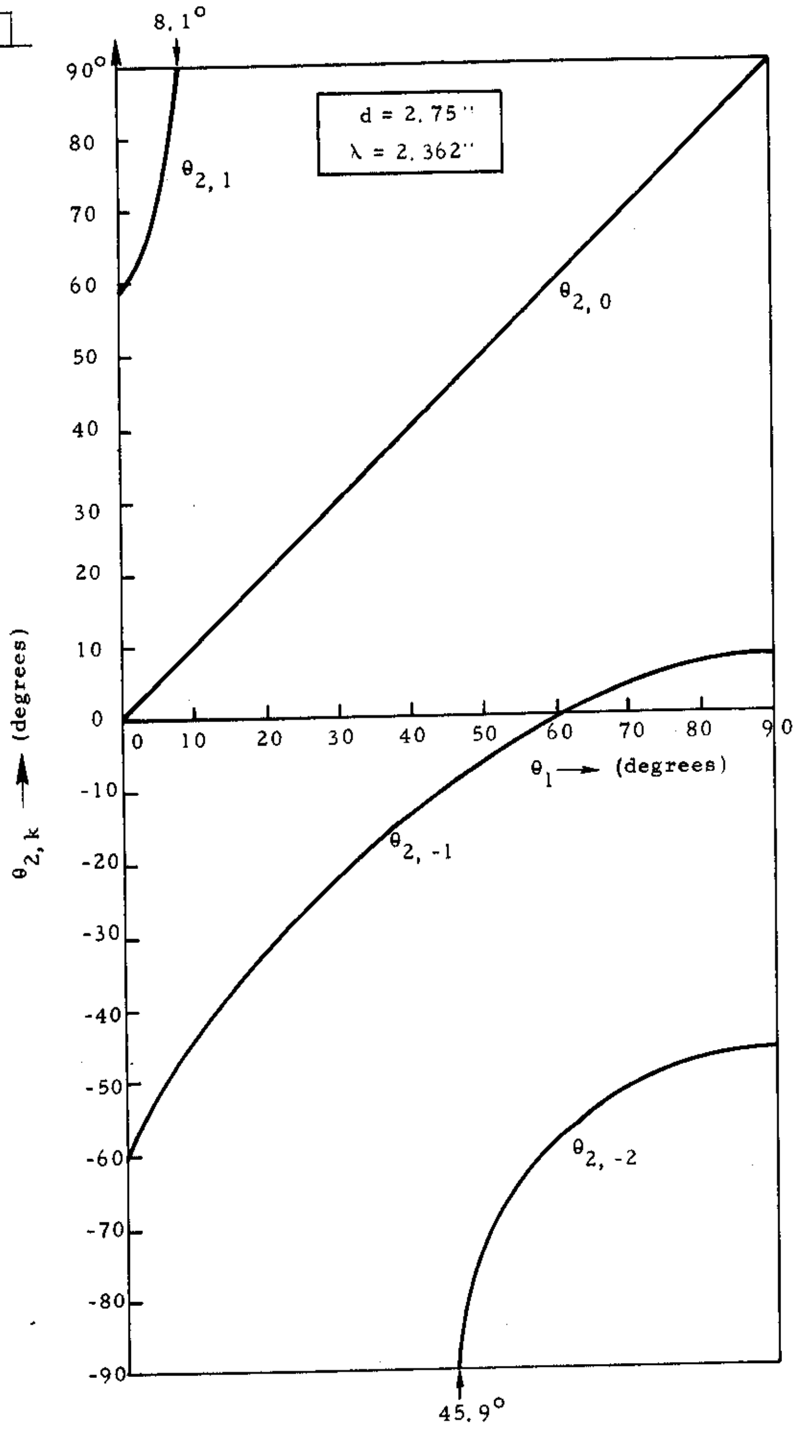

Fig. B3. θ_{2k}, vs θ_1 for $d/\lambda = 1.16$.

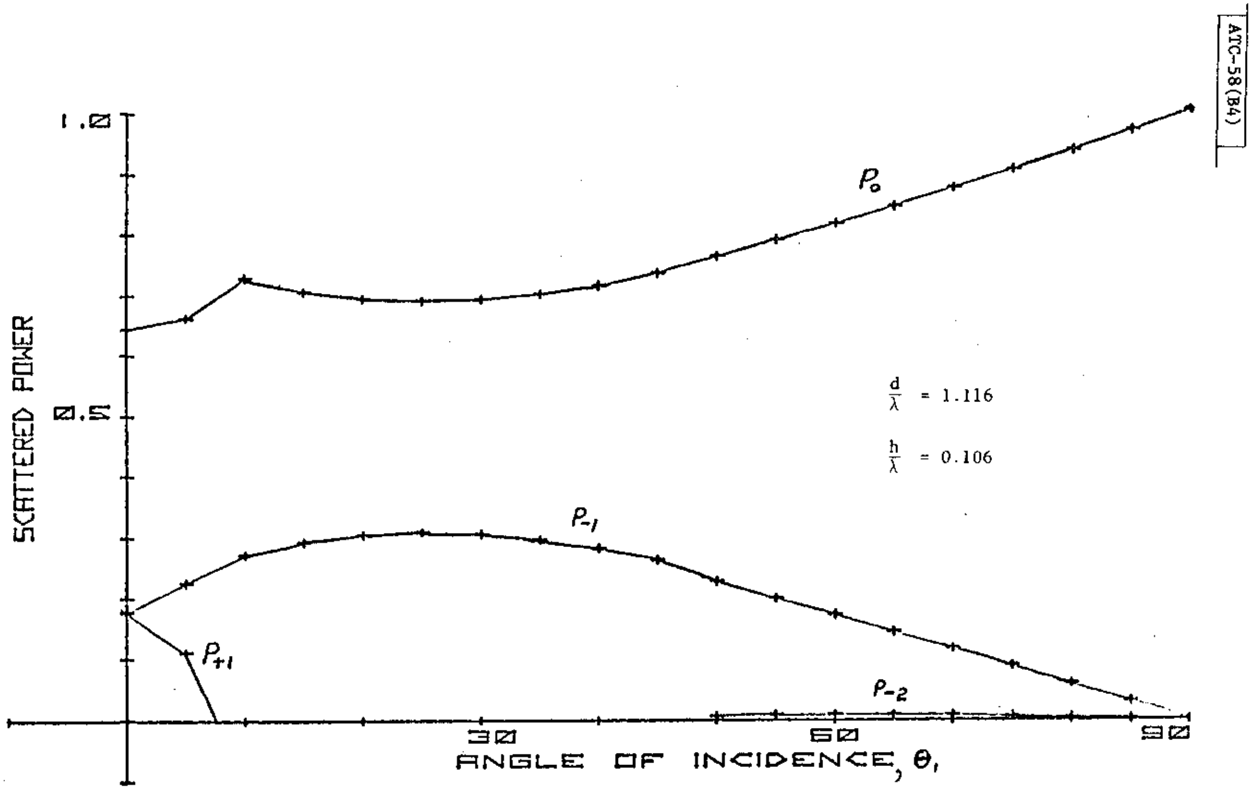

Fig. B4. Plots of $P_k(\theta_1)$ for S1 and vertical polarization.

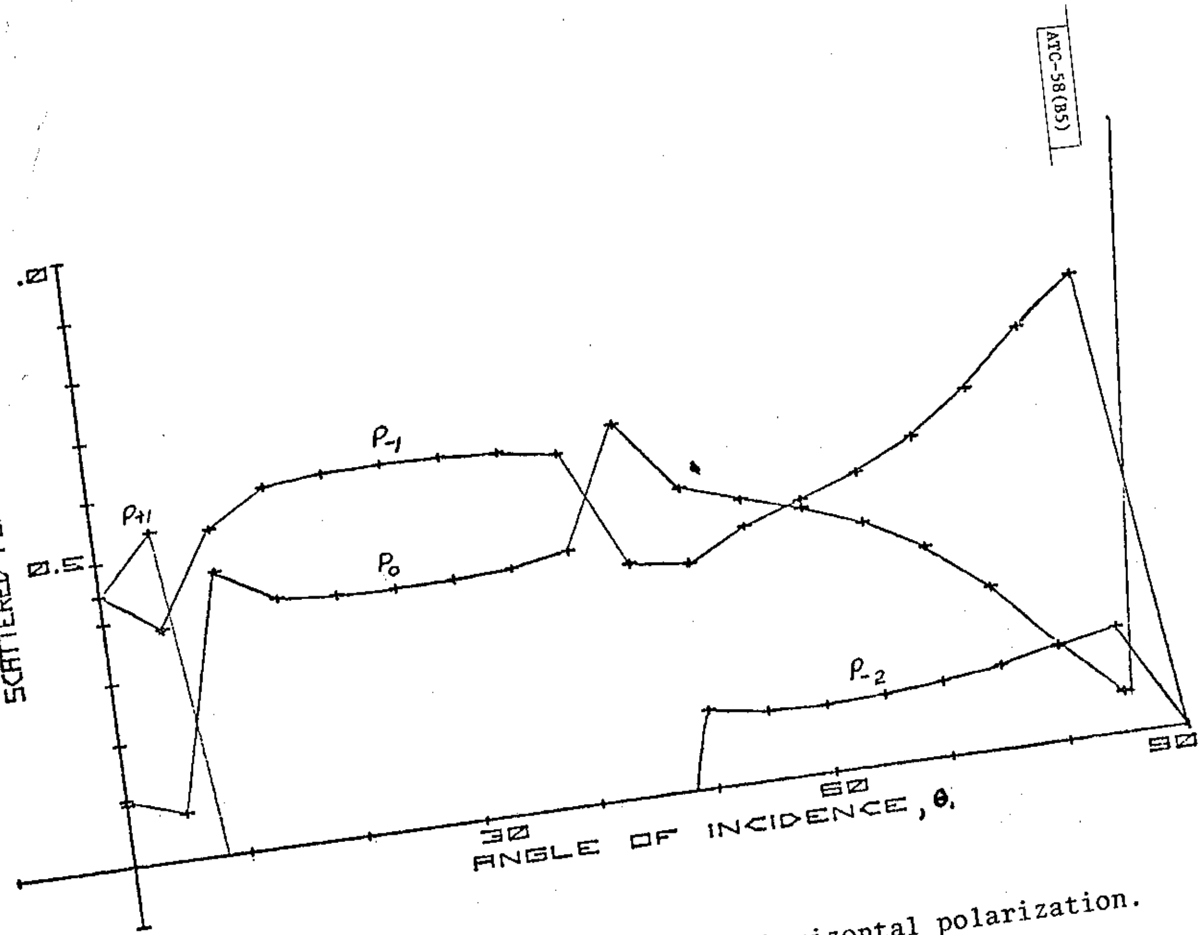

Fig. B5. Plots of $P_k(\theta_1)$ for S1 and horizontal polarization.

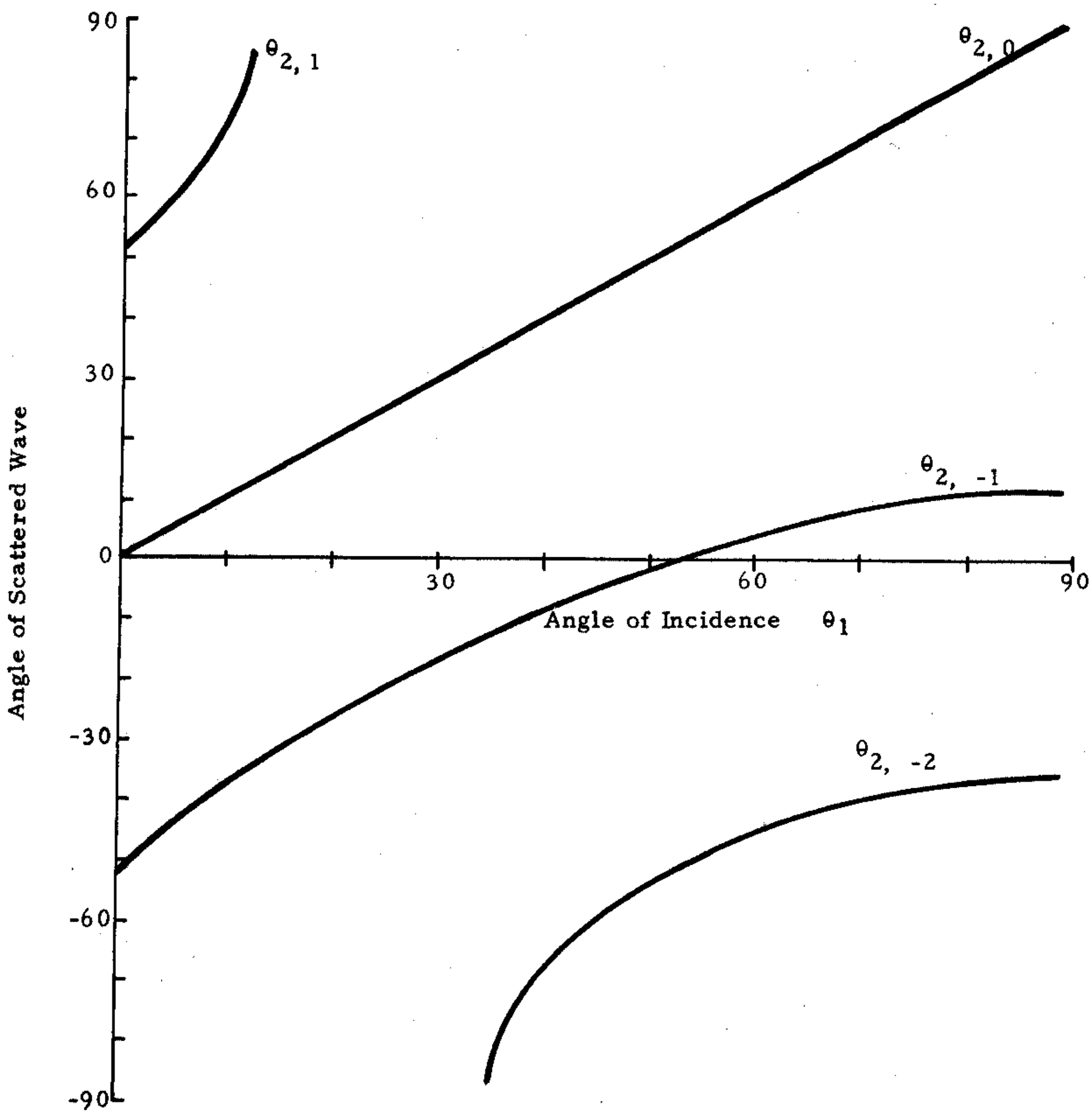

Fig. B6. $\theta_{2,k}$ vs θ_1 for $d/\lambda = 1.27$.

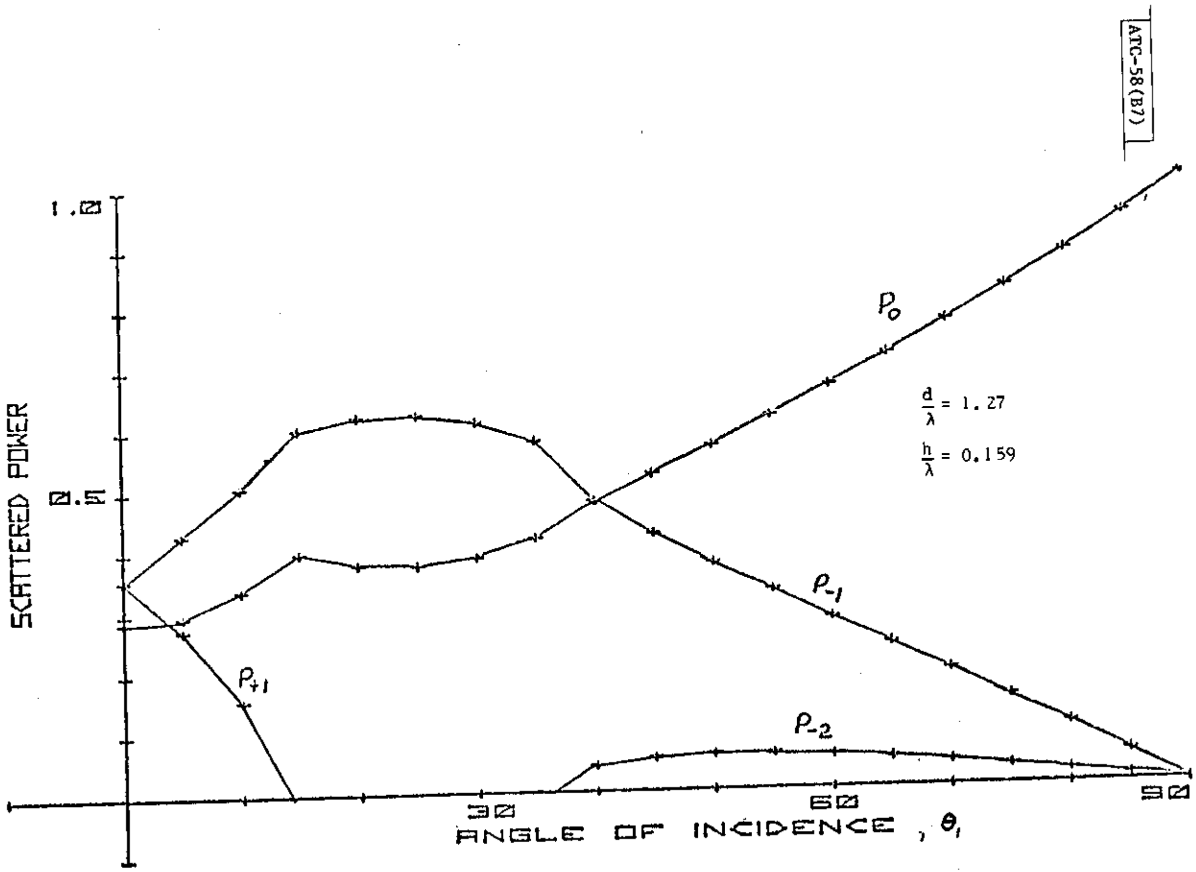

Fig. B7. Plots of $P_k(\theta_1)$ for S_2 and vertical polarization.

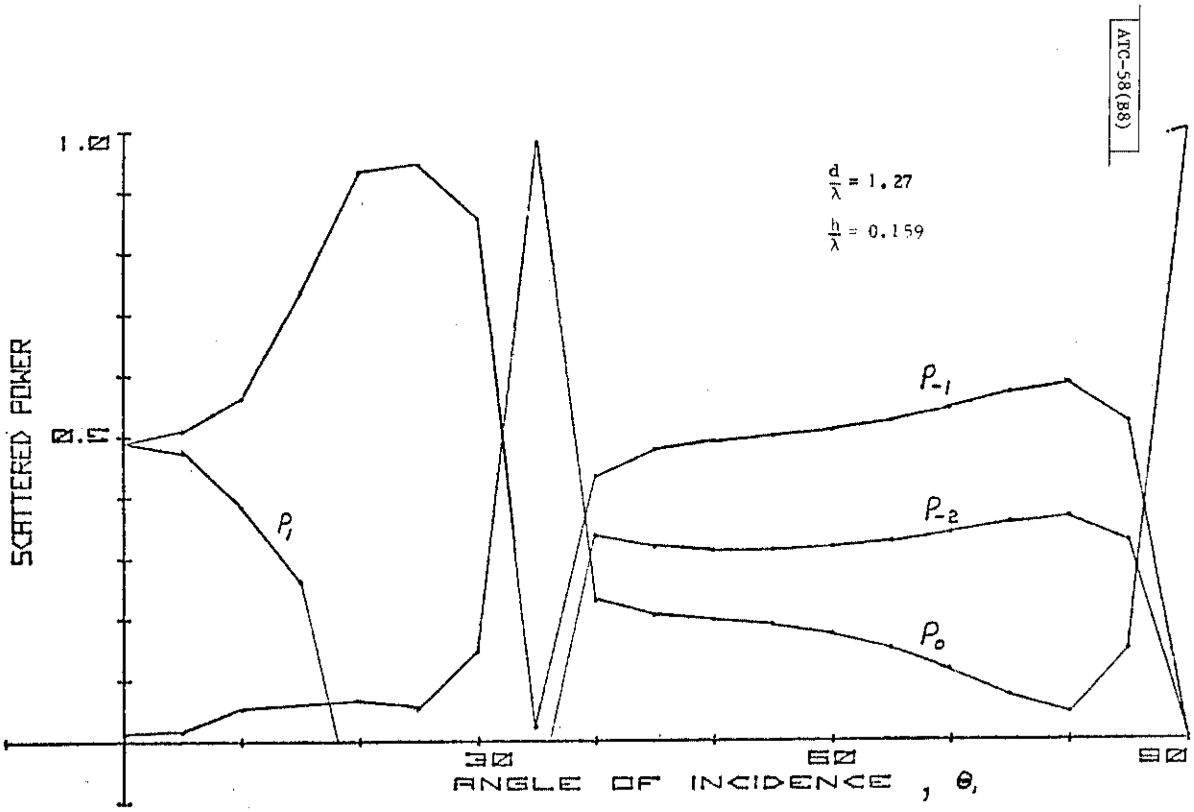

Fig. B8. Plots of $P_k(\theta_1)$ for S_2 and horizontal polarization.

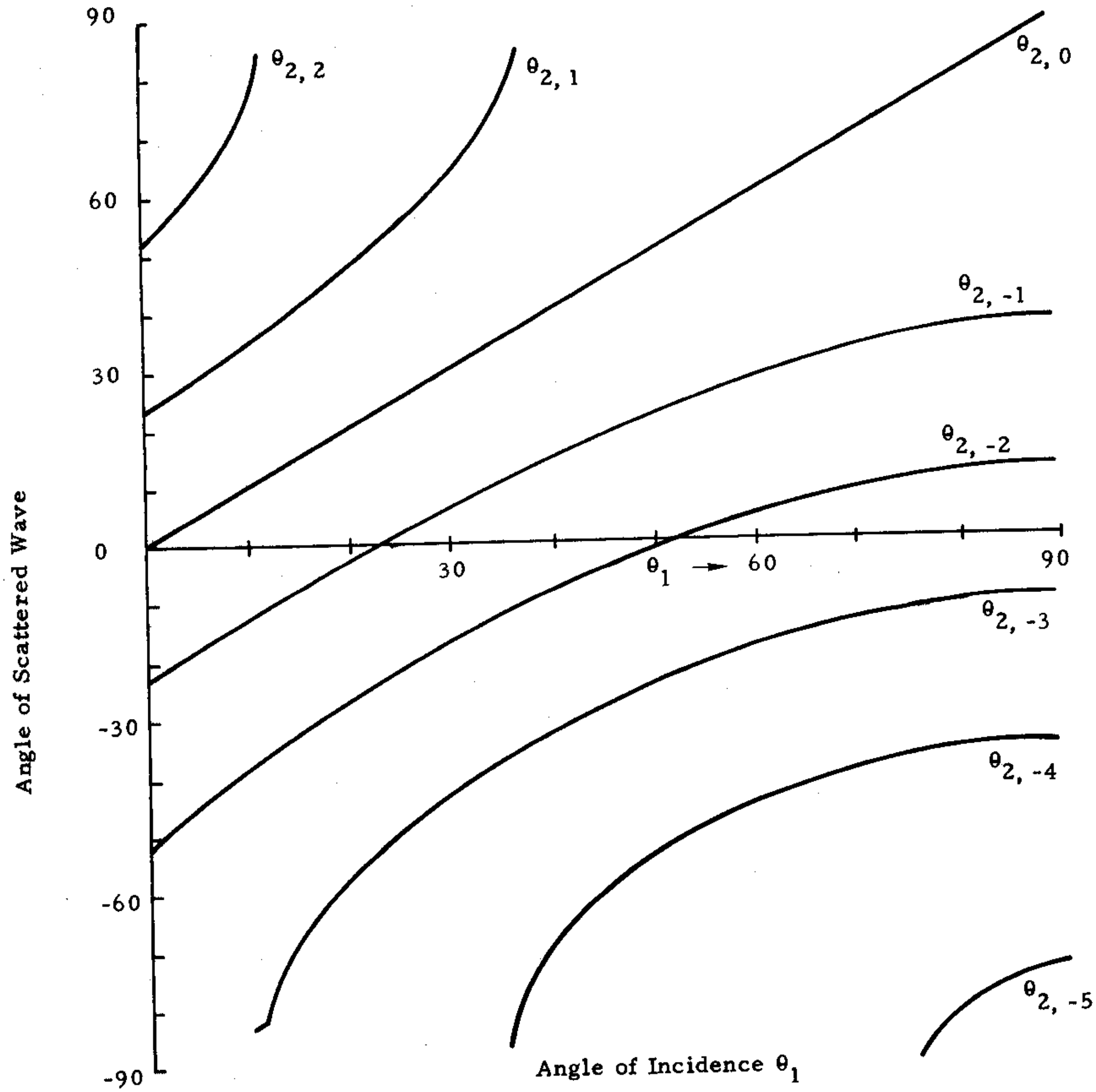

Fig. B9. $\theta_{2,k}$ vs θ_1 for $d/\lambda = 2.54$.

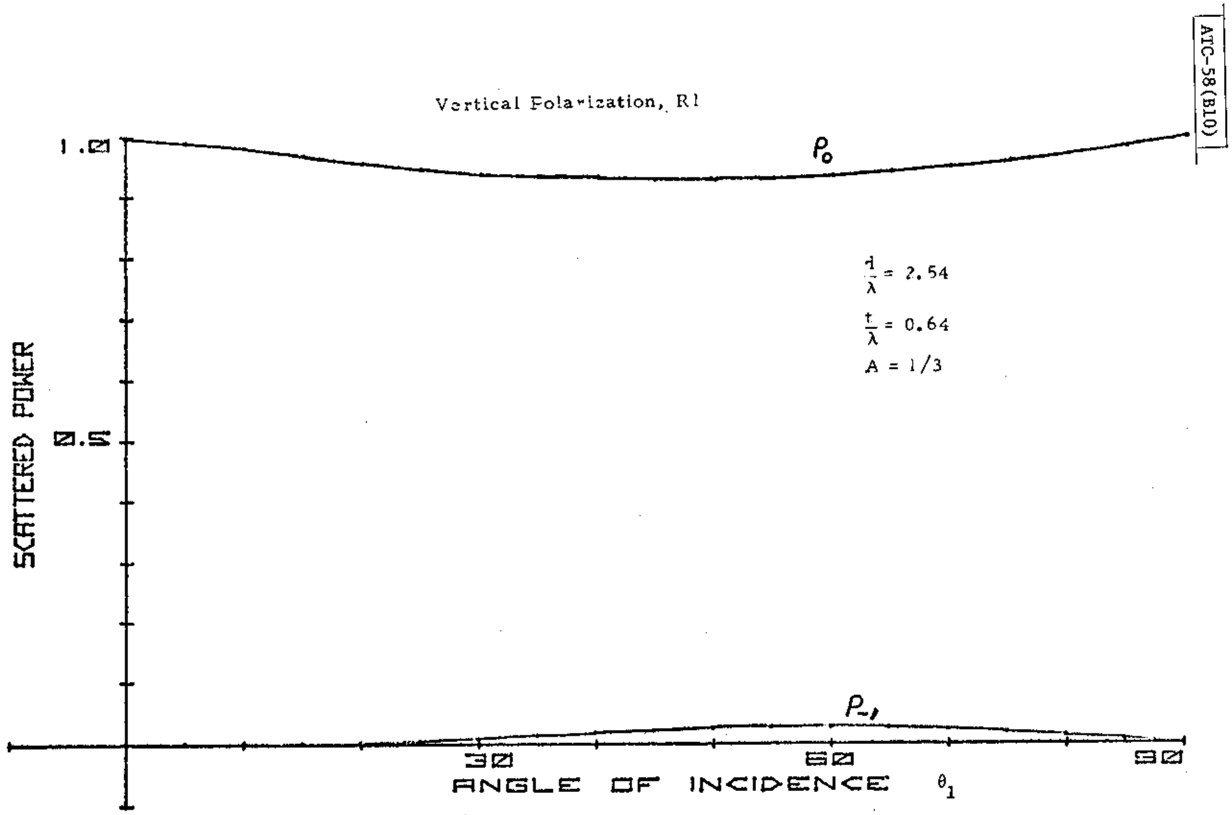

Fig. B10. Plots of $P_k(\theta_1)$ for R1 and vertical polarization.

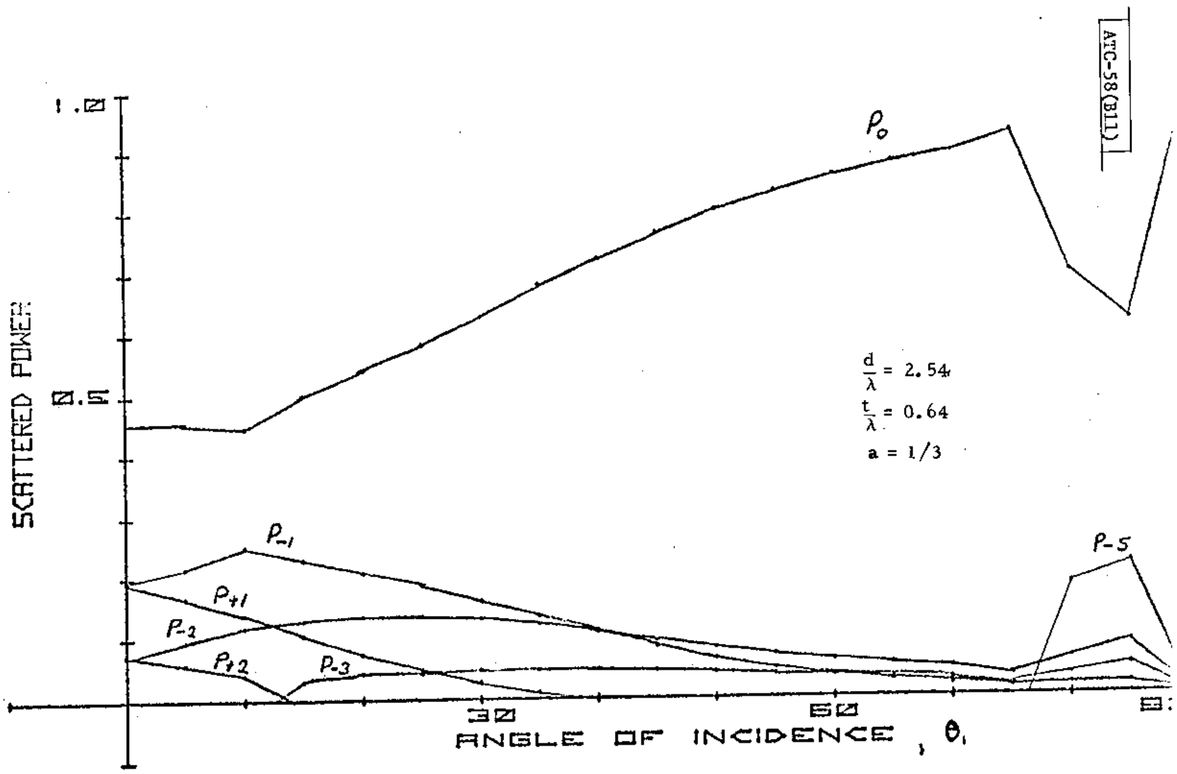

Fig. B11. Plots of $P_k(\theta_1)$ for R1 and horizontal polarization.

References

1. D.E. Kerr, Propagation of Short Radio Waves, Radiation Laboratory Series 1951 (McGraw-Hill, New York; also Dover, New York, 1965).

2. T.C.M. Tong and T.B.A. Senior, "Scattering of Electromagnetic Waves by a Periodic Surface with Arbitrary Profile," Scientific Report No. 13, AFCRL-72-0258, University of Michigan (April 1972).

3. A. Hessel and J. Shmoys, "Computer Analysis of Propagation/Reflection Phenomena," Scientific Report Contract Number DAAB07-73-M-2716, Polytechnic Institute of Brooklyn (August 1973).

4. K.A. Zaki and A.R. Neureuther, "Scattering from a Perfectly Conducting Surface with a Sinusoidal Height Profile: TE-Polarization," IEE Trans. Antennas Prop. AP-19, 208-214 (1971).

5. K.A. Zaki and A.R. Neureuther, "Scattering from a Perfectly Conducting Surface with a Sinusoidal Height Profile: TM-Polarization," IEEE Trans. Antennas Prop. AP-19, 747-751 (1971).

☆U.S. GOVERNMENT PRINTING OFFICE:1976--600-223--(42) 27